Université Fédérale

Toulouse Midi-Pyrénées

THÈSE

En vue de l'obtention du

DOCTORAT DE L'UNIVERSITÉ DE TOULOUSE

Délivré par :

Université Toulouse 3 Paul Sabatier (UT3 Paul Sabatier)

Cotutelle internationale avec l'Université Libanaise (Beyrouth)

Présentée et soutenue par :
Saleem HAMADY
le mardi 16 décembre 2014

Titre :

Nouveaux concepts de transistors de puissance à haute mobilité électronique (HEMT) en Nitrure de Gallium (GaN)

École doctorale et discipline ou spécialité :
ED GEET : Composants et Systèmes de gestion de l'Énergie

Unité de recherche :
LAAS-CNRS

Directeur/trice(s) de Thèse :

Frédéric MORANCHO, Professeur, Université Toulouse 3, LAAS-CNRS
Professeur Bilal BEYDOUN, Professeur, Université Libanaise

Jury :

Jean-Guy TARTARIN, Professeur, Université Toulouse 3, LAAS-CNRS	Président
Yvon CORDIER, Directeur de Recherche CNRS, CRHEA-CNRS	Rapporteur
Clovis FRANCIS, Professeur, Université Libanaise	Rapporteur
Mathieu GAVELLE, Ingénieur CEA Tech	Examinateur
Fabrice LETERTRE, Directeur Général, EXAGAN	Examinateur
Farid MEDJDOUB, Chargé de Recherche CNRS, IEMN	Examinateur

Université Libanaise

École Doctorale
Sciences et Technologies

UNIVERSITÉ TOULOUSE III PAUL SABATIER
Université de Toulouse

THESE EN COTUTELLE

Pour obtenir le grade de Docteur délivré par

l'Université Paul Sabatier

Ecole Doctorale Génie Electrique Electronique, Télécommunications
Spécialité : Composants et Systèmes de gestion de l'Énergie

et

l'Université Libanaise

Ecole Doctorale des Sciences et Technologies
Spécialité : MicroNano Systèmes - Physique Appliquée

Présentée et soutenue publiquement par :

Saleem HAMADY

le mardi 16 décembre 2014

Nouveaux concepts de transistors de puissance à haute mobilité électronique (HEMT) en Nitrure de Gallium (GaN)

Directeurs de thèse **:**

Prof. Frédéric MORANCHO

Prof. Bilal BEYDOUN

Membres du Jury

M. Jean-Guy TARTARIN	Professeur des universités, Université Toulouse III	Président
M. Yvon CORDIER	Directeur de Recherche, CNRS-CRHEA	Rapporteur
M. Clovis FRANCIS	Professeur des universités, Université Libanaise	Rapporteur
M. Mathieu GAVELLE	Docteur, Ingénieur CEA Tech	Examinateur
M. Fabrice LETERTRE	Directeur Général, EXAGAN	Examinateur
M. Farid MEDJDOUB	Chargé de Recherche, CNRS-IEMN	Examinateur

Dedicated to my beloved family

Yousef, Aida, Faisal, Hind and Kareem

New concepts for normally-off power Gallium Nitride (GaN) High Electron Mobility Transistor (HEMT)

Table of Contents

Abstract v

Acknowledgments vii

List of Acronyms ix

Introduction 1

Chapter 1 State of the art 5

1.1. Introduction 7

1.2. Power devices 7

1.2.1. Silicon power devices 7

1.3. Theoretical limits for power devices 9

1.4. Wide bandgap power devices 12

1.5. Gallium Nitride (GaN) 14

1.5.1. Gallium Nitride physical properties 14

1.5.2. Elastic and piezoelectric properties 16

1.6. Bound charge 17

1.7. AlGaN/GaN High electron mobility transistor 20

1.7.1. Basic structure 20

1.7.2. Band diagram of conventional HEMTs 22

1.7.3. Source of the 2DEG 26

1.7.4. Normally-off HEMT 28

1.7.4.1. Gate recess structure 28

1.7.4.2. Thin barrier layer 29

1.7.4.3. Gate Injection Transistor 29

1.7.4.4. P-GaN Gate HEMT 30

1.7.4.5. Fluorine implantation 30

1.8. MIS-HEMTs 31

1.9. Conclusion 32

Chapter 2 TCAD Simulation 35
2.1. Introduction 37
2.2. Silvaco framework overview 37
2.3. Simulation of AlGaN/GaN HEMT 38
2.3.1. Meshing 38
2.3.2. Physical Models 39
2.3.3. Simulator calibration 45
2.3.4. Normally-off structures simulated 48
2.3.4.1. Fluorine implantation below the channel 48
2.3.4.2. Buried p-region 50
2.4. Conclusion 51
Chapter 3 A normally-off HEMT with Fluorine implantation below the channel 53
3.1. Introduction 55
3.2. HEMT with Fluorine implanted below the channel 55
3.2.1. Fluorine implantation below the channel 55
3.2.2. Comparison between implantation in the barrier layer and implantation below the channel 57
3.2.3. Variations of the threshold voltage with the distance "d" 58
3.2.4. Breakdown voltage and off-state current 61
3.2.5. Forward gate voltage 62
3.3. MIS-HEMT with Fluorine below the channel 62
3.3.1. Effect of Fluorine concentration 63
3.3.2. Variation of the threshold voltage with thickness of the insulator 66
3.3.3. Variations with the permittivity of the insulator 67
3.4. Effect on the transconductance 69
3.5. AlN interlayer for better transconductance 71
3.6. Conclusion 72

Chapter 4 A normally-off HEMT with a buried p-GaN region 75
4.1. Introduction 77
4.2. HEMT with buried p-region 77
4.2.1. Effect of the width of the p-region P_w 79
4.2.2. Effect of the thickness of the p-region P_{th} 80
4.2.3. Effect of x-mole fraction: decreasing the download push of the triangular well 83
4.2.4. Effect of p-doping concentration 84
4.2.5. Effect of the distance "d" between p-region and the AlGaN/GaN interface 86
4.3. MIS-HEMT with a buried p-region 87
4.3.1. Variation with doping concentration 88
4.3.2. Variations of the threshold voltage with thickness of the insulator 89
4.3.3. Variations with the permittivity of the insulator 89
4.4. Comparison between the HEMT with a buried p-region and the Gate Injection Transistor (GIT) 92
4.4.1. Gate Injection Transistor 92
4.4.2. HEMT with a buried p-region versus GIT 93
4.4.3. Hybrid normally-off GIT with a buried p-region 95
4.5. New structures easing the fabrication of normally-off HEMTs with a buried p-region 98
4.5.1. Structure #1 98
4.5.1.1. Device design and fabrication process 98
4.5.1.2. Conditions for operation 99
4.5.1.3. Band diagram 101
4.5.1.4. Sensitivity analysis 102
4.5.2. Structure #2 105
4.5.2.1. Device design and fabrication process 105
4.5.2.2. Sensitivity analysis 106
4.6. Conclusion 107

Chapter 5 General conclusion and future work 109
5.1. General conclusion 111
5.2. Future work 113
5.2.1. Structure for fabrication 113
5.2.2. Develop and implement a new mobility model 113
5.2.3. Linking the equivalent interfacial charge to the Gaussian profile 114
5.2.4. AC and transient analysis 114
References 115

Abstract

AlGaN/GaN HEMTs are very promising candidates for high frequency applications with high power and low noise. While switching applications strongly demand normally-off operation, conventional HEMTs attain a channel populated with electrons at zero gate voltage making them normally-on. For the sake of achieving normally-off HEMTs, several structures have been proposed such as recessed gate structures, Fluorine ion treatment, P-GaN gate structures, thin AlGaN barrier and Gate Injection transistor.

The effectiveness of the agent used to obtain normally-off, whether it is recessing the gate, introducing a cap layer or implanting Fluorine, increases as the agent comes closer to the AlGaN/GaN interface. Unfortunately, when introducing a cap layer or recessing the gate, coming closer to the interface means decreasing the barrier thickness, which strongly affects the density of the 2DEG. In the case of Fluorine implantation, getting closer will increase the probability of Fluorine ions getting into the channel and hence degrade the mobility of the 2DEG.

In this work we propose two new concepts to achieve normally-off operation. We suggest the introduction of negative Fluorine ions on one hand or a p-GaN region on the other hand, below the channel, under the AlGaN/GaN interface and away from high current density regions. After calibrating the simulator using experimental results from a normally-on HEMT device, we will show that our proposed structures are more effective: the concentration required to achieve normally-off operation is lower than in the other existing solutions, and the confinement of the two dimensional electron gas below the gate is better.

The proposed ideas were also applied to Metal Insulator Semiconductor HEMT (MIS-HEMT) and Gate Injection Transistor (GIT), giving rise to a normally-off HEMT with high controllable threshold voltage.

Acknowledgments

This research would not have been possible without the guidance and the help of several individuals who in one way or another contributed and extended their valuable assistance in the preparation and completion of this study.

In the first place, I would like to record my gratitude to my advisors Prof. Bilal Beydoun and Prof. Frédéric Morancho for their supervision, advice, extraordinary patience and guidance from the very early stage of this research.

To Danial, Saleh, Amin, Bahaa, Haytham, Taher, Wisam, Osama, Jamal, Amin and Alaa, thank you for your thoughts, prayers, phone calls, e-mails, texts, visits and being there whenever I needed a friend. You all are the best friends anyone could ever ask for.

To Hadi, thanks for listening, offering me advice, and supporting me through this entire process.

Thanks to Dr. Yehya Amer for his endless support, care and encouragement

Special thanks for my friends at LAAS, Housam, Nadim, Serge, Ayyad and Mostapha. The debates, dinners, rides to the airport, and general help and friendship were all greatly appreciated.

I am grateful to all the administrative staff at the Lebanese and Paul Sabatier Universities and at the LAAS laboratory, for the practical support throughout my PhD, including, Ms. Camille Cazeneuve, Ms. Marie-Thérèse Funch, Ms. Claire Bardet, Ms. Zeinabou Sabatier, Ms. Ascension De Sousa, Ms. Isabelle Izarié and Ms. Zeinab Ibrahim.

To Mr Denis Griot and Prof. Augustin Martinez, thanks for the friday meetings, for giving me insight on the market of GaN and for believing in my potential.

My thanks go to my thesis reporters, Prof. Yvon Cordier and Prof. Clovis Francis and for the jury members for their comments and remarks.

I would like to extend my gratitude to the Azm and Saada association and for the LAAS laboratory for financing this research project.

Words fail me to express my appreciation to my parents, Yousef and Aida Hamady for their love and support. My life has been extremely blessed to have two wonderful, loving parents whose love and support of anything I do has never been in doubt. To my brothers Faisal and Kareem and to my sister Hind thanks for all the emotional support, loving entertainment, and caring. I thank god for my family to whom I dedicate this thesis.

Saleem HAMADY

List of Acronyms

2DEG	Two dimensional electron gas
AC	Alternating current
AlGaN	Aluminum Gallium Nitride
DC	Direct current
GaN	Gallium Nitride
GIT	Gate injection transistor
Grid T&D	Grid Transmission & Distribution
GTO	Gate turn-off thyristor
HEMT	High electron mobility transistor
HVAC	Heating, ventilation, and air conditioning
HVDC	High voltage direct current
IGBT	Insulated gate bipolar transistor
MOSFET	Metal insulator semiconductor field effect transistor
Si	Silicon
SiC	Silicon Carbide
UPS	Uninterruptible power supply
VTR	Video tape recording

Introduction

Electronic devices have truly blended in with our lives and expand our capabilities and potential. Development and innovation in this field will shape the future of mankind. In the electronic devices we use today, solid-state devices are utilized to control or convert electric power into different forms. This domain is known as power electronics. In our smart phones, tablets, PDAs and almost every mobile device, a DC/DC converter is used to maintain a fixed output voltage regardless of the battery voltage level. Most of the electronic devices connected to the mains (laptops, TVs, etc) utilize an AC/DC converter, which are also known as rectifiers. DC/AC converters, also known as inverters, are used in hybrid vehicles, renewable energy systems, UPS and emergency lighting systems. After storing AC voltage in DC batteries, the batteries can later be used to generate AC voltage with the help of an inverter. AC/AC converters are found in international power adapters, light dimmer, fan with controllable speeds and many other applications that require a change in the frequency or voltage level of an AC signal.

Improving the efficiency of power electronic devices is crucial to reduce switching losses and hence lower the CO_2 emission. Today, the vast majority of power devices are made from silicon. Unfortunately, the intrinsic physical properties of silicon set a theoretical limit on the capabilities of silicon power devices hindering them, in some domains, from being the candidates for future power electronics. With silicon power devices reaching their theoretical limits, design engineers are facing the challenge of increasing the ratings of converters in terms of operating voltage, operating temperature and efficiency. The quest for a solution to silicon limitations leads researchers to the doorstep of wide bandgap materials such as Silicon Carbide (SiC) and Gallium nitride (GaN). Compared to silicon, the main benefits of these materials are a good operation over a wide temperature range, high critical electric field and high saturation velocity.

SiC power components have been a subject of extensive research in the past fifteen years. However, despite the remarkable results obtained by several teams, SiC must be grown on native substrates which are expensive and relatively small in size (100 mm in diameter). On the other hand, GaN can be grown on silicon substrates which are of low cost and large size (150 to 200 mm in diameter). Moreover, GaN is better than SiC for creating heterostructures due to their built-in polarization field. Therefore, for devices such as HEMT, GaN is the material of choice.

The polarization doped High Electron Mobility Transistor (HEMT) is a field effect transistor in which two layers of different bandgap and polarization field are grown upon each other. As

a consequence of the discontinuity in the polarization field, surface charges at the heterointerface are created. If the induced charge is positive, electrons will tend to compensate the induced charge resulting in the formation of the channel. Since in the HEMT the channel electrons are confined in a quantum well in a very narrow spatial region at the heterointerface, the channel electrons are referred to as a Two Dimensional Electron Gas (2DEG). This confinement grants the electrons high mobilities surpassing the bulk mobility of the material in which the electrons are flowing. Thanks to the GaN properties and the HEMT's topology, AlGaN/GaN HEMTs are now promising devices for high frequency applications with high power and low noise, such as microwave and millimeter wave communications, imaging and radars.

While power switching applications strongly demand normally-off operation with a threshold voltage above 3V, conventional HEMTs attain a channel populated with electrons at zero gate voltage making them normally-on. Several normally-off structures have been proposed such as recessed gate structures, fluorine ion treatment, P-GaN gate structures, thin AlGaN barrier and the Gate Injection Transistor. The effectiveness of the agent used to obtain normally-off, whether it is recessing the gate, introducing a cap layer or implanting fluorine, increases as the agent comes closer to the AlGaN/GaN interface. Unfortunately, in introducing a cap layer or recessing the gate, coming closer to the interface means decreasing the barrier thickness, which strongly affects the density of the 2DEG. In the case of fluorine implantation, getting closer to the interface increases the probability of fluorine ions getting into the channel and hence the degradation of the mobility of the 2DEG.

In this work, two new normally-off concepts are proposed. To examine their electric characteristics, a commercial TCAD simulation tool from Silvaco is used. Technology Computer Aided Design (TCAD) tools are simulation tools used to model the processing and behavior of electronic devices. The simulator can predict the electrical behavior of semiconductor devices at specified bias conditions.

After introducing the structure, composition and features of the conventional HEMT in chapter 1, the device simulator is explained in chapter 2 showing the input to the simulator, the fitting strategy and the models used. In chapters 3 and 4, the two new normally-off designs are shown along with the results of the sensitivity analysis for the HEMT with Fluorine implanted below the channel and HEMT with buried p-region respectively.

Chapter 1
State of the art

1.1. Introduction

The reduction of CO_2 emission has always been a subject of extensive research. In the domain of power electronics, the reduction of CO_2 emission can be achieved by increasing the efficiency of power converters by reducing the switching losses in power devices [1]. Today, the vast majority of power devices are made from silicon. Unfortunately, silicon is reaching its theoretical limit in terms of device performance. The quest for a solution to silicon limitations leads researchers to the doorstep of wide bandgap materials, such as Silicon Carbide (SiC) and Gallium nitride. When compared to SiC, GaN is a better candidate to fabricate heterostrucutres and, unlike SiC, can be grown on silicon substrates. This chapter shows the fundaments of the HEMT device fabricated using GaN based materials. Afterwards, the state of the art normally-off HEMT structures are explained and shown.

1.2. Power devices

For ultimate efficiency in power conversion, an ideal switch is required. An ideal switch has zero voltage drop and no limit on the current level carried during the on-state. During the off-state, it attains infinite resistance (zero leakage current) and can sustain unlimited voltages. The time to switch between the on and off-state is zero [2].

The quest for the ideal switch results in the development of various power components, each resembles in a way a characteristic of the ideal switch. In practical switches, there is a trade-off between voltage, current and frequency ratings.

1.2.1. Silicon power devices

Figure 2 shows the split of the main power devices depending on their current, voltage and frequency rating. The power MOSFETs are found in applications demanding small inverters (Watt to kW range) such as VTRs, mobile phones, communication devices, audio equipments and many others.

The IGBT performance is regularly improving as technology evolves and has already replaced the bipolar transistor in power applications. Moreover, IGBT power modules, parallelly combining several IGBT devices, are attractive for power levels up to several Megawatts. The operating frequency of the IGBT is relatively low mainly because of a problem during turn-off known as current-tail. IGBTs and IGBT modules are utilized in applications using inverters with a switching power ranging from kW to MW such as air conditioners, refrigerators, railways, paper making, etc.

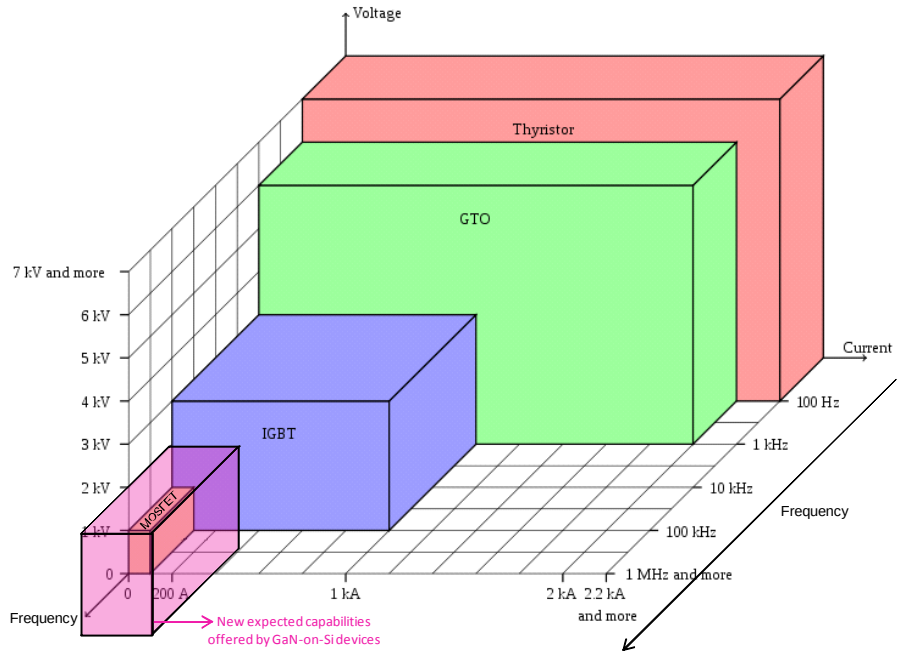

Figure 1.1 Classification of the main power devices according to their switching frequency, voltage and current ratings

Thyristor-based devices are the only choice at very high power. The problem with thyristors is that once it starts conducting, the gate loses its control over the device. To solve this problem, the gate turn-off thyristor (GTO) was later introduced which is a fully controllable switch that can be turned on and off. However, while thyristors are used in medium to high voltage applications, GTO are used at medium voltages only. Thyristors and thyristor-based devices are used in AC drives, HVDC and Grid T&D [3].

It is worth mentioning that recent improvements of Si devices (superjunction, high speed IGBT) and the introduction of new materials (SiC, GaN) will mix the performance and open new device choices. For instance, GaN on Silicon devices are expected to be faster than IGBTs and more powerful than MOSFETs. GaN-based power solutions are expected to increase efficiency, reduce system size, and simplify overall product design and can eliminate up to 90% of all electric conversion losses from heating, ventilation, and air-conditioning systems (HVAC). Therefore GaN power devices are expected to replace silicon MOSFETS and IGBT modules in applications like VTRs, communication devices, audio equipments, AC adapters and electric/hybrid vehicles [3].

1.3. Theoretical limits for power devices

When increasing the applied voltage across a power device, the electric field within the device begins to increase. Once the electric field approaches a critical level E_c, the power device tends to undergo avalanche breakdown. To allow simple comparison between similar systems with different material compositions, an abrupt one-dimensional P+/N diode is studied [4]. In this study, it is assumed that the voltage is supported across only one side of the structure. This assumption holds true for an abrupt P+N junction since the doping concentration on one side is very high compared to the other. Moreover, since the P+ region is taken very thin and highly doped compared to the n-region, the depletion region extends primarily in the N-doped region [4].

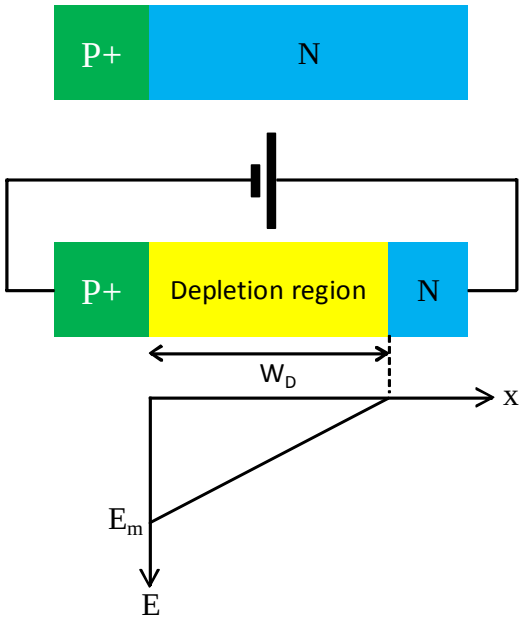

Figure 1.2. Schematic cross-section of an abrupt P^+N junction showing the electric field distribution inside the depletion region when the junction is reversed biased

When this diode is reverse biased, a depletion region is formed in the N-region (the depletion in the P+ region can be neglected). The electric field in the depletion region can be extracted from the Poisson's equation:

$$\nabla^2 V = -\frac{\rho}{\varepsilon_s} \tag{1.1}$$

$$E = -\nabla . V \tag{1.2}$$

where V is the electrostatic potential, ρ is the charge density, ε_s is the dielectric constant of the semiconductor and E is the electric field.

In our case (one dimensional case):

$$\frac{d^2V}{dx^2} = -\frac{dE}{dx} = -\frac{\rho}{\varepsilon_s} = -\frac{qN_D}{\varepsilon_s} \tag{1.3}$$

The charge within the depletion region due to the presence of ionized donors can be expressed as qN_D, q is the proton charge and N_D is the donor concentration in the uniformly doped N-region. The solution of equation 1.3, with the use of the boundary conditions $E(W_D) = 0$ and $V(0) = 0$, yields the following expressions for the electric field and the electrostatic potential:

$$E(x) = -\frac{qN_D}{\varepsilon_s}(W_D - x) \tag{1.4}$$

$$V(x) = \frac{qN_D}{\varepsilon_s}\left(W_D x - \frac{x^2}{2}\right) \tag{1.5}$$

W_D can be related to the applied voltage by using the condition $V(W_D) = V_a$, where V_a is the applied reverse voltage.

$$W_D = \sqrt{\frac{2\varepsilon_s V_a}{qN_D}} \tag{1.6}$$

At breakdown $V_a = V_{BR}$ and $E_m = E(0) = E_c$

$$W_D = \sqrt{\frac{2\varepsilon_s V_{BR}}{qN_D}} \tag{1.7}$$

$$E_c = -\frac{qN_D}{\varepsilon_s} W_D \Rightarrow W_D = \frac{-\varepsilon_s E_c}{qN_D} \tag{1.8}$$

Combining equations 1.7 and 1.8, we get:

$$N_D = \frac{\varepsilon_s {E_c}^2}{2qV_{BR}} \tag{1.9}$$

$$W_D = \frac{2V_{BR}}{E_c} \tag{1.10}$$

The specific on resistance per unit area of the ideal uniformly doped drift region is:

$$R_{on,sp} = \frac{W_D}{q\mu_n N_D} \tag{1.11}$$

Combining equations 1.9 and 1.10, we obtain:

$$R_{on,sp} = \frac{4\,V_{BR}}{\varepsilon_s \mu_n E_c^3} \tag{1.12}$$

The denominator of this equation ($\varepsilon_s \mu_n E_c^3$) is commonly referred to as Baliga's figure of merit for power devices [5]. It is an indicator of the impact of the semiconductor material properties on the resistance of the drift region. An accurate modeling of the specific on resistance requires taking into account the dependence of the critical electric field and mobility on the doping concentration.

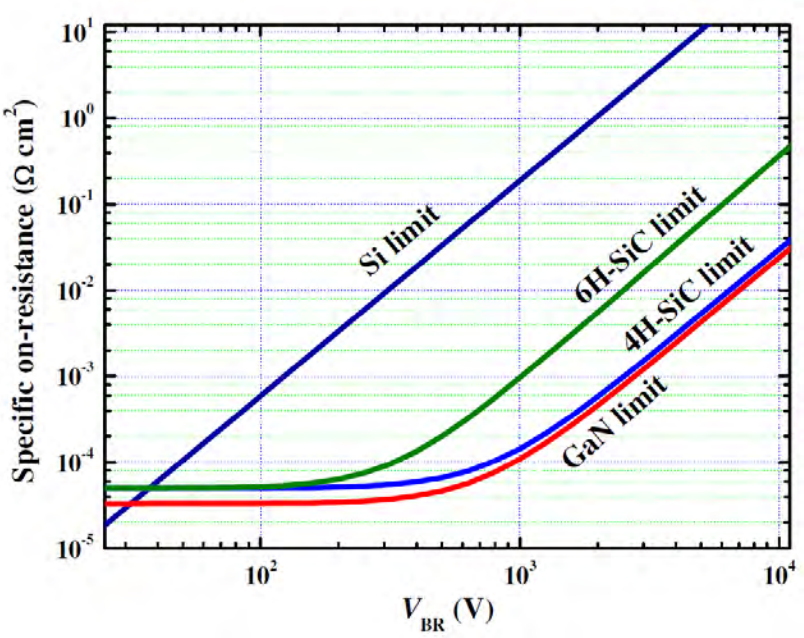

Figure 1.3. Theoretical on-resistance versus breakdown voltage for different materials showing an advantage for wide bandgap semiconductors [5]

Practical specific ON-resistance estimation is calculated using the following approximation [6]:

$$E_c \propto N_D^y$$

$$\mu_n \propto N_D^{-x}$$

$$R_{ON}(\Omega.cm^2) \propto V_{BR}^{\eta}$$

$$\eta = \frac{2-x-y}{1-2y}$$

For Si [4]: $R_{ON}(\Omega.cm^2) = 5.93 \times 10^{-9}\ {V_{BR}}^{2.5}$ (1.13)

For 4H-SiC [4]: $R_{ON}(\Omega.cm^2) = 2.97 \times 10^{-12}\ {V_{BR}}^{2.5}$ (1.14)

For 6H-SiC [7]: $R_{ON}(\Omega.cm^2) = 1.45 \times 10^{-11} V_{BR}{}^{2.6}$ (1.15)

For GaN [7]: $R_{ON}(\Omega.cm^2) = 2.4 \times 10^{-12} V_{BR}{}^{2.5}$ (1.16)

Figure 1.3 shows the plot of equations 1.13, 1.14, 1.15 and 1.16 [5]. It is clear that the theoretical limit of wide bandgap materials is much higher than that of silicon. This means that, for the same breakdown voltage, devices based on wide bandgap materials offer a significantly lower ON-resistance.

1.4. Wide bandgap power devices

With silicon power devices reaching their theoretical limits in terms of temperature and power operation, design engineers are facing the challenge of increasing the ratings of converters in terms of operating voltage, operating temperature and efficiency. The quest for a solution to silicon limitations leads researchers to the doorstep of wide bandgap materials such as Silicon Carbide (SiC) and Gallium Nitride (GaN).

Item	Unit	Si	4H-SiC	GaN
Band gap	eV	1.1	3.26	3.4
Electron mobility	$cm^2/V.s$	1300	900	900 - 2000
Breakdown field strength	V/cm	0.3×10^6	3×10^6	3.5×10^6
Saturated electron speed	cm/s	1×10^7	2×10^7	2.5×10^7
Thermal conductivity	W/cm.K	1.5	3.7	1.3

Table 1 Physical properties of Silicon (Si), Silicon Carbide (4H-SiC) and Gallium Nitride (GaN)

Wide bandgap materials show superior advantages over silicon such as large bandgap, high critical breakdown field strength and high thermal conductivity in some cases (SiC). The values are illustrated in table 1. The translation of these superior physical properties to the devices is shown in figure 1.4. The high critical electric field and the wide energy gap enable operation at high voltages and elevated temperatures. The high switching frequency is attributed to the high saturation electron velocity and high mobilities. From figure 1.4, it can be concluded that SiC will stay the preferred choice for high temperature applications. GaN has an extra advantage compared with SiC as a result of the enhanced mobility of electrons in the two dimensional electron gas (2DEG). This translates into a GaN device with a smaller size for a given on-resistance and breakdown voltage.

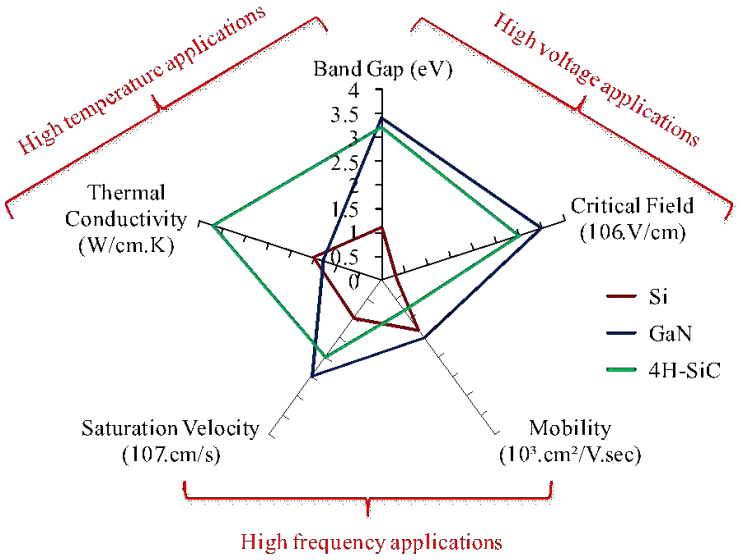

Figure 1.4 Comparison between Silicon, Gallium Nitride and Silicon Carbide based on their physical properties

The applications for various power devices along with the material capabilities are shown in figure 1.5 [3]. It is clear that high power and high frequency applications are demanding more than silicon can offer. SiC is expected to cover the high power low frequency applications while GaN covers the high frequency relatively low power applications. The competition between SiC and GaN will be at intermediate frequencies and moderate power.

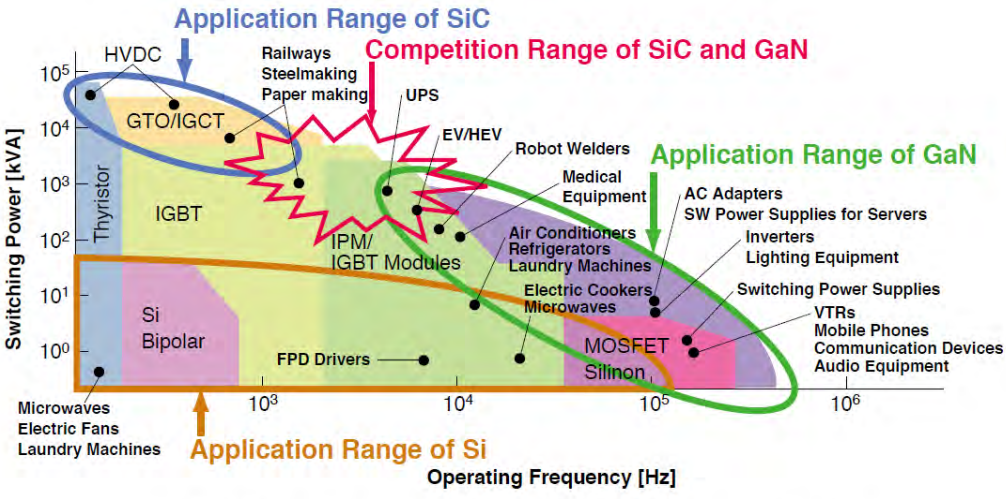

Figure 1.5 Applications for various power devices along with the material capabilities [3]

1.5. Gallium Nitride (GaN)

1.5.1. Gallium Nitride physical properties

Gallium Nitride (GaN) is a semiconductor material belonging to the III-V semiconductor family. Its crystal structure may differ between Wurtzite and Zinc blend. The two structures are shown in figure 1.6 [8]. Since AlGaN/GaN HEMTs are grown on the Wurtzite phase, only this crystal structure will be further explained. The unit cell of the III-N Wurtzite structure is the hexagonal cell consisting of two intercepting Hexagonal Closed Packed (HCP) sub-lattices, each formed by one type of atoms. The structure is fully defined by three lattice constants: the side's length of the hexagonal base "a", the height of the cell "c" and the shift, along the c-axis, between the 2 sub-lattices "u". In an ideal Wurtzite structure, when atoms are considered to be touching hard spheres, the ratio of these parameters is $c_o/a_0 = \sqrt{8/3} = 1.633$ and $u_o/c_0 = 3/8 = 0.375$. GaN can be doped with silicon (Si) or with oxygen to n-type [9] and with magnesium (Mg) to p-type [10].

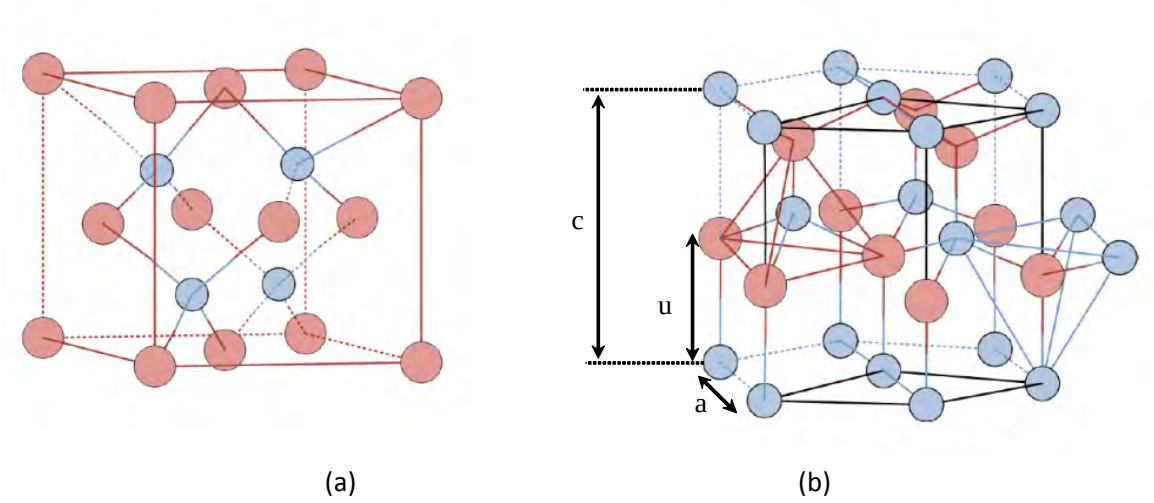

Figure 1.6 Crystal structure of GaN (a) Zinc blend and (b) Wurtzite structure [8]

Beside the advantage of Wurtzite structure being favored at room temperature due to its stability, it possesses a built-in polarization field named the spontaneous polarization P_{sp}. This field springs up due to the ionic nature of the gallium-nitrogen bond and the lack of inversion symmetry within some planes within the crystal. The values of the spontaneous polarization of some binary and trinary III-N alloys is shown in figure 1.7 [11].

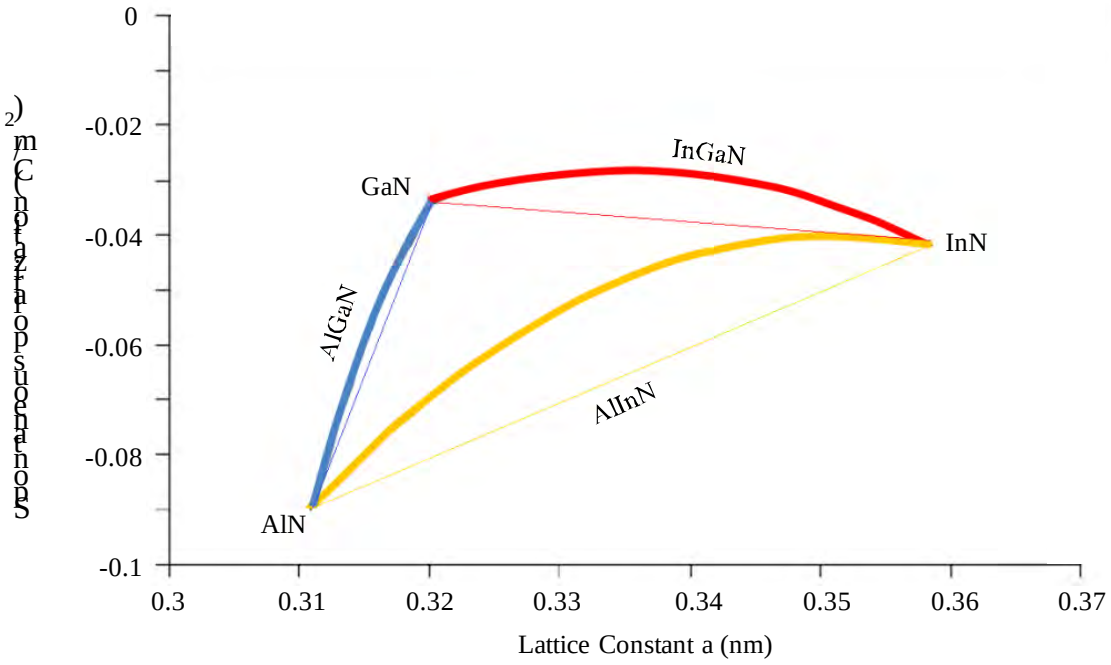

Figure 1.7. Spontaneous polarization of III-N binary and ternary alloys. The thin lines show linear interpolation while the thick ones show second order approximation [11]

Planes lacking inversion symmetry will attain a polarization field along their normal vector. In Wurtzite GaN (w-GaN), the (0001) plane, named the c-plane, attains spontaneous polarization, while the $(1\bar{1}00)$ and $(11\bar{2}0)$ planes, named m- and a-planes respectively, do not. Some of the polar and non-polar planes are shown in figure 1.8.

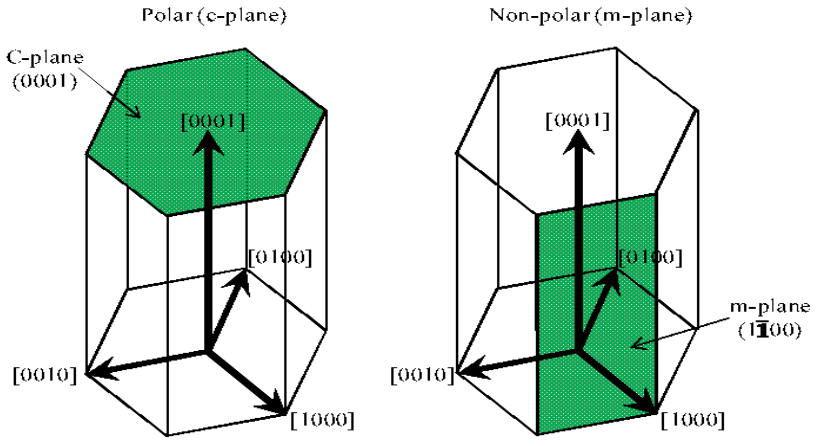

Figure 1.8 To the left the polar plane known as c-plane (0001) and to the right a non-polar plane ($\mathbf{1\bar{1}00}$) known as the m-plane

In order to take advantage of the spontaneous polarization, GaN is grown perpendicularly to the c-plane. The resulting surface is either the (0001) also known as Ga-faced or $(000\bar{1})$

known as N-faced. The orientation of the polarized field in N-faced plane is opposite to that in the G-faced. Distinction between these two orientations can be done by variety of techniques including wet chemical etching, characterization of physical morphology, and convergent beam electron diffraction [12]. The atomic arrangement in GaN-face and N-face GaN is shown in figure 1.9 [13]

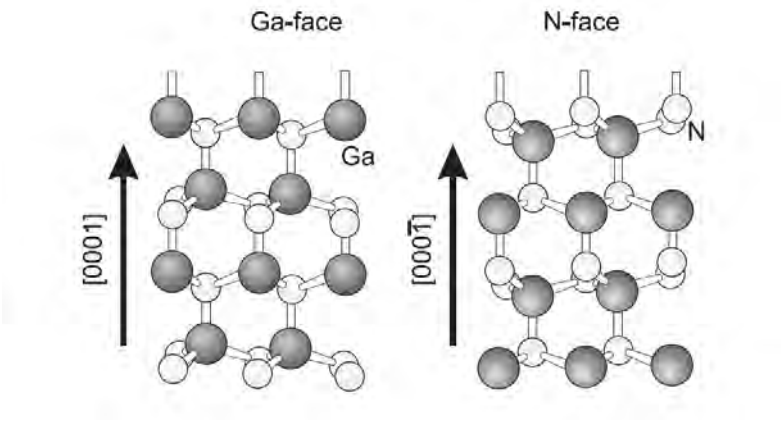

Figure 1.9 Atomic arrangement in Ga-face and N-face GaN [14]

1.5.2. Elastic and piezoelectric properties

In addition to the spontaneous polarization, GaN as well as GaN alloys possess piezoelectric properties. When an external electric field is applied to piezoelectric materials, they mechanically deform. Conversely, these materials generate an electric field in response to an applied mechanical stress/strain. When growing two materials with different lattice constant upon one another, at certain conditions discussed in 1.4.3.3, the above layer will stretch or shrink so that its lattice constant matches the layer upon which it is grown. This stretch/strain will generate a polarization field named piezoelectric polarization P_{pz}.

The piezoelectric polarization is simply expressed as:

$$P_{pz} = e_{33}\varepsilon_3 + e_{13}.(\varepsilon_1 + \varepsilon_2) \tag{1.17}$$

$$\text{where:} \quad \varepsilon_1 = \varepsilon_2 = \frac{(a - a_o)}{a_o} \ , \ \varepsilon_3 = \frac{(c - c_o)}{c_o} \tag{1.18}$$

$$\text{and:} \quad \varepsilon_3 = -2\,\frac{C_{13}}{C_{33}}\,\varepsilon_1 \tag{1.19}$$

a_o and c_o are the equilibrium value of the lattice constant (base material), a and c are the lattice constants of the material that is to be deposited (stretched or strained material), e_{33} and e_{13} are piezoelectric coefficients, C_{33} and C_{13} are elastic constants, ε_3 is the strain along the c axis, ε_1 and ε_2 are the in-plane strains that are assumed to be isotropic. Hence P_{pz} can be written as:

$$P_{pz} = 2\,\frac{a - a_o}{a_o}\left(e_{31} - e_{33}\frac{C_{13}}{C_{33}}\right) \tag{1.20}$$

1.6. Bound charge

When two layers with different polarization fields are grown upon one another, a bound charge at their interface will be created. Depending on the divergence of the polarization field, this charge can be positive or negative. The bound charge can be calculated using the following equation:

$$\rho_f = -\nabla.\mathbf{P} \tag{1.21}$$

where ρ_f is the bound charge density and **P** is the polarization field.

Figure 1.10 shows the bound charge created at the interface of AlGaN/GaN in two different cases. The GaN layer is assumed to be relaxed and hence attains only spontaneous polarization. On the other hand, the AlGaN layer is strained and therefore attains both spontaneous and piezoelectric polarizations.

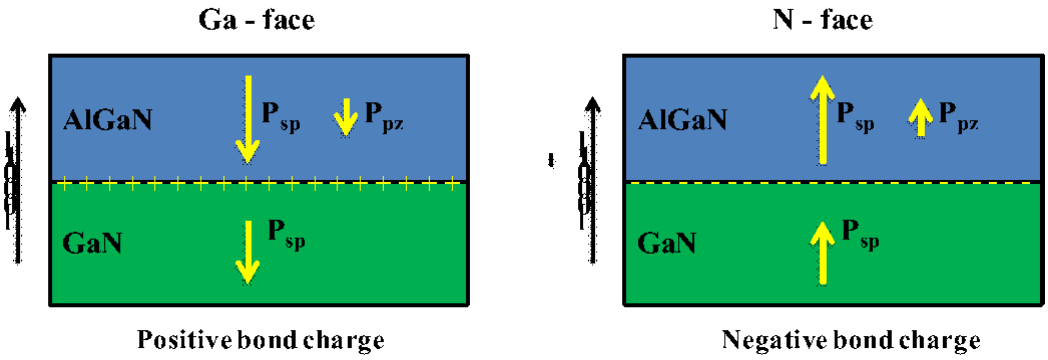

Figure 1.10 Bound charge at the AlGaN/GaN interface for (left) Ga-face and (right) N-Face

The sign of the bound charge is derived from equation 1.21. Figure 1.11 shows a detailed derivation of the bound charge.

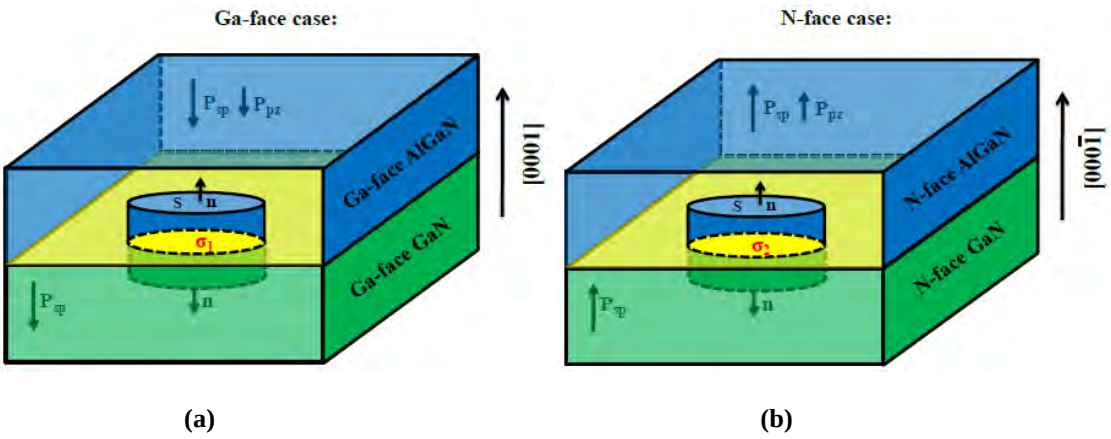

Figure 1.11 A cylindrical closed surface is used to solve equation 1.23 to calculate the bound charge the interface in (a) Ga-face AlGaN on top of Ga-face GaN and in (b) N-face AlGaN on top of N-face GaN

We have from equation 1.21:

$$\nabla . \boldsymbol{P} = -\rho_f$$

Integrating on both sides, we get:

$$\iiint \nabla . \boldsymbol{P}\, dv = -\iiint \rho_f\, dv \tag{1.22}$$

$$\iiint \rho_f\, dv = Q_b \tag{1.23}$$

where Q_b is the bound charge at the interface.

Using divergence theorem and equation 1.23 we get:

$$\oiint \boldsymbol{P} . d\boldsymbol{S} = \oiint (\boldsymbol{P} . \boldsymbol{n})\, dS = -Q_b \tag{1.24}$$

A cylindrical closed surface is chosen as shown in figure 1.11.

$\boldsymbol{n}$ is the vector perpendicular to the surface of the cylindrical closed surfaces.

In the case of growing in the [0001] direction figure 1.11 (a), the resulting bound charge is positive.

$$\oiint (\boldsymbol{P} . \boldsymbol{n})\, dS = -Q_b \implies -P_{AlGaN} S + P_{GaN} S = -Q_b \implies P_{AlGaN} - P_{GaN} = \frac{Q_b}{S} = \sigma_1$$

$$P_{AlGaN} > P_{GaN} \implies \sigma_1 > 0$$

In the case of growing in the [000$\bar{1}$] direction (figure 1.11 (b)), the resulting bound charge is negative.

$$\oiint (\boldsymbol{P}.\boldsymbol{n})dS = -Q_b \implies P_{AlGaN}S - P_{GaN}S = -Q_b$$

$$\implies P_{GaN} - P_{AlGaN} = \frac{Q_b}{S} = \sigma_2$$

$$P_{AlGaN} > P_{GaN} \implies \sigma_2 < 0$$

A third configuration can be used to increase the divergence in the polarization field and hence increase the density of bound charge at the interface. If a Ga-face AlGaN layer is grown on top an N-face GaN layer (figure 1.12) the resulting bound charge would be:

$$\oiint (\boldsymbol{P}.\boldsymbol{n})dS = -Q_b \implies -P_{AlGaN}S - P_{GaN}S = -Q_b$$

$$\implies P_{AlGaN} + P_{GaN} = \frac{Q_b}{S} = \sigma_3 > 0$$

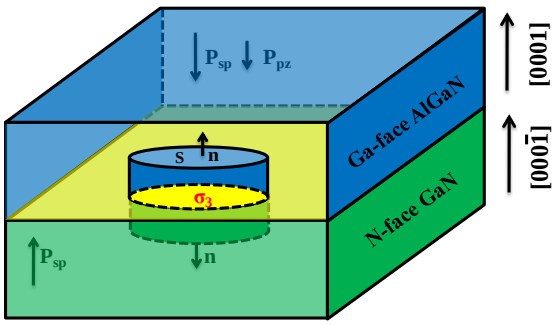

Figure 1.12 A cylindrical closed surface is used to solve equation 1.23 to calculate the bound charge at Ga-face AlGaN / N-face GaN interface

To numerically compare σ_3 to σ_1 , the x-mole fraction in the AlGaN is taken 0.25.

For the case of Ga-face AlGaN / Ga-Face GaN:

$$\sigma_1 = 5.1 \times 10^{-6} - 2.9 \times 10^{-6} = 2.2 \times 10^{-6} \frac{C}{cm^2}$$

For the case of Ga-face AlGaN / N-Face GaN:

$$\sigma_3 = 5.1 \times 10^{-6} + 2.9 \times 10^{-6} = 8 \times 10^{-6} \frac{C}{cm^2}$$

$$\frac{\sigma_3}{\sigma_1} = 3.63$$

Although this approach may theoretically results in a much higher bound charge, it will introduce a large number of defects at the AlGaN/GaN interface making it useless.

1.7. AlGaN/GaN High electron mobility transistor

1.7.1. Basic structure

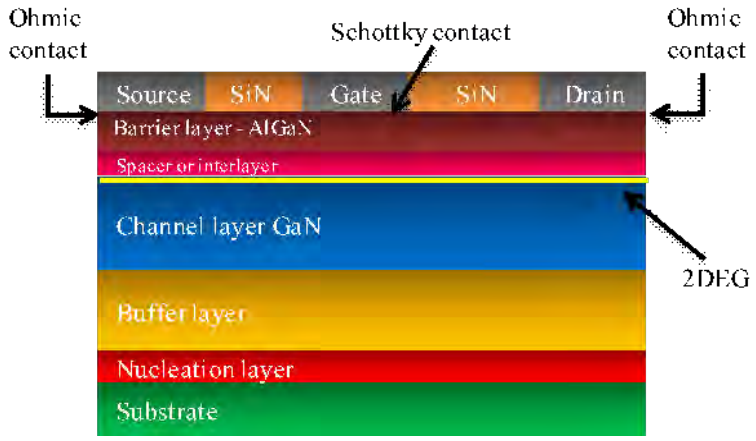

Figure 1.13 Schematic cross-section of the conventional high electron mobility transisitor (HEMT)

The high electron mobility transistor (HEMT) is a field effect transistor in which two layers of different bandgaps and polarization fields are grown upon one another. As a consequence of the discontinuity in the polarization field, surface charges at the heterointerface are created. If the induced charge is positive, electrons will tend to compensate the induced charge resulting in the formation of a two dimensional electron gas (2DEG). The 2DEG represents the channel of the HEMT and the current flow between the drain and the source is controlled by the gate of the device. The schematic cross-section of the conventional HEMT is shown in figure 1.13

The substrate is used as the base for the growing process. HEMTs are currently grown on Silicon [14][15][16][17], sapphire [18][19][20], Silicon Carbide [21][22][23] and GaN substrates [24]. Figure 1.14 [3] compares the four substrates according to the available size, cost, thermal conductivity, difference in heat expansion and lattice constant when compared to Gallium Nitride [3]. Silicon Carbide and sapphire substrates were the first to be studied, benefiting from the existing experience and tool sets in the LED industry. However, the successful growth of GaN on Silicon attracts the industry because of the availability of large silicon wafers at low cost. Currently the best results, which are obtained on SiC substrates, are likely reproduced by using Silicon substrates.

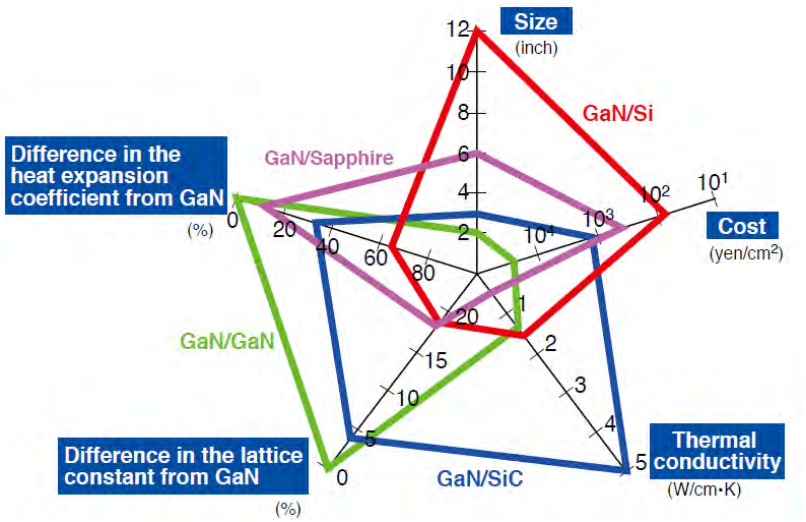

Figure 1.14 Comparison between different substrates on which GaN can be grown [3]

As for the GaN substrates, although there is no lattice mismatch problem, these substrates remain undesirable because of their small size and extreme high cost.

Nucleation buffer layers: When GaN is grown on foreign substrates (except for saphire), due to the lattice mismatch, a tensile strain arises favoring the creation of cracks. To prevent this cracking, intermediate layers are introduced between the substrate and the channel layer to compensate for the significant lattice mismatch between GaN and the substrate.

Channel layer: On the buffer layer a GaN layer is grown mostly along the [0001] direction to benefit from the spontaneous polarization of the c-plane within the GaN Wurtzite crystal. Within this layer the channel will be formed, hence, it is sometimes referred to as the channel layer.

Barrier layer: On top of the channel layer, a layer with higher bandgap and lesser electron affinity is grown. Due to the conduction band offset and the difference in the polarization between the barrier and the channel layer, a potential quantum well will be created underneath the hetero-interface, trapping the electrons inside, and consequently creating the channel. The depth of the well is associated with the difference of electron affinity. In GaN HEMTs, AlGaN is usually used as a barrier layer. The barrier layer can be either doped or intrinsic. In GaAs HEMTs, since the barrier layer is doped, a thin intrinsic layer known as spacer layer, with the same material as the barrier, is introduced between the channel and the barrier to prevent ionized impurity scattering between the electrons in the channel and the dopant atoms [25]. In GaN HEMTs, an interlayer of AlN [26] is sometimes used to enhance the confinement of the channel electrons and increase their density.

Passivation layer: it is usually SiN, which reduces the response of the surface traps which in return suppress the effect of current collapse [27].

Electrodes, named the source and the drain, are placed on highly doped semiconductor to achieve ohmic contacts. However, the third electrode, named the gate, is placed on non-heavily doped semiconductor to generate the Schottky barrier. The Schottky gate controls the carrier concentration in the channel layer below the interface. As the gate voltage decreases, the carrier concentration below the gate electrode decreases. The gate bias required to pinch-off the channel is called the threshold voltage (V_{th}). Below V_{th}, channel becomes depleted from carriers, and thus, no current can flow between the drain and source. When the threshold voltage is negative, the HEMT is called a depletion-mode (D-mode) HEMT or normally-on and, when it is positive the device is then called an enhancement-mode (E-mode) HEMT or normally-off. Conventional AlGaN/GaN HEMTs are D-mode transistors.

1.7.2. Band diagram of conventional HEMTs

To understand the behavior of the HEMT, one must understand the variation of the energy band diagram with the applied voltage. If an AlGaN layer is grown on a GaN layer, assuming no positive bound charge at their interface due to the discontinuity of the polarization field, the band diagram looks like the illustration in figure 1.15.

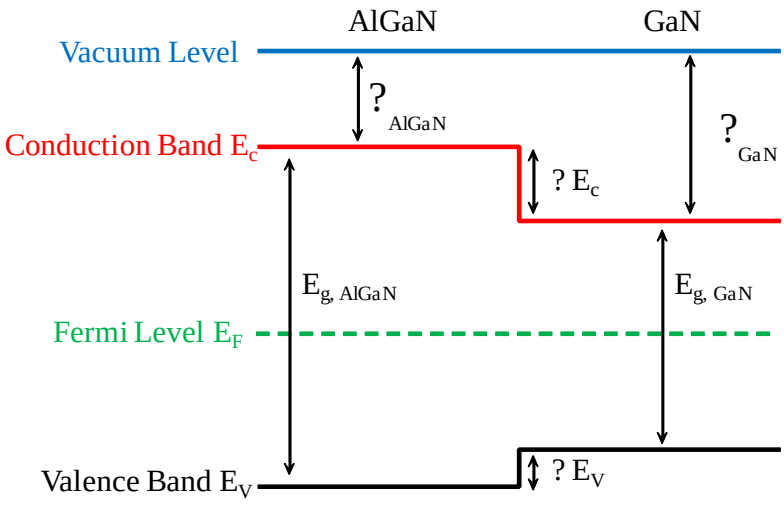

Figure 1.15 Band diagram of an AlGaN/GaN hetero-structure without the consideration of the positive bound charge at the AlGaN/GaN interface

To draw this figure no built-in potential is assumed and hence the Vacuum level is drawn first. Afterwards, knowing that the difference between the conduction band and the Fermi

level is equal to the electron affinity χ of the material, the conduction band is drawn. Then from the conduction band, by knowing the bandgap of the material, the valence band can be located. The Fermi level, at equilibrium, must be constant throughout the layers. In figure 1.15, we have assumed, to reduce complexity, that the Fermi level is pre-aligned before enforcing equilibrium conditions. However, in real cases, a constant Fermi level must be drawn first, then the conduction and valence bands, and finally the Vacuum level. The position of the conduction band with respect to the constant Fermi level is separately drawn in each region according to the doping concentration. In n-doped semiconductors, the Fermi level is higher than that of the intrinsic semiconductor and lies closer to the conduction band. On the other hand, in p-doped semiconductors, the Fermi level is lower than that of the intrinsic semiconductor and lies closer to the valence band. The severity of the shift of the Fermi level from the intrinsic level depends on the doping concentration. As the doping concentration increases, the shift from the intrinsic level increases.

The conduction band offset, known as ΔE_c, can be extracted from the difference of the electron affinity of the two layers.

$$\Delta E_c = \chi_{GaN} - \chi_{AlGaN} \tag{1.25}$$

The conduction band offsets changes from 74% to 72% of ΔE_g with increasing Al content in an AlGaN/GaN system [28].

In fact, conventional AlGaN/GaN HEMTs have a Schottky gate contact and a positive bound charge at the AlGaN/GaN interface. These two factors strongly affect the band diagram. The domain of interest in HEMT transistors is at the hetero-interface (AlGaN/GaN interface), Hence, the study will be focused on that region. The schematic cross-section of a normally-on HEMT and an illustration of its band diagram are shown in figure 1.16. The first important point is that the conduction band at the Gate/AlGaN interface is pinned to the Schottky barrier $\Phi_B$which can be calculated as:

$$\Phi_B = W_m - \chi_{AlGaN} \tag{1.26}$$

where W_m is the workfunction of the metal and χ_{AlGaN} is the electron affinity of AlGaN.

The second important point is the impact of the bound charge on the band diagram. In figure 1.15, the conduction band is above the Fermi level throughout the two layers. However, when positive bound charge is added at the AlGaN/GaN interface, the conduction band at the interface bends. As the charge concentration increases, the bending increases. This bending,

if high enough, will cause part of the conduction band in the vicinity of the interface to go below the Fermi level.

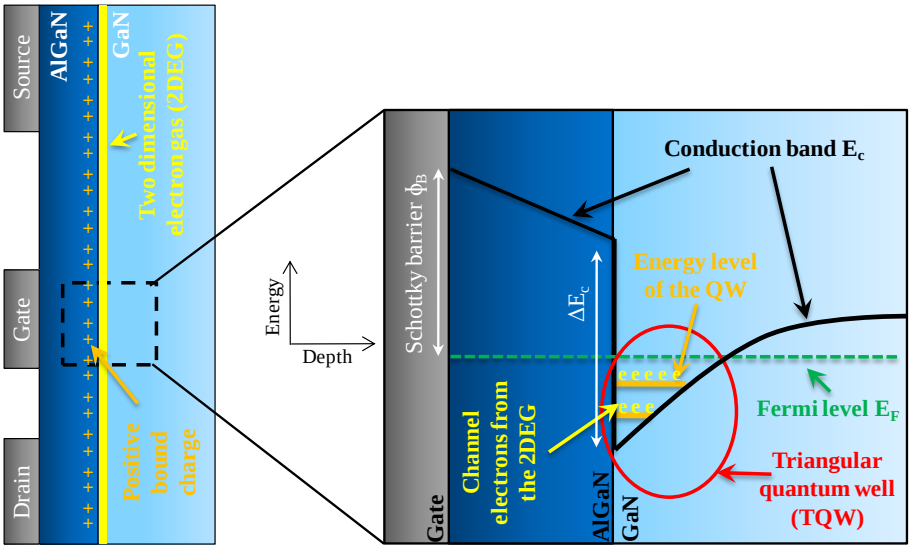

Figure 1.16 Schematic band diagram of a conventional normally-on HEMT. At the gate/AlGaN interface, the conduction band energy is equal to the Schottky barrier. The positive bound charge at the AlGaN/GaN interface bends the conduction band causing the creation of the triangular well. Electrons occupying the energy levels of the triangular well form the HEMT's channel

In that region (Fermi level above the conduction band) electrons will populate on the energy levels of the triangular quantum well formed at the AlGaN/GaN interface. These electrons form the HEMT's channel and are known as the Two Dimensional Electron Gas (2DEG).

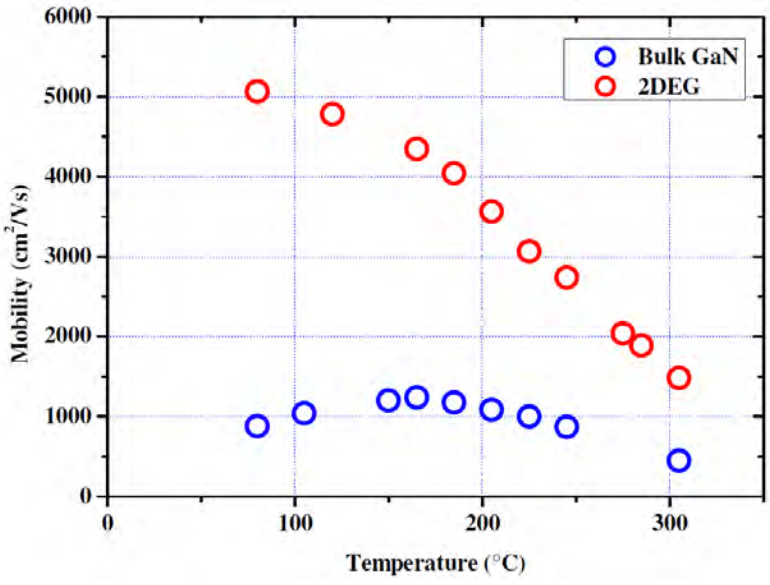

Figure 1.17 Variations of the electron mobility versus temperature for 2DEG in $Al_{0.1}GaN/GaN$ and for bulk n-GaN with $N_D = 10^{17}$ cm^{-3} [30]

The confinement of the channel electrons in the quantum well grants them two-dimensional features, which strongly enhance their mobility. Figure 1.17 [29] shows the variation of the electron mobility versus temperature for 2DEG in $Al_{0.1}GaN/GaN$ and for bulk *n*-GaN with an n-doping concentration 10^{17} cm^{-3}. It is clear that the mobility of the 2DEG is higher at all temperatures.

To manipulate the density of electrons in the channel, and hence switch the HEMT ON and OFF, the voltage at the gate is varied. Here, it is worth defining the threshold voltage V_{th} as the voltage required to populate electrons at the interface and hence giving the channel conduction privilege. Figure 1.18 shows the triangular quantum well at three different biasing conditions.

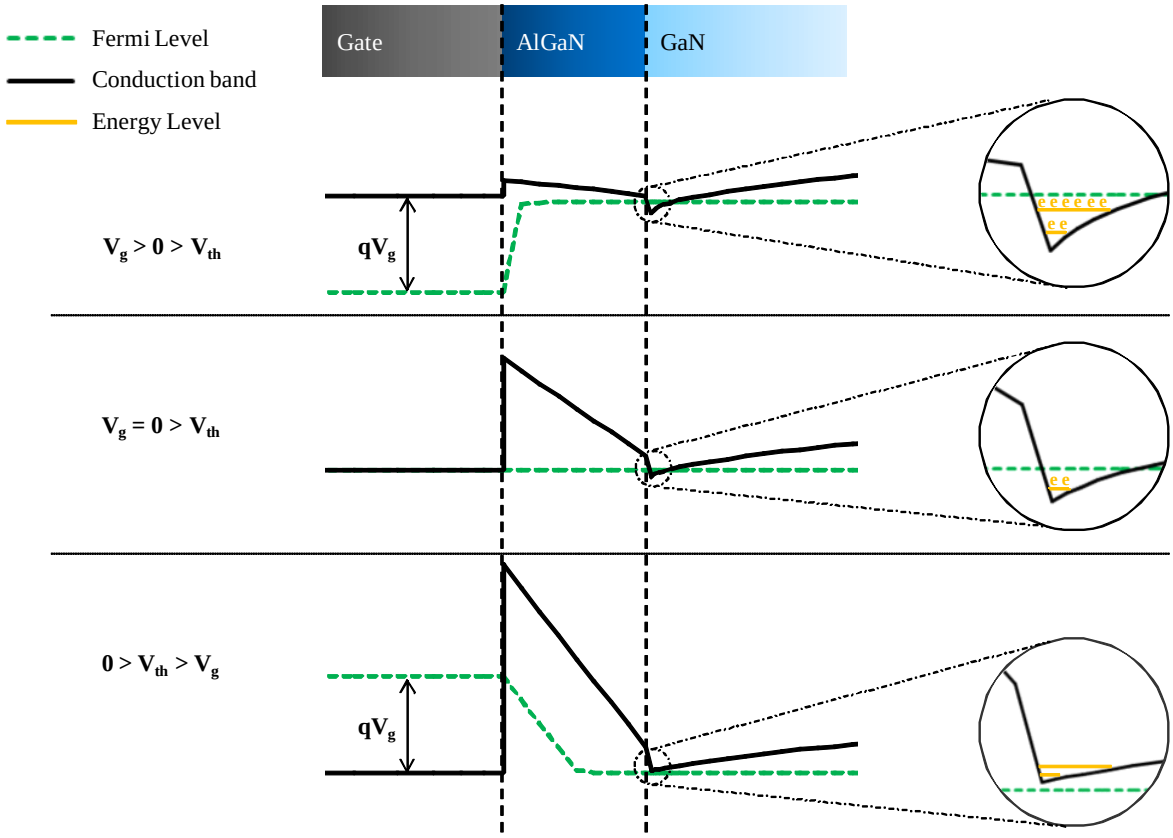

Figure 1.18 Position of the Fermi level with respect to the conduction band at various biasing conditions. The zoomed parts illustrate the status of the triangular well at the AlGaN/GaN interface to show the depletion of channel electrons (2DEG) as the gate voltage goes below the threshold voltage

Channel electrons occupy energy levels that are positioned below the Fermi level. When the gate voltage is much higher than the threshold voltage ($V_{gs} >> V_{th}$), the Fermi level in the triangular well is above several energy levels. This enables high population of channel

electrons and hence high current density. When the gate voltage decreases, the Fermi level goes downwards with respect to the triangular well. Therefore fewer energy levels are populated and hence the concentration of channel electrons, below the gate, decreases. Once the gate voltage goes below the threshold voltage, all energy levels are above the Fermi level. This causes channel depletion and the HEMT turns OFF.

1.7.3. Source of the 2DEG

Surface traps are energy states in the band-gap of a semiconductor. They originate from factors such as crystal defects, dislocations, or the presence of impurities. Classification of these traps depends on the relative position of their energy level inside the band gap. Traps with energy above the Fermi level are acceptor-like, attaining negative charge when occupied. However, traps with energy below the Fermi level are donor-like, positively charged when empty and neutral when occupied.

Donor-like surface traps at the upper surface of the AlGaN barrier layer are one of the most important sources of the 2DEG in the channel. However, this only applies for specific barrier thickness. Consider a thin barrier layer with relatively small thickness; the surface trap is below the Fermi energy. Nonetheless, as the barrier thickness increases, the energy of the surface trap approaches the Fermi energy until, at a critical thickness, it coincides with it as shown in figure 1.19. At this point, electrons filling this state are pulled to the channel by the strong polarization-induced electric field found in the barrier to form the 2DEG.

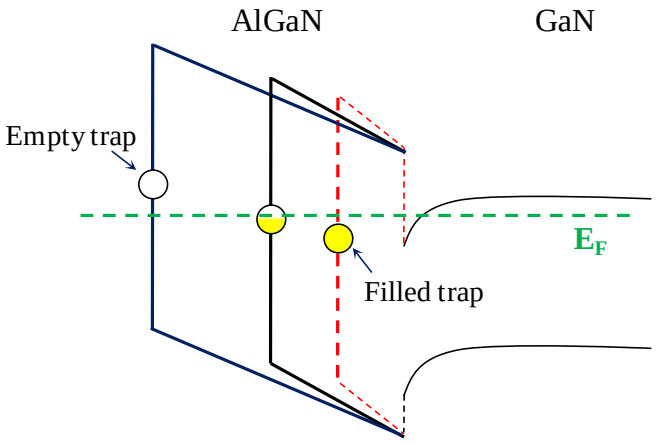

Figure 1.19 Schematic band diagram of an AlGaN/GaN hetero-structure showing the distance at which electrons in the donor interface traps are pulled to the HEMT's channel

If the surface traps are completely depleted, further increase in the barrier thickness will not increase the 2DEG density (figure 1.20). Actually, if the channel layer fails to stretch the

barrier layer, the later will relax. Upon relaxation, defects are created at the AlGaN/GaN interface and the piezoelectric polarization will vanish causing deterioration in the density of the 2DEG.

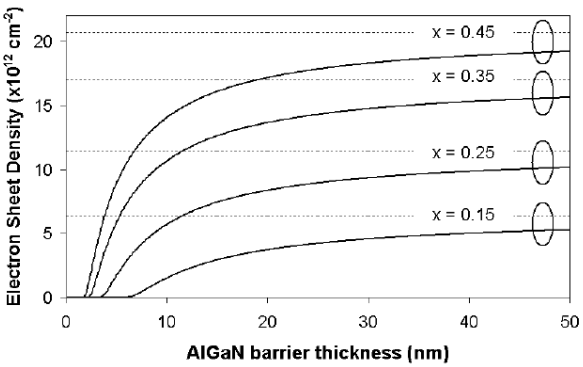

Figure 1.20 Variations of the two dimensional electron gas density with the thickness of the barrier layer at various x-mole fractions

The thickness of the barrier is not the only factor that affects the 2DEG density. The x-mole fraction also plays a crucial role. The piezoelectric polarization in the stretched barrier layer (case of AlGaN) strongly depends on the x-mole fraction. With increasing the x-mole fraction, the lattice contact shrinks (see figure 1.7). This leads to a higher stretch in the AlGaN layer, which increases the piezoelectric polarization. The increase in the divergence of the polarization field between the barrier and the channel layer causes higher bound charge density. This is shown in figure 1.21 where the bound charge density increases with increasing the x-mole fraction.

However, like the thickness of AlGaN, further increase in the x-mole fraction causes a relaxation in the AlGaN layer and hence a deterioration in the density of 2DEG. This is shown in figure 1.21 [11]. As the x-mole fraction increases, the total polarization (P^{total}), which is the sum of the spontaneous (P^{sp}) and piezoelectric polarizations (P^{pz}), increases. However, while the spontaneous polarization continues to increase for x-mole fractions above 0.4, the piezoelectric polarization undergoes a sudden decrease signaling the relaxation of the AlGaN layer [30]. It is worth noting that, when smaller x-mole fractions are used, higher strained AlGaN thicknesses can be grown.

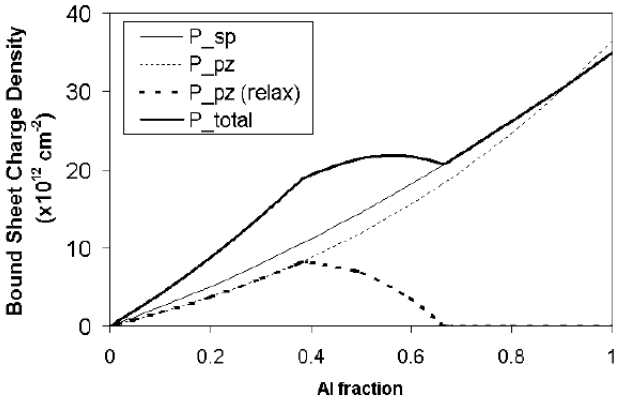

Figure 1.21 Variations of the bound charge density with the x-mole fraction in the barrier layer. A sudden drop in the piezoelectric polarization signals the relaxation of the barrier layer [11]

1.7.4. Normally-off HEMT

Although conventional HEMTs seem to be very promising candidates for power switching applications, they are depletion mode transistors (normally-on; $V_{th} < 0$). It means that a negative voltage must be applied on the gate in order to block the current. But in order to reduce the circuit complexity and eliminate standby power consumption, normally-off HEMTs ($V_{th} > 0$) are strongly required. Several normally-off structures have been proposed. The main structures are:

1.7.4.1. Gate recess structure

In this structure, the barrier structure is etched and the gate is brought closer to the AlGaN/GaN interface. As the gate electrode approaches the AlGaN/GaN interface, the threshold voltage increases. Once the depletion region created by the Schottky contact reaches the AlGaN/GaN interface and depletes the channel at zero gate voltage, normally-off operation is achieved. Figure 1.22 shows a schematic cross-section of the gate recess structure [31]–[33].

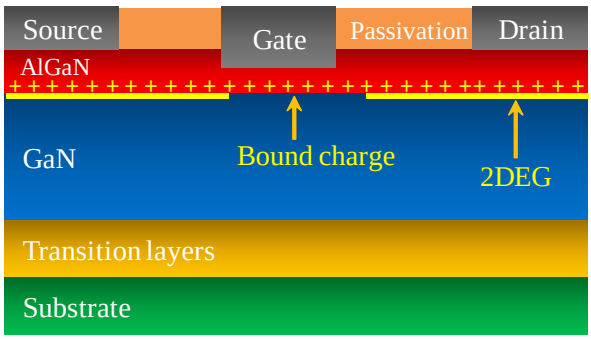

Figure 1.22 Schematic cross-section of the normally-off HEMT using the gate recess technique

1.7.4.2. Thin barrier layer

This structure also achieves normally-off operation by approaching the gate electrode towards the AlGaN/GaN interface. But this time, instead of etching the relatively thick barrier layer to approach the AlGaN/GaN interface, a very thin AlGaN barrier is used. The x-mole fraction in this thin barrier is sometimes increased to unity to compensate the low 2DEG density resulting from a thin barrier (figure 1.23) [34]–[36].

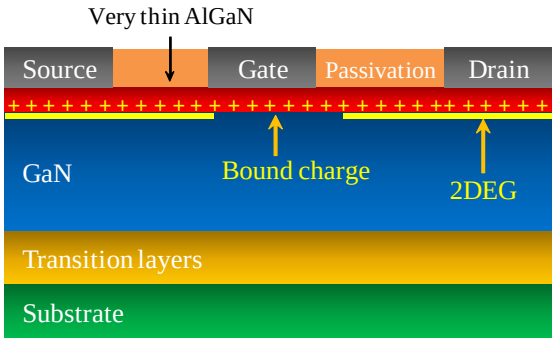

Figure 1.23 Schematic cross-section of the normally-off HEMT using a thin AlGaN barrier layer

1.7.4.3. Gate Injection Transistor

In this structure, a p-AlGaN region is introduced below the gate as shown in figure 1.24. It is well known that, in p-type semiconductors, the Fermi level shifts towards the valence band. However, since at equilibrium the Fermi level is constant, this shift will manifest itself through uplifting the conduction band. The uplift of the conduction band in the p-doped region will elevate the triangular well at the AlGaN/GaN interface.

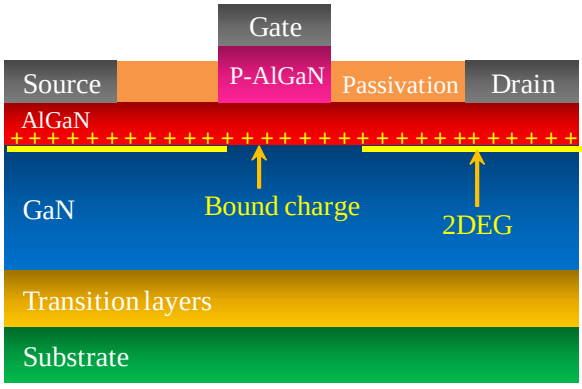

Figure 1.24 Schematic cross-section of the normally-off Gate Injection Transistor using a p-AlGaN cap layer

If the doping concentration is strong enough to raise the triangular well above the Fermi level, normally-off operation will be achieved. It is worth noting that the p-AlGaN cap layer

not only shifts the threshold voltage to positive values but also increases the forward gate voltage of the HEMT [37], [38].

1.7.4.4. P-GaN Gate HEMT

The schematic cross-section of the normally-off p-GaN gate HEMT is shown in figure 1.25. In this structure, the lift in the conduction band is not due to p-doping of the cap layer (which is the case in the p-AlGaN cap) but rather to the discontinuity in the polarization between the barrier and the cap layers. This discontinuity creates a negative bound charge at the p-GaN/AlGaN interface, which lifts up the triangular well at the AlGaN/GaN interface and causes normally-off operation. The p-doping though still helps in increasing the forward gate voltage [39]–[44].

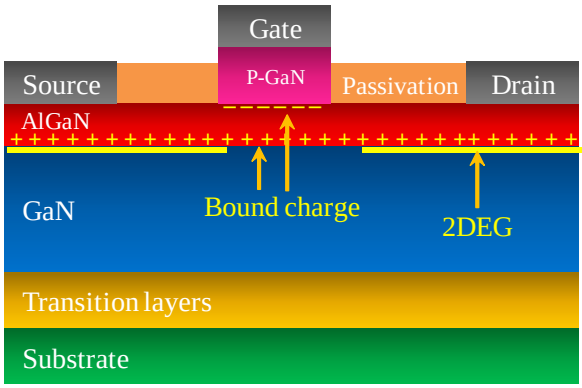

Figure 1.25 Schematic cross-section of the normally-off p-GaN gate HEMT using a p-GaN cap layer

1.7.4.5. Fluorine implantation

This approach relies on implanting negative Fluorine ions $^{19}F^{+}$ in the barrier layer as shown in figure 1.26. The conduction band is uplifted in the region where Fluorine is implanted, causing an elevation in the triangular well at the AlGaN/GaN interface band above the Fermi level. Unfortunately, during implantation, a small amount of Fluorine ions penetrates into the channel and present themselves as impurities that could lead to mobility degradation [45]–[49].

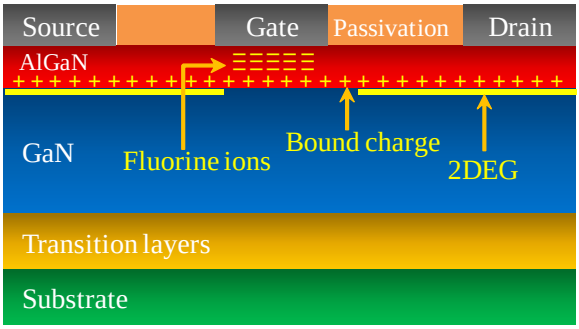

Figure 1.26 Schematic cross-section of the normally-off HEMT using Fluorine implantation in the barrier layer

1.8. MIS-HEMTs

The problem with the previously mentioned normally-off HEMTs is that their threshold is around 1 V. A threshold voltage above 3 V is required in order to prevent the misoperation caused by noise [50]. Moreover, since most of these structures use a Schottky gate, the gate leakage limits the increase in the threshold voltage and in the current density of the device. Therefore, to achieve higher threshold voltages and to eliminate gate leakage, an insulating layer below the gate has to be introduced. This will give rise to the so called MIS-HEMT, Metal Insulator Semiconductor High Electron Mobility Transistor. The insulating material, also known as the gate dielectric, varies from SiO_2 [51], SiN_x [52], [53], HfO_2 [54] to Al_2O_3 [55], [56]. Most of the normally-off MIS-HEMTs use one [57]–[59], or a combination [60] of the above mentioned techniques. Figure 1.27 shows a schematic cross-section of a conventional normally-on MIS-HEMT.

Although a high threshold voltage (greater than 3 V) is obtained in the case of MIS-HEMT with recessed gate or with Fluorine implantation, several drawbacks exist in these structures. In the MIS-HEMT with a recessed gate, the barrier layer is etched. This introduces many defects in the barrier layer and damage the density and mobility of the 2DEG resulting in a very poor current density. In the case of Fluorine implantation, as mentioned in section 1.7.4.5, small amount of negative Fluorine ions penetrate into the channel during implantation and cause mobility degradation.

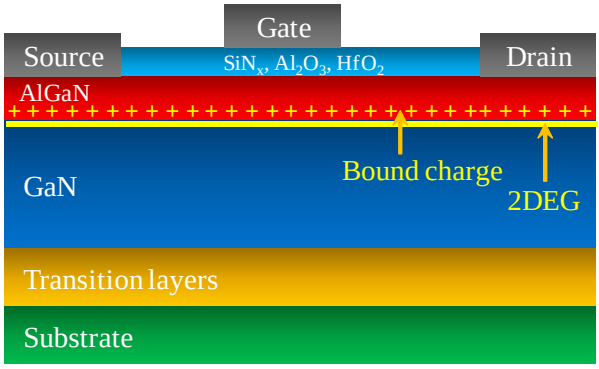

Figure 1.27 Schematic cross-section of a conventional Metal Insulator Semiconductor High electron mobility transistor (MIS-HEMT)

In MIS-HEMTs, the insulating layer results in the creation of an additional charge at the insulator/barrier interface. This charge can be positive or negative. For instance, a recent study reported negative charge when using Al_2O_3 and positive charge in the case of HfO_2 [61]. Moreover, the charge can be distributed inside the insulating layer. The location of charge created can be concluded from the variation of the threshold voltage with the thickness of the insulator. For instance, in Al_2O_3, a quadratic dependence of V_{th} of the thickness of the insulator signals the distribution of charge inside the insulator, while a linear dependence indicates that the charge is located at the insulator/AlGaN interface [62].

1.9. Conclusion

Today, the vast majority of power devices are made from silicon. Improving their efficiency is crucial to reduce switching losses and hence lower the CO_2 emission. Unfortunately, power devices based on silicon, are reaching their theoretical limits. Design engineers are now facing the challenge of increasing the ratings of converters in terms of operating voltage, operating temperature and efficiency. The quest for a solution to silicon limitations leads researchers to the doorstep of wide bandgap materials such as Silicon Carbide (SiC) and Gallium nitride (GaN). Compared to silicon, the main benefits of these materials are a good operation over a wide temperature range, high critical electric field and high saturation velocity.

Despite the remarkable results obtained by several teams working on Silicon Carbide, SiC must be grown on native substrates which are expensive and relatively small in size. On the other hand, GaN can be grown on silicon substrates which are large and of low cost. Moreover, GaN is better than SiC for creating heterostructures due to their built-in polarization field. Therefore, for devices such as HEMT, GaN is the material of choice.

The High Electron Mobility Transistor (HEMT) is a field effect transistor in which two layers of different bandgap and polarization field are grown upon each other. As a consequence of the discontinuity in the polarization field, surface charges at the heterointerface are created. If the induced charge is positive, electrons will tend to compensate the induced charge resulting in the formation of the channel. Since in the HEMT the channel electrons are confined in a quantum well in a very narrow spatial region at the heterointerface, the channel electrons are referred to as a Two Dimensional Electron Gas (2DEG). This confinement grants the electrons high mobilities surpassing the bulk mobility of the material in which the electrons are flowing.

Conventional HEMTs attain a channel populated with electrons at zero gate voltage making them normally-on. For power switching applications normally-off operation is required. Several normally-off structures have been proposed such as recessed gate structures, fluorine ion treatment, P-GaN Gate, thin AlGaN barrier, and the Gate Injection Transistor. The problem with the previously mentioned normally-off HEMTs is that their threshold is around 1 V. A threshold voltage above 3 V is required in order to prevent the misoperation caused by noise. Moreover, since most of these structures use a Schottky gate, the gate leakage limits the increase in the threshold voltage and in the current density of the device. Therefore, to achieve higher threshold voltages and to eliminate gate leakage, an insulating layer below the gate has to be introduced. This will give rise to the so called MIS-HEMT, Metal Insulator Semiconductor HEMT. Although, the threshold voltage of the normally-off MIS-HEMT can be reach values above 3 V, the techniques used degrades the channel mobility resulting in low current densities.

Chapter 2
TCAD Simulation

2.1. Introduction

Technology Computer Aided Design (TCAD) tools are simulation tools used to model the processing and behavior of electronic devices. The simulator can predict the structure resulting from several processing steps (process simulation) or foretell the electrical behavior of semiconductor devices at specified bias conditions (device simulation). The inputs of the device simulator are the material properties from which the device is made along with the dimensions and doping profiles of all the regions in the device. Moreover, physical models, describing the behavior of carrier are added. Afterwards a structure is discretized by creating a mesh and associating all the physical properties of the regions with nodes (mesh points). The simulator will then solve a set of physical equations along with the defined models to predict the electric behavior of the device. In this work, the electric characteristics of the new normally-off structures were examined using a commercial TCAD simulation tool from Silvaco, Inc [63]. In this chapter the simulator is explained along with the calibration strategy.

2.2. Silvaco framework overview

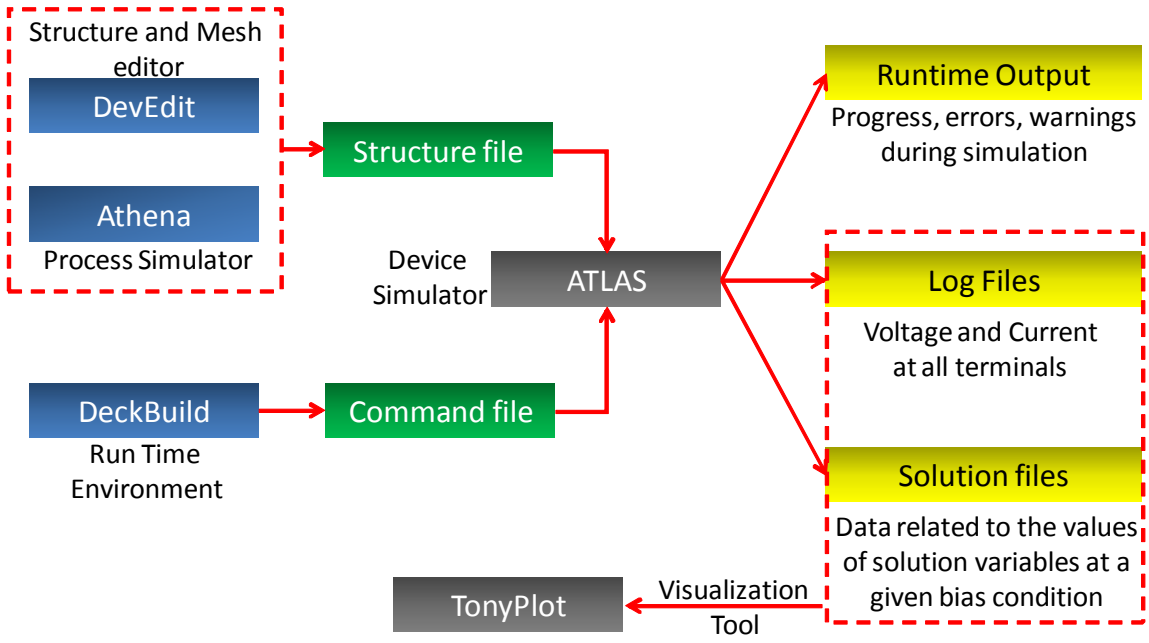

Figure 2.1 Simulation flow in Silvaco showing the inputs and outputs of ATLAS

To simulate a structure via Silvaco, different tools are employed. In this work, we will focus on ATLAS that is a physically-based two and three dimensional device simulator that predicts the electrical behavior of semiconductor devices at specified bias conditions. The

device structure containing the doping profiles and the mesh are inputted to ATLAS. One way to create the file is to start by the tool ATHENA to simulate the processing steps required to obtain the desired structure and then mesh it with a tool called DEVEDIT. Another way to create the structure file is by writing a script a DECKBUILD defining the mesh and the physical composition of the structure along with the doping profile.

The models, biasing conditions and numerical methods used to attain the electric characteristics are defined in ATLAS.

ATLAS will then generate three types of files: the runtime output which shows the progress of the simulation, the log files storing the current and voltage values at each electrode and finally the structure files containing information about various physical quantities inside the structure at certain biasing conditions. To visualize the output results, a tool called TONYPLOT is used to display the log and structures files. In this work, for better visualization, the results were extracted from TONYPLOT and plotted in Microsoft Excel.

2.3. Simulation of AlGaN/GaN HEMT

2.3.1. Meshing

In every conventional device simulator, to solve the physical equations governing the behavior of carrier transport, the device that is to be simulated is discretized into a grid and the equations are solved at each grip point. The grid and grip points are sometimes referred to as the mesh and nodes respectively. In our simulated structures, the mesh was generated in DECKBUILD. The most sensitive region in the HEMT transistor is the AlGaN/GaN interface. Therefore, as shown in figure 2.2, a very fine mesh was created in that region where the node-to-node distance in the y-direction was reduced down to 0.5 nanometers.

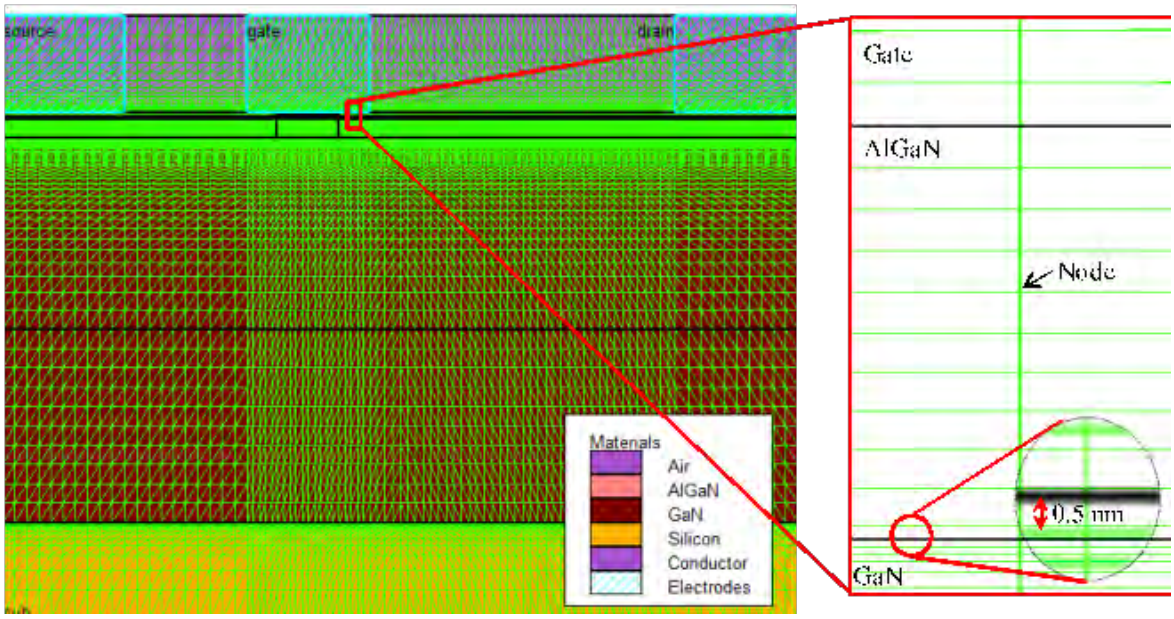

Figure 2.2 The mesh with the cross-section of the HEMT viewed from the visualization tool Tonyplot showing a refined mesh at the AlGaN/GaN interface

Moreover, it is crucial to refine the mesh at hetero-interfaces where an abrupt change in the physical properties occurs. Furthermore, during breakdown simulation, high electric field intensities are obtained at the electrode edges. Therefore, it is recommended to further refine the mesh in these regions. Although finer meshes may yield more accurate solutions, the numerical efficiency is greater when fewer grid points are used. Indeed, the simulation time increases with increasing the number of grid points in the simulated structure. In ATLAS, for two-dimensional simulations, the maximum number of nodes is limited to 20,000. In this work, during the parametrical study, a dynamic mesh was carefully created to always ensure a number of grid points lower than 20,000 nodes throughout the simulated physical dimensions, while enough refinement in the sensitive areas. The mesh used to simulate the HEMT devices is shown in figure 2.2.

2.3.2. Physical Models

After defining the mesh, a set of fundamental semiconductor equations is solved at each node. These equations include, but not limited to, Poisson’s equation, continuity equations and transport equations. The above mentioned equations are all derived from the Maxwell's laws [63].

Poisson's Equation

The Poisson's Equation relates the electrostatic potential and the electric field to the space charge density. It can be expressed as:

$$\nabla^2\varphi = -\boldsymbol{\nabla}.\boldsymbol{E} = {}^{\rho}/_{\varepsilon} \tag{2.1}$$

where φ is the electrostatic potential, ε is the local permittivity, and ρ is the local space charge density.

ρ can be expressed as the sum of all mobile and fixed charges, including free electrons (n) and holes (h) concentrations, ionized donor (N_D^+) and acceptor (N_A^-) impurity concentrations, and charge due to the presence of traps and defects (Q_T). Therefore, equation 2.1 can be written as:

$$\rho = q\,(\,n - p + N_D^+ - N_A^-) + Q_T \tag{2.2}$$

where q is the proton charge.

Continuity equation

The continuity equations for electrons and holes are defined by equations 2.3 and 2.4:

$$\frac{\partial n}{\partial t} = \frac{1}{q}\nabla.J_N - r_n + g_n \tag{2.3}$$

$$\frac{\partial p}{\partial t} = \frac{-1}{q}\nabla.J_p - r_p + g_p \tag{2.4}$$

where n and p are the electron and hole concentrations, J_N and J_p are the electron and hole current densities, r_n and r_p are the recombination rates for electrons and holes, g_n and g_p are the generation rates for electrons and holes.

The Poisson's and continuity equations provides the general framework. However, further models are required for the current densities, generation and recombination rates of electrons and holes.

Transport equations

Charge transport models are usually obtained by applying approximations and simplifications to the Boltzmann Transport Equation. The simplest model of charge transport that was recently adequate for nearly all devices that were technologically feasible is the Drift-Diffusion Model.

In this model, the current densities of electrons and holes can be expressed as:

$$J_N = qn\mu_n E + qD_n \nabla n \tag{2.5}$$

$$J_p = qn\mu_p E - qD_P \nabla p \tag{2.6}$$

where μ_N and μ_p are the electron and hole mobilities, D_n and D_p are electron and hole diffusivities. The first term in the equation ($qn\mu E$) represents the drift current, while the second term ($qD\nabla n$) represents the diffusion current.

Carrier Mobility

The carrier mobility describes the speed of the carriers in response to an external electric field. In this work two different low field mobility models where used. The first is the constant low field mobility, which is the default mobility model. It uses constant low-field mobilities within each region of a device. This default model is independent of doping concentration, carrier densities and electric field. It does account for lattice scattering due to temperature according to:

$$\mu_{n0} = MUN \left(\frac{T_L}{300}\right)^{-TMUN} \tag{2.7}$$

$$\mu_{p0} = MUP \left(\frac{T_L}{300}\right)^{-TMUP} \tag{2.8}$$

where T is the lattice temperature. The low-field mobility parameters: MUN, MUP, TMUN and TMUP can be specified in the MOBILITY statement.

The other low field mobility used is the Albrecht Model which was developed by Albrecht et al [64]. This model is dependent on the doping concentration and the lattice temperature.

$$\frac{1}{\mu(N,T_L)} = \frac{AN.ALBRCT}{N0N.ALBRCT}\left(\frac{T_L}{T0N.ALBRCT}\right)^{-3/2} ln\left[1 + 3\left(\frac{T_L}{T0N.ALBRCT}\right)^{2}\left(\frac{N}{N0N.ALBRCT}\right)^{-2/3}\right] + BN.ALBRCT \times \left(\frac{T_L}{T0N.ALBRCT}\right)^{3/2} + \frac{CN.ALBRCT}{\exp(T1N.ALBRCT/T_L) - 1} \tag{2.9}$$

where μ(N,T) is the mobility as a function of doping and lattice temperature, N is the total doping concentration, and T_L is the lattice temperature. AN.ALBRCT, BN.ALBRCT, CN.ALBRCT, N0N.ALBRCT, T0N.ALBRCT and T1N.ALBRCT are user-specifiable parameters on the MOBILITY statement. Similar expression is used for holes with the user-defined parameters AP.ALBRCT, BP.ALBRCT, CP.ALBRCT, N0P.ALBRCT, T0P.ALBRCT and T1P.ALBRCT.

To take the saturation effect into account, the Parallel Electric Field-Dependent Mobility is used which models the saturation velocity [65].

$$\mu_n(E) = \mu_{n0}\left[\frac{1}{1+\left(\frac{\mu_{n0}\,E}{VSATN}\right)^{BETAN}}\right]^{\frac{1}{BETAN}} \tag{2.10}$$

$$\mu_p(E) = \mu_{p0}\left[\frac{1}{1+\left(\frac{\mu_{p0}\,E}{VSATP}\right)^{BETAP}}\right]^{\frac{1}{BETAP}} \tag{2.11}$$

Here, E is the parallel electric field and μ_{n0} and μ_{p0} are the low-field electron and hole mobilities respectively.

Impact ionization model

In high electric field regions, free carriers accelerate and collide with the crystal atoms. If the energy acquired by the electrons reaches the ionization energy, more free carriers will be generated. If the generation rate of these free carriers is sufficiently high, this process will eventually lead to avalanche breakdown. Equation 2.12 describes the general impact ionization process.

$$\boldsymbol{G = \alpha_n\left|\vec{J}\right|_n + \alpha_p\left|\vec{J}\right|_p} \tag{2.12}$$

Here, G is the local generation rate of electron-hole pairs, $\boldsymbol{\alpha_n}$ and $\boldsymbol{\alpha_p}$ are the ionization coefficients for electrons and holes and $\boldsymbol{J_n}$ and $\boldsymbol{J_p}$ are their current densities. The ionization coefficient represents the number of electron-hole pairs generated by a carrier per unit distance travelled. In this work, the model relating the impact ionization coefficients to the electric field in the direction of the current is used. This is the most physically sound and is

the default model for the field dependence of the impact ionization coefficients. Equation 2.12 can be written as:

$$\boldsymbol{G = \alpha_N \left(\left| \frac{E.J_n}{J_n} \right| \right) J_n + \alpha_p \left(\left| \frac{E.J_p}{J_p} \right| \right) J_p} \tag{2.13}$$

If the dot product of *E* and *J* is negative, then the field component is taken as 0. Consequently, impact ionization may only occur when a current is dominated by the drift term.

Selberherr's Impact Ionization Model

The ionization rate model proposed by Selberherr [66] is a variation of the classical Chynoweth model [67]. The Selberherr model is based upon the following expressions [68]:

$$\boldsymbol{\alpha_n} = \text{AN}\, e^{\left(\frac{-BN}{E}\right)^{BETAN}} \tag{2.14}$$

$$\boldsymbol{\alpha_p} = \text{AP}\, e^{\left(\frac{-BP}{E}\right)^{BETAP}} \tag{2.15}$$

where *E* is the electric field in the direction of current flow at a particular position in the structure and the parameters AN, AP, BN, BP, BETAN, and BETAP are specified by the user.

The bound charge at the AlGaN/GaN interface:

The introduction of the positive bound charge at the AlGaN/GaN interface is one of the most important steps for the simulation of the HEMT. In all the simulated HEMTs, the GaN and AlGaN layers are grown in the [0001] direction i.e. Ga-face. Moreover, the GaN layer is assumed to be relaxed while the AlGaN layer is stretched so that its lattice constant matches that of GaN. This will result in the formation of a positive bound charge as explained in section 1.6.

$$\sigma = P_{AlGaN} - P_{GaN} \tag{2.16}$$

where P_{AlGaN} and P_{GaN} are the magnitudes of the polarization fields in the AlGaN and GaN layers respectively. Since the GaN layer is assumed to be relaxed and the AlGaN layer stretched, we get:

$$P_{GaN} = P_{GaN}^{sp} \tag{2.17}$$

$$P_{AlGaN} = P_{AlGaN}^{sp} + P_{AlGaN}^{pz} \tag{2.18}$$

where P^{sp} and P^{pz} are the spontaneous and piezoelectric polarization fields.

The spontaneous polarization of the AlGaN layer is calculated as:

$$P_{Al_xGaN}^{sp} = x.P_{AlN}^{sp} + (1-x)P_{GaN}^{sp} \tag{2.19}$$

The piezoelectric polarization in the AlGaN layer is expressed in equation 1.20 as:

$$P^{pz} = 2\,\frac{a-a_o}{a_o}\left(e_{31} - e_{33}\frac{C_{13}}{C_{33}}\right)$$

Figure 2.3 shows the band diagram of the HEMT before and after introducing the positive bound charge.

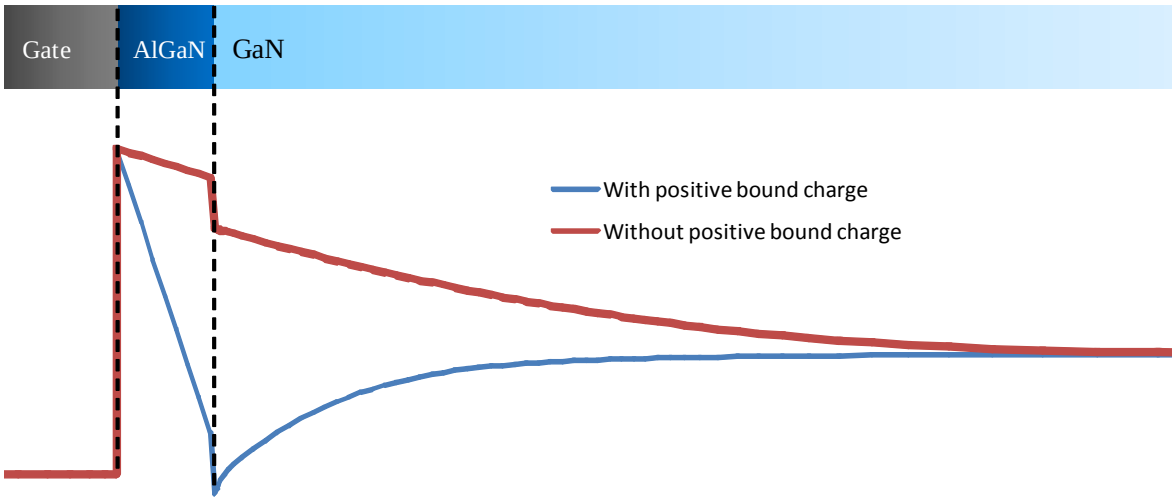

Figure 2.3 Band diagram with and without the positive bound charge at the AlGaN/GaN interface showing the creation of the triangular well after the bending of the conduction band due to the introduced positive charge

The addition of the positive polarization charge bends the conduction band at the AlGaN/GaN interface. This will result in the formation of a triangular well. At equilibrium, the electrons populating in the region where the Fermi level is above the triangular well, have an enhanced mobility that was manually introduced to the simulator (2DEG mobility).

The values of the spontaneous polarization (P^{sp}), lattice (a_0), elastic and strain constants (e_{31}, e_{33}, C_{13}, C_{33}) are shown in table 2.1 [69][70][71].

	Unit	GaN	AlN	$Al_{0.25}GaN$
P^{sp}	C/m^2	-0.081	-0.029	-0.068
e_{31}	C/m^2	-0.49	-0.60	-0.5175
e_{33}	C/m^2	0.73	1.46	0.9125
C_{13}	GPa	103	108	104.25
C_{33}	GPa	405	373	397
a_o	nm	0.3189	0.3112	0.316975
ε_r	/	9.5	9	9.375

Table 2.1 The values of the spontaneous polarization, lattice, elastic and strain constants for GaN and AlN [69][70][71]

To calculate the above mentioned parameters for AlGaN a linear interpolation was used as shown in equation 2.20

$$Z_{Al_xGaN} = x.Z_{AlN} + (1-x)Z_{GaN} \tag{2.20}$$

2.3.3. Simulator calibration

To calibrate the simulation, experimental results from a normally-on HEMT device were used. The schematic cross-section of the normally-on HEMT used for calibration is shown in figure 2.4. The thicknesses of the AlGaN and GaN layers are 30 nm and 1.1 µm respectively.

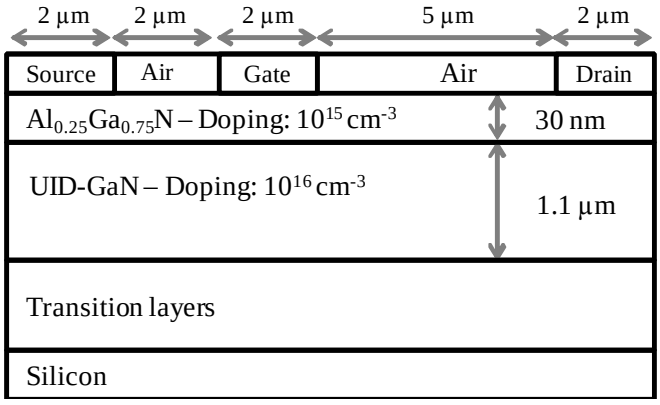

Figure 2.4 Geometrical and technological parameters used for the normally-on HEMT structure and the calibration of the TCAD simulations

In ATLAS, the transition layers were substituted by a GaN layer with a doping concentration of 10^{12} cm^{-3} as shown in figure 2.5. Electrically, this layer has the same effect as the transition layers. They are both semi-insulating.

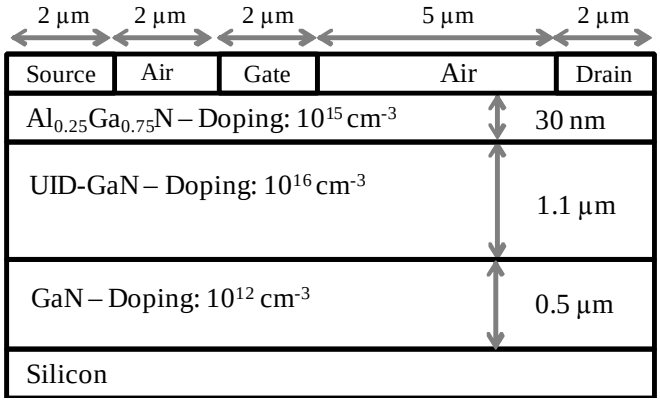

Figure 2.5 Schematic cross-section of the simulated structure

The thickness of the GaN layer substituting the transition layers was increased to 0.5 µm so that the simulated breakdown voltage reaches 280 V, which is the experimental breakdown voltage of the studied HEMT. The default impact ionization parameters used for the simulations are shown in table 2.2 [72].

	AN	AP	BN	BP	BETAN	BETAP
Unit	cm^{-1}		V/cm		-	
	2.52×10^{8}	5.37×10^{6}	3.41×10^{7}	1.96×10^{7}	1	1

Table 2.2 Default impact ionization parameters used during the simulation of the breakdown voltage

To calibrate the simulator, the density and energy of acceptor traps (in GaN and AlGaN layers) as well as the density of the two dimensional electron gas were tuned. As shown in figure 2.6, the threshold voltage, transconductance and off-state current of the simulated structure match the ones experimentally measured.

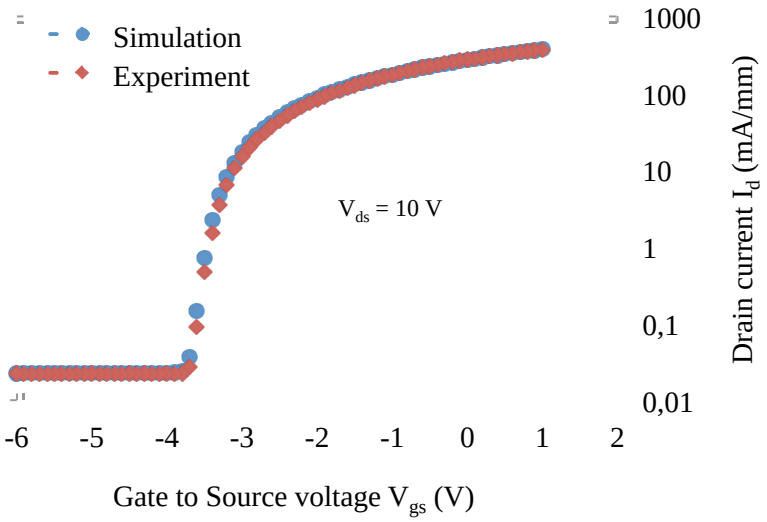

Figure 2.6 Comparison of experimental and simulated $I_d(V_{gs})$ transfer characteristics showing a clear match for the threshold voltage and transconductance

To change the density of the 2DEG, the bound charge at the AlGaN/GaN interface was multiplied by a fitting parameter K as shown in equation 2.21:

$$\sigma = K * \left(\frac{Ps_{GaN} + Ppz_{GaN} - Ps_{AlGaN} - Ppz_{AlGaN}}{q} \right) \tag{2.21}$$

K: Fitting parameter (used to fit the threshold voltage)

A list of parameters used during the simulation are shown in table 2.3[73][74].

Electron affinity of GaN	4.1 eV
Gate workfunction	5.1 eV
Density of acceptor traps	10^{17} cm^{-3}
Energy of acceptor traps as measured from the conduction band	0.368 eV
Conduction band offset ΔE_c	0.7

Table 2.3 List of parameters used during the simulation

Other parameters are derived from the constants shown in table 2.2 such as:

Bandgap of AlGaN [75]:

$$E_G^{AlGaN} = x.E_G^{AlN} + (1-x).E_G^{GaN} - 1.3.x.(1-x) \tag{2.22}$$

Affinity of AlGaN:

$$\chi_{AlGaN} = \chi_{GaN} - \Delta E_c \tag{2.23}$$

2.3.4. Normally-off structures simulated

After calibrating the simulator, two new concepts for normally-off HEMT structures are proposed. Until now, all the proposed normally-off structures introduced external agents inside or at the top of the barrier layer. The idea behind the two concepts is to introduce an external agent below the gate, under the AlGaN/GaN interface to control the density of channel electrons below the gate. In this work, the external agents are either negative Fluorine ions or a p-doped region.

2.3.4.1. Fluorine implantation below the channel

In this structure, we propose the implantation of negative Fluorine ions below the AlGaN/GaN interface. To simulate the effect of the implanted Fluorine ions, negative charge was added inside the GaN layer. To do that using ATLAS, the layer in which negative ions are to be implanted was split into two layers with the same material. This will generate a homo-interface inside the layer. At this interface, a fixed negative charge is added as shown in figure 2.7. The position of the charge can be varied by changing the thickness of the split layer.

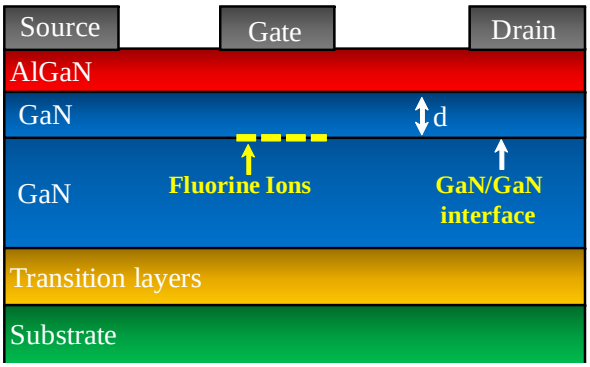

Figure 2.7 Strategy used to simulate the effect of Fluorine ions using ATLAS

The profile of the concentration of Fluorine ions, resulting from this approach, differs from the experimental profile. However, its effect on the transfer characteristics can be imitated by varying the concentration of negative charge at the interface. The use of a Fluorine equivalent interface charge was used by [76] to derive a comprehensive analytical model for the threshold voltage of fluorinated MOS-HEMTs.

To confirm the use of a Fluorine equivalent interface charge, the structures proposed in [49] (conventional normally-on HEMT and new normally-off HEMT with Fluorine in the AlGaN layer) were studied using the simulator with the previously tuned parameters. In figure 2.8, the experimental results and the simulated ones are compared and show a clear match.

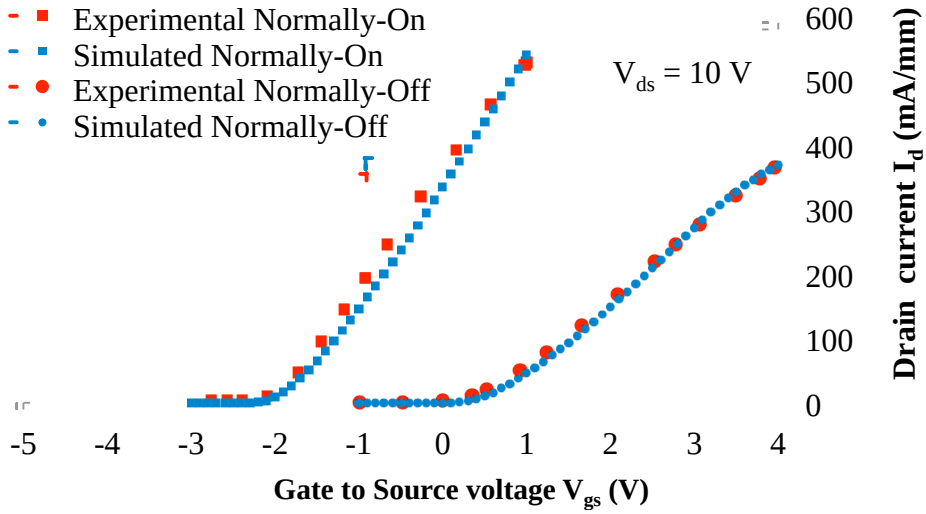

Figure 2.8 Comparison between the experimental transfer characteristics $I_d(V_{gs})$ obtained in [46] and the simulated ones using the calibrated simulator, for normally-on HEMT and HEMT with Fluorine implanted in the barrier layer

It is worth noting that the mobility of the 2DEG in the normally-off HEMT structure (after Fluorine implantation in the AlGaN layer) was used as a fitting parameter and was reduced from 1500 cm^2/V.sec to 500 cm^2/V.sec. This mobility degradation is due to the scattering between the electrons and the Fluorine ions present in the channel.

When studying the normally-off structure with Fluorine implantation, the constant low field mobility was used. The parameters used are shown in table 2.4

	MUN	MUP
GaN bulk	900	10
AlN bulk	300	10
2DEG	1500	10

Table 2.4 Parameters for the constant low field mobility used during the simulation of the normally-off HEMT with Fluorine implantation

2.3.4.2. Buried p-region

In this structure, we propose the introduction of a p-region below the gate under the AlGaN/GaN interface i.e. below the channel of the HEMT. A schematic cross-section of this structure is shown in figure 2.9.

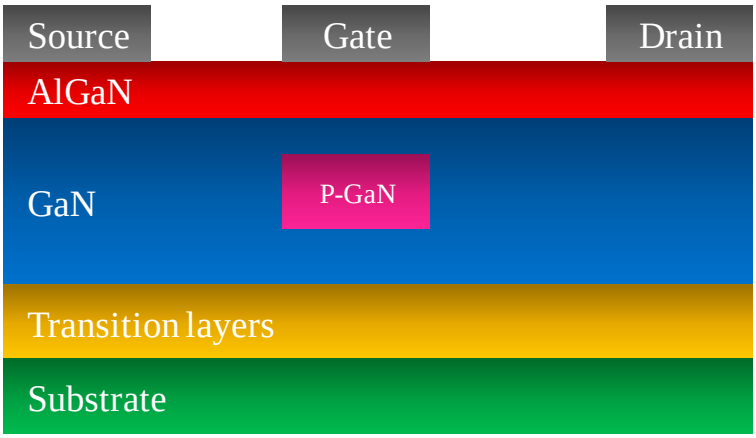

Figure 2.9. Schematic cross-section of the HEMT with a buried p-region

When studying the structures with buried p-regions or the Gate Injection Transistors (figure 1.24), the ALBRCT low field mobility was used to take into account the variation of the mobility with the doping concentration. The parameters used during the simulation for the ALBRCT model are shown in table 2.5.

	AN.ALBRCT	BN.ALBRCT	AN.ALBRCT	BN.ALBRCT
GaN bulk	5×10^4	5×10^4	0.07	0.07
2DEG	1.5×10^4	1.5×10^4	0.07	0.07
P-GaN	1.5	1.5	0.07	0.07

Table 2.5 Parameters for the ALBRCT low field mobility used during the simulation of the normally-off HEMT with buried p-region and the GIT

Since in the HEMT the current flows in a very narrow region at the AlGaN/GaN interface, the output current of the device is not very sensitive to the mobility in the bulk of AlGaN and GaN layers.

In the following chapters, the new proposed normally-off structures are shown. The structure with Fluorine implanted below the channel is discussed in Chapter 3. In Chapter 4, the normally-off HEMT with a buried P-region will be examined.

2.4. Conclusion

To examine the electric characteristics of our proposed normally-off HEMT design, the commercial TCAD simulation tool from Silvaco was used. The simulator was calibrated using experimental data from a normally-on HEMT device. The energy and density of the accepter traps as well as the density of the two dimensional electron gas were tuned so that the simulated transconductance, threshold voltage and off state current match the ones experimentally measured. Moreover, the transition layers were substituted by an intrinsic GaN layer. The thickness of this layer was increased to fit the vertical breakdown voltage of the device. In the proposed normally-off designs, Fluorine ions or p-regions are introduced below the channel. To simulate the effect of Fluorine implantation, fixed negative sheet charge was introduced.

Chapter 3
A normally-off HEMT with Fluorine implantation below the channel

3.1. Introduction

The implantation of negative Fluorine ions is a well-known method used to achieve normally-off operation in HEMTs [45][46][47][48][49]. For now, all the normally-off HEMTs based on this technique implant the Fluorine ions above the channel. Although this method is capable of achieving normally-off operation, small amount of negative Fluorine ions penetrate into the channel during implantation and cause mobility degradation [48].

In this chapter, we propose the implantation of negative Fluorine ions below the channel rather than above it. To introduce the negative Fluorine ions, the strategy explained in section 2.3.4.1 is used. The dimensions and physical properties of the studied structure are the same as the normally-on HEMT used for calibration.

3.2. HEMT with Fluorine implanted below the channel

3.2.1. Fluorine implantation below the channel

A schematic cross-section of the simulated structure is shown in figure 3.1. The distance "d" between the Fluorine ions and the AlGaN/GaN interface is 15 nm. The width of the region where negative charge is introduced is equal to 1 µm.

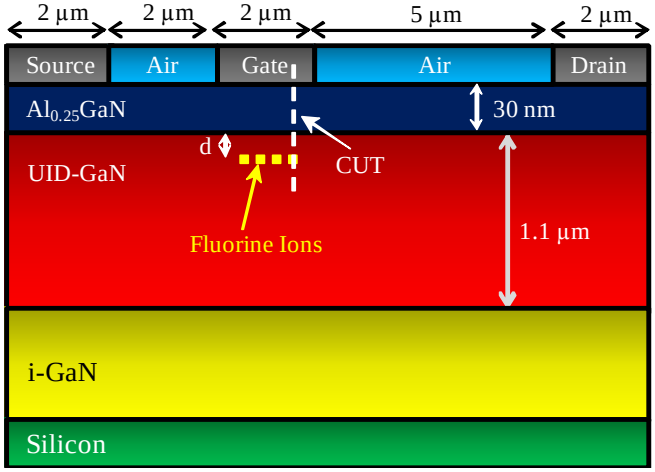

Figure 3.1 Schematic cross-section of the HEMT with Fluorine implanted in GaN below the channel

The concentration of the Fluorine ions, called F_{imp}, is varied. It can be seen from figure 3.2 that the threshold voltage increases with increasing Fluorine concentration. When the Fluorine concentration reaches 8×10^{12} cm^{-2}, the HEMT becomes normally-off with a threshold voltage of 0.5 V.

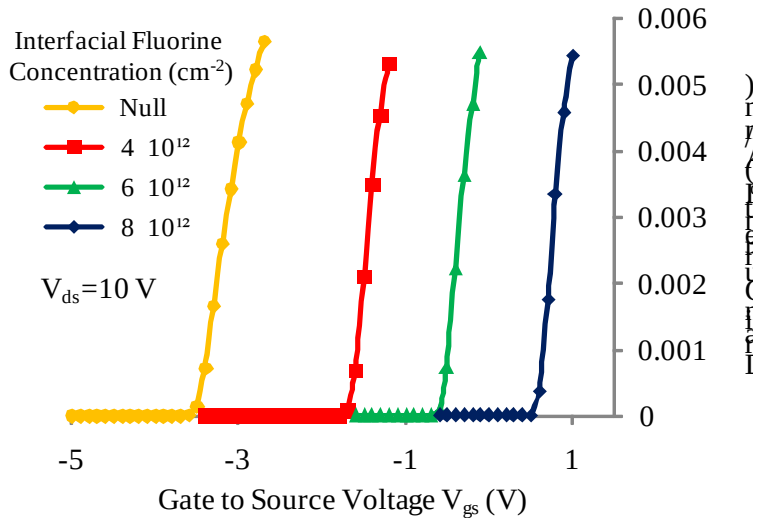

Figure 3.2 Simulated $I_{ds}(V_{gs})$ transfer characteristics showing the increase in the threshold voltage with the Fluorine concentration

To explain the increase in the threshold voltage with the Fluorine concentration, the band diagram through CUT in figure 3.1, is shown in figure 3.3.

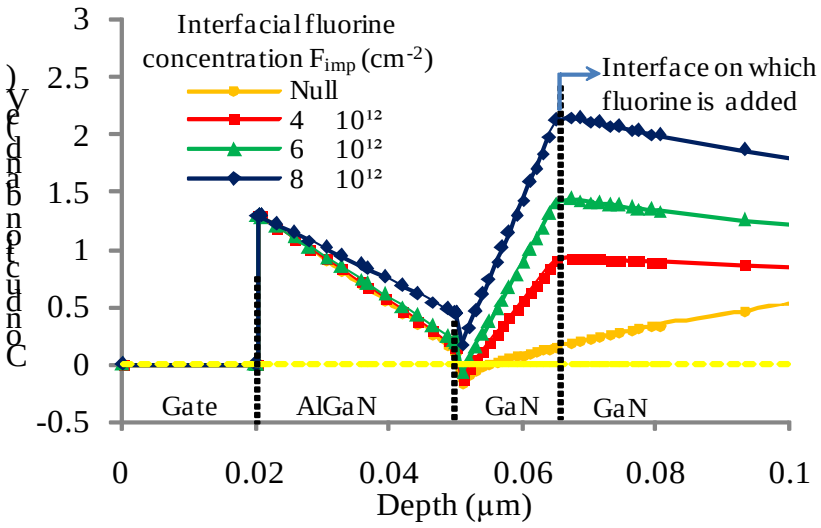

Figure 3.3 *Conduction band along CUT - see figure 3.1 - at various Fluorine concentrations showing the uplifting of the triangular well at high Fluorine concentration*

The energy gap between the conduction band and the Fermi level increases as the Fluorine concentration increases. This is manifested through the uplifting in the conduction band in the region where Fluorine is implanted. This raise causes the elevation of the conduction band at the AlGaN/GaN interface. If the Fluorine concentration is strong enough to raise the conduction band at the interface above the Fermi level, normally-off HEMT can be achieved as shown in figure 3.3, with a concentration of 8×10^{12} cm^{-2}.

3.2.2. Comparison between implantation in the barrier layer and implantation below the channel

In order to compare the implantation in the barrier layer (i.e. in the UID-GaN layer) to that below the channel (i.e. in the AlGaN layer), the transfer characteristics of the conventional normally-on HEMT ("Null") and HEMT with Fluorine implanted in AlGaN layer, at various concentrations, are simulated and shown in figure 3.5. For a fair comparison, the Fluorine ions are located 15 nm above the AlGaN/GaN interface as shown in figure 3.4.

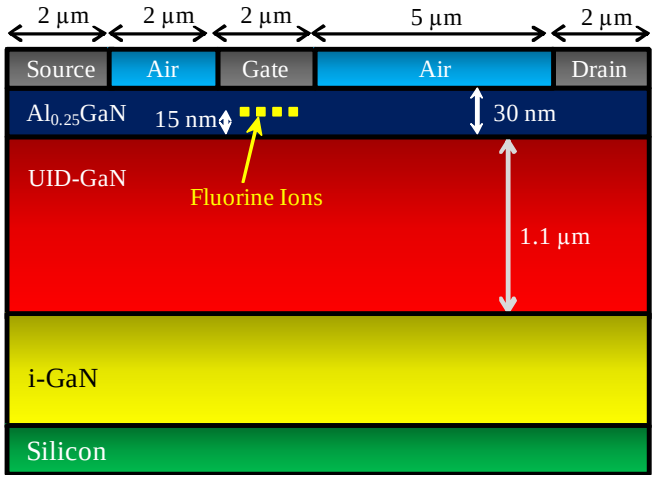

Figure 3.4 Schematic cross-section of the HEMT with Fluorine implanted in the AlGaN layer (barrier layer)

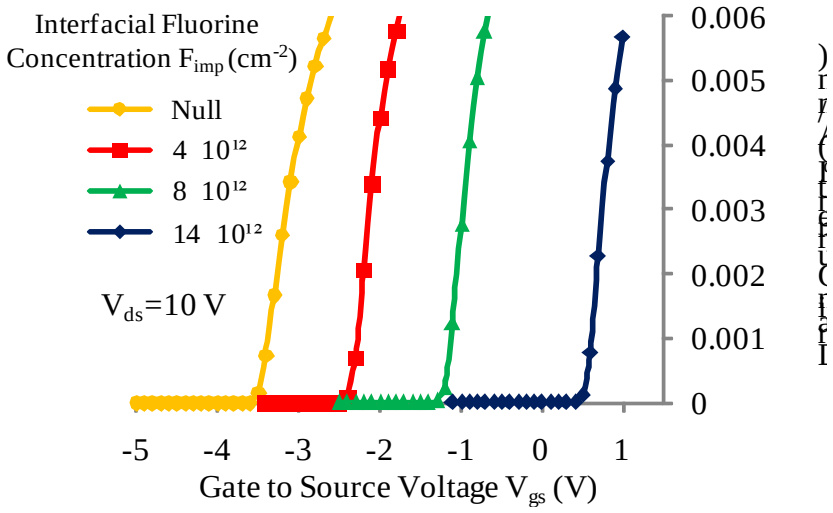

Figure 3.5 I_d (V_{gs}) transfer characteristics of the conventional normally-on HEMT and HEMTs with Fluorine implanted in AlGaN at various concentrations

Although the threshold voltage also increases with increasing the Fluorine concentration, the concentration required to achieve normally-off operation with a threshold voltage of 0.5 V is

equal to 14×10^{12} cm^{-2}. In the case of implantation below the channel, a concentration of only 8×10^{12} cm^{-2} was required to achieve the same threshold voltage. This makes our proposed technique more efficient.

To explain the better efficiency, the band diagrams for the two structures are shown in figure 3.6. In both cases, the threshold voltage is 0.5 V. Since HEMTs attain a Schottky gate, the conduction band at the top of the AlGaN layer is pinned at a fixed energy equal to the Schottky barrier. If it was not for that pinning, the conduction band in AlGaN would have risen higher when Fluorine is implanted, causing a higher shift in the threshold voltage.

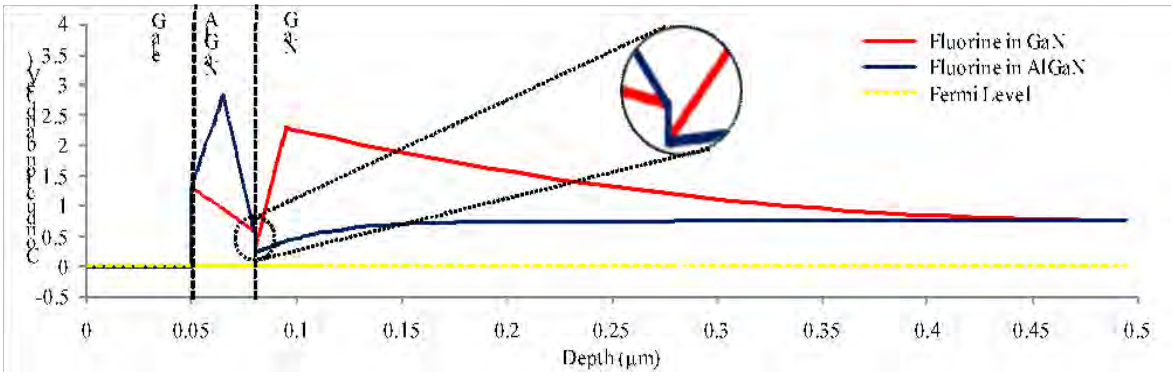

Figure 3.6 Band diagrams of HEMT with Fluorine implanted in AlGaN at concentration 14×10^{12} cm^{-2} and HEMT with Fluorine in GaN at concentration $8 \times 10^{12} cm^{-2}$; both HEMTs attain a threshold voltage of 0.5 V

Moreover, it can be noted from the band diagram that the confinement of the 2DEG under the gate is superior in the case of Fluorine implanted in GaN (see zoom in Figure 3.6).

3.2.3. Variations of the threshold voltage with the distance "d"

Figure 3.7 shows the variations of the threshold voltage with respect to the distance "d" between the AlGaN/GaN interface and the Fluorine ions (figure 3.1), for three different Fluorine concentrations.

It can be seen that, as the distance increases, the threshold voltage decreases. However, the rate of decrease is more significant after exceeding a certain critical distance $d_{critical}$. In addition, the results show that $d_{critical}$ decreases with the increase in the Fluorine concentration: for example, the critical distances at Fluorine concentration of 6×10^{12}, 7×10^{12} and 8×10^{12} cm^{-2} are 48, 33 and 25 nm respectively. The rate of decrease seems to be independent on the Fluorine concentration when $d < d_{critical}$.

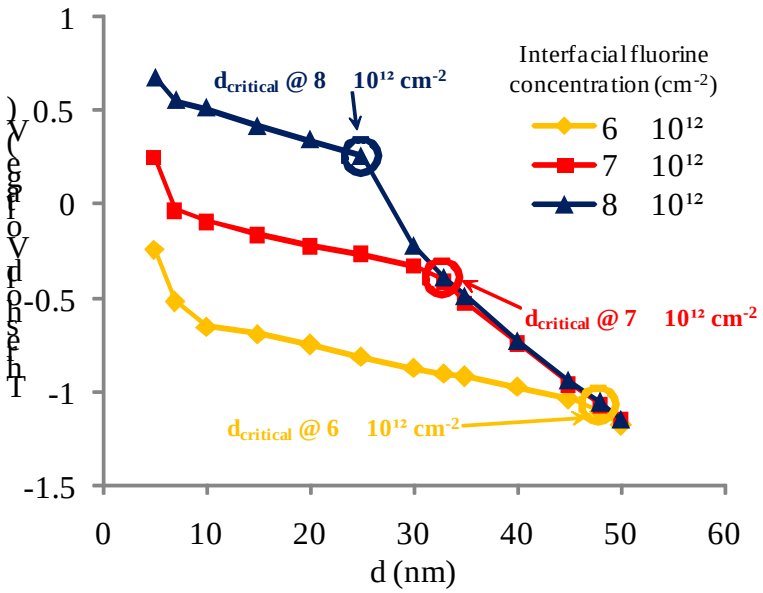

Figure 3.7 Variations of the threshold voltage with the distance "d" between the Fluorine ions and the AlGaN/GaN interface at various Fluorine concentrations

Moreover, it can be noted that the distance d must be below the critical distance for the threshold voltage to increase with increasing the Fluorine concentration (as mentioned in figure 3.2). For example, for a Fluorine concentration of 6×10^{12} cm^{-2} and d = 35 nm, V_{th} = - 0.91 V. Since at this concentration $d < d_{critical}$ (35 < 48), an increase in the Fluorine concentration from 6×10^{12} to 7×10^{12} cm^{-2} will increase V_{th} from - 0.91 V to - 0.48 V. However, at a Fluorine concentration of 7×10^{12} cm^{-2}, $d > d_{critical}$ (35 > 33): therefore, the increase in the Fluorine concentration from 7×10^{12} to 8×10^{12} cm^{-2} does not increase the threshold voltage and V_{th} remains equal to - 0.48 V.

$d_{critical}$ can be extracted and explained from the band diagram. However, it is worth pointing out three important aspects of the band diagram.

The first is the band bending due to the introduction of charge. Positive charge, like the bound charge at the AlGaN/GaN interface, decreases the gap between the Fermi level and the conduction band. On the other hand, negative charge, like the implanted Fluorine ions, increases the gap between the conduction band and the Fermi level. However, since at equilibrium the Fermi level is constant, the variation in the gap manifests itself through pushing the conduction band downwards in the case of positive charge and upwards in the case of negative charge.

The second aspect is the width of the gap at different Fluorine concentrations. A Fluorine concentration of 6×10^{12} cm^{-2} can increase the gap up to 3.404 eV. A higher concentration of

8×10^{12} cm^{-2} can achieve higher gap width up to 3.412 eV. The difference between the maximum gap values, at different Fluorine concentrations, is very low (0.008 eV) and it is not the reason behind the higher increase in the threshold voltage. Actually, it is the reason why the threshold voltage does not increase when $d > d_{critical}$ (will be discussed in more details below).

The third aspect is that the width of the gap, in the region where Fluorine is implanted, is strongly affected by the neighboring positive bound charge at the AlGaN/GaN interface. While the positive bound charge pulls the conduction band downwards, the negative Fluorine ions push it upwards. Therefore, the negative Fluorine ions will not be able to increase the gap to its maximum value unless parting a certain distance from the positive bound charge. Figure 3.8 shows the band diagram, along CUT in figure 3.1, with Fluorine implanted at various distances d from the AlGaN/GaN interface. The Fluorine concentration is taken equal to 7×10^{12} cm^{-2}. The distance at which the gap, in the region where Fluorine is implanted, reaches its maximum value, is $d_{critical}$. The gap remains constant for $d > d_{critical}$. From figure 3.8, we can see that $d_{critical}$ is equal to 33 nm.

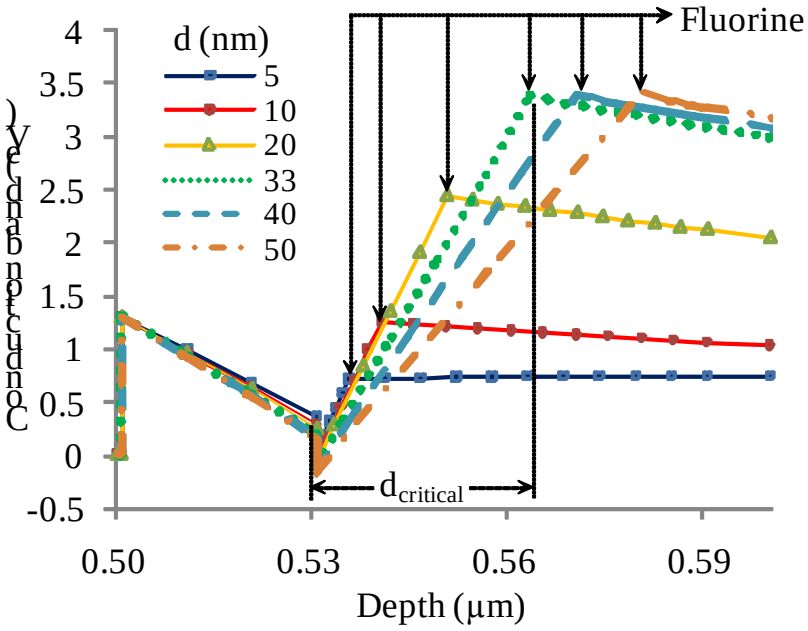

Figure 3.8 Band diagrams, along CUT in figure 3.1, with Fluorine implanted at various distances from the AlGaN/GaN interface. The Fluorine concentration is equal to 7×10^{12} cm^{-2}

But it is worth noting that, at a given distance below $d_{critical}$, as the Fluorine concentration increases, the upward push in the conduction band increases (see figure 3.3), hence the

maximum gap value can be reached at relatively short distances. That is why $d_{critical}$ decreases with increasing the Fluorine concentration.

The threshold voltage will not increase with the Fluorine concentration at $d > d_{critical}$ since at that distance, the gap reaches its maximum value, and further increase in the Fluorine concentration will slightly increase the gap (recall second aspect: the increase in the Fluorine concentration from 6×10^{12} cm^{-2} to 8×10^{12} cm^{-2} increases the gap by 0.008 eV).

3.2.4. Breakdown voltage and off-state current

To examine the off-state current and the breakdown voltage, the structure shown in figures 3.1 and 3.4 were studied. However, due to convergence problems at high voltages in the normally-off HEMT with high Fluorine concentrations, a smaller x-mole fraction of 0.15 was used instead. In this case, a smaller Fluorine concentration of 4.2×10^{12} cm^{-2} is needed to achieve normally-off operation with a threshold voltage of 0.5 V. The same HEMT (x-mole fraction of 0.15) with no Fluorine implantation attains a threshold voltage of -2 V.

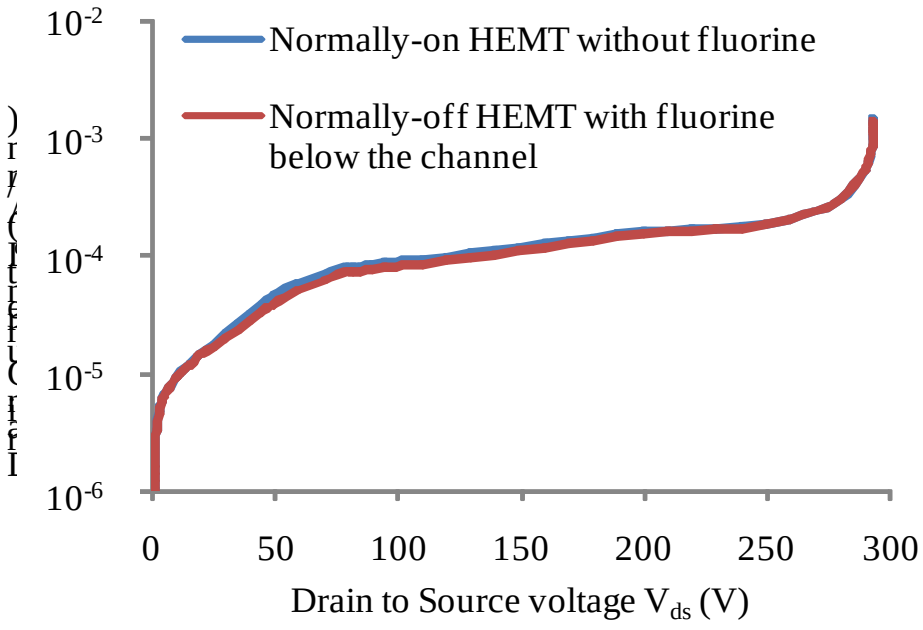

Figure 3.9 Simulated $I_d(V_{ds})$ characteristics in the off-state, showing the off-state current and the breakdown voltage of the normally-on HEMT and the normally-off HEMT with Fluorine implantation below the channel

Figure 3.9 shows the variation of the drain current with the applied drain to source voltage $I_d(V_{ds})$. In order to study the two HEMTs in the off-state, i.e. below their threshold voltage, the applied gate to source voltage is: $V_{gs} = V_{th} - 1$ V. It is clear that neither the vertical

breakdown voltage, nor the off-state current are affected by the implanted Fluorine ions. A breakdown voltage of 280 V was obtained in both cases.

3.2.5. Forward gate voltage

Although this approach helps increasing the threshold voltage, its disadvantage is that the forward gate voltage (the gate voltage at which the gate leaking occurs) decreases with increasing the Fluorine concentration. Figure 3.10 shows the variations of the forward gate voltage and the threshold voltage with the Fluorine concentration. It can be seen that this decrease in the forward gate voltage limits the increase in the threshold voltage.

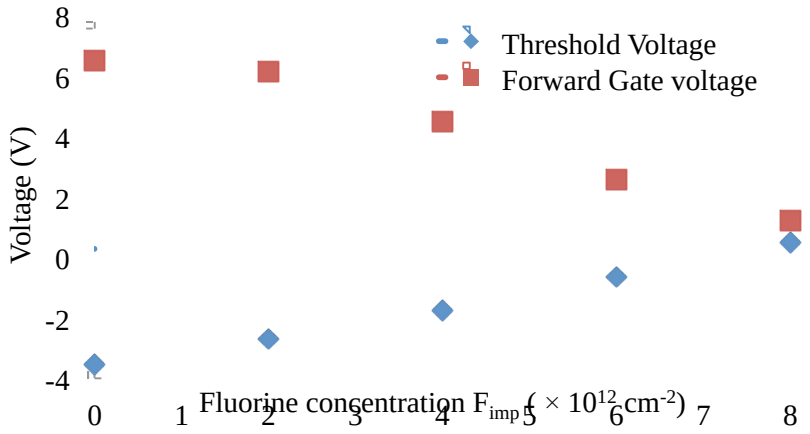

Figure 3.10 Variations of the threshold voltage and forward gate voltage with the Fluorine concentration at V_{ds}=10 V

To eliminate the gate leakage, and hence push further the limitations of the device, the Schottky gate has to be replaced by a MIS gate. This is done by introducing an insulating layer below the gate electrode.

3.3. MIS-HEMT with Fluorine below the channel

The low forward gate voltage in the above proposed normally-off HEMT limits the increase in the threshold voltage. Therefore, to eliminate the gate leakage, an insulating layer is introduced below the gate.

In this work, three different insulators are used: Silicon Oxide (SiO_2), Silicon Nitride (Si_3N_4) and Hafnium Oxide (HfO_2). An ideal case is studied in which no fixed charge is present inside the insulator or at the insulator/barrier interface. The aim of using different types of insulators is to see the effect of the permittivity of the insulator on the transfer characteristics

of the device. The relative permittivity (ε_r) of SiO_2, Si_3N_4 and HfO_2 are 3.9, 7.5, and 25 respectively.

Now, after introducing the insulating layer, the increase in the threshold voltage with the Fluorine concentration will not be limited by the forward gate voltage. Therefore, the effect of increasing the Fluorine concentration is studied again to address the limitations of this technique.

3.3.1. Effect of Fluorine concentration

The simulated structure is shown in figure 3.11. The insulator used is Si_3N_4 with a thickness of 10 nm. The distance between the AlGaN/GaN interface and the implanted Fluorine ions is equal to 10 nm. The concentration of the implanted Fluorine ions "F_{imp}" will be varied.

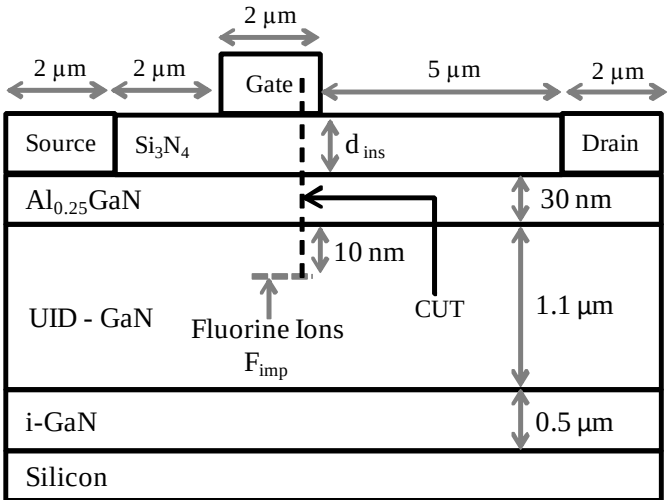

Figure 3.11 Schematic cross-section of the simulated MIS-HEMT with Fluorine implanted in GaN below the channel

Although the aim of Fluorine implantation is to achieve normally-off operation, it also can be used to reduce the off-state current of a normally-on MIS-HEMT. Figure 3.12 shows the transfer characteristics $I_d(V_{gs})$ for a MIS-HEMT with Fluorine implanted below the channel at various concentrations. Implanting Fluorine ions helps to reduce the off-state current. It is worth noting that further increase in the Fluorine concentration ($F_{imp} > 4 \times 10^{12}$ cm^{-2}) will not cause further reduction in the off-state current. The lowest off-state current reached is equal to that of the normally-on HEMT (the one used for calibration).

As for the threshold voltage, as expected, it increases with increasing the Fluorine concentration. However, a point is reached where further increase in the Fluorine concentration does not affect the threshold voltage.

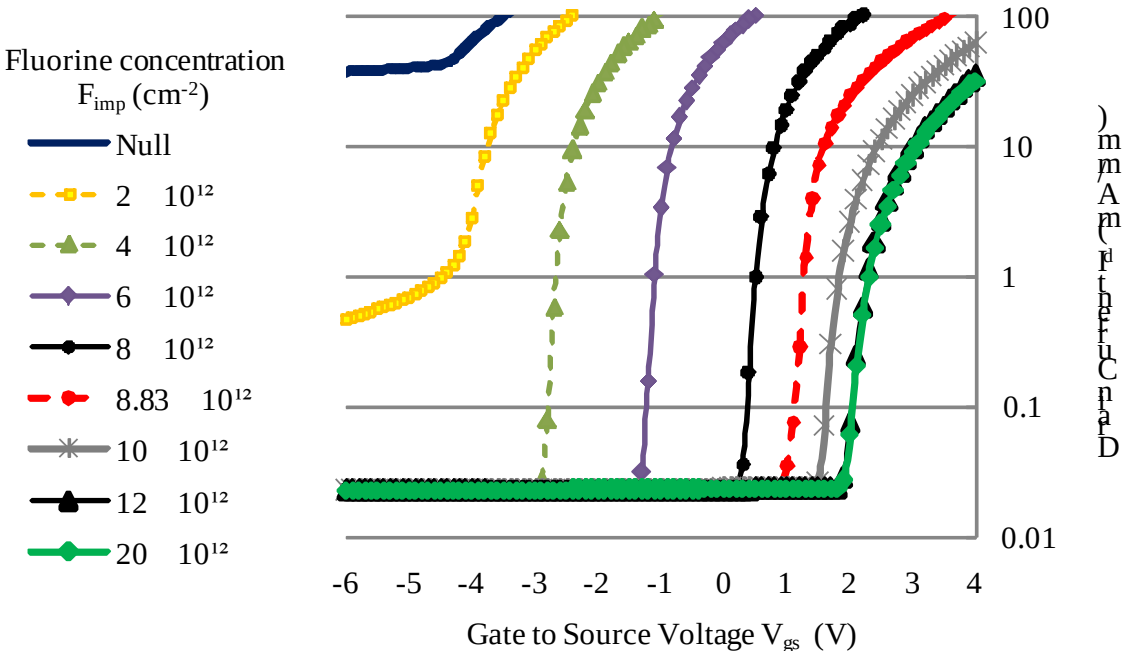

Figure 3.12 $I_{ds}(V_{gs})$ transfer characteristics of the MIS-HEMT at various Fluorine concentrations for d_{ins} = 10 nm

In figure 3.13, the variations of the threshold voltage with F_{imp}, at d_{ins} = 10, 20 and 40 nm, are illustrated. It is clear that the threshold voltage increases with increasing the Fluorine concentration. However, a point is reached ($F_{imp} = F_{optimum} = 12 \times 10^{12}$ cm^{-2}), where a further increase in the concentration no longer affects the threshold voltage. To explain this limitation, the band diagram along the CUT of figure 3.11, is shown in figure 3.14. As mentioned before, introducing Fluorine ions in a semiconductor will shift the Fermi level towards the valence band, thus increasing the gap between the conduction band and the Fermi level. However, since at equilibrium the Fermi level is constant, the increase in the gap will manifest itself through uplifting the conduction band. Nonetheless, the gap between the Fermi level and the conduction band cannot surpass the bandgap of the material in which Fluorine is implanted, which is GaN in our case.

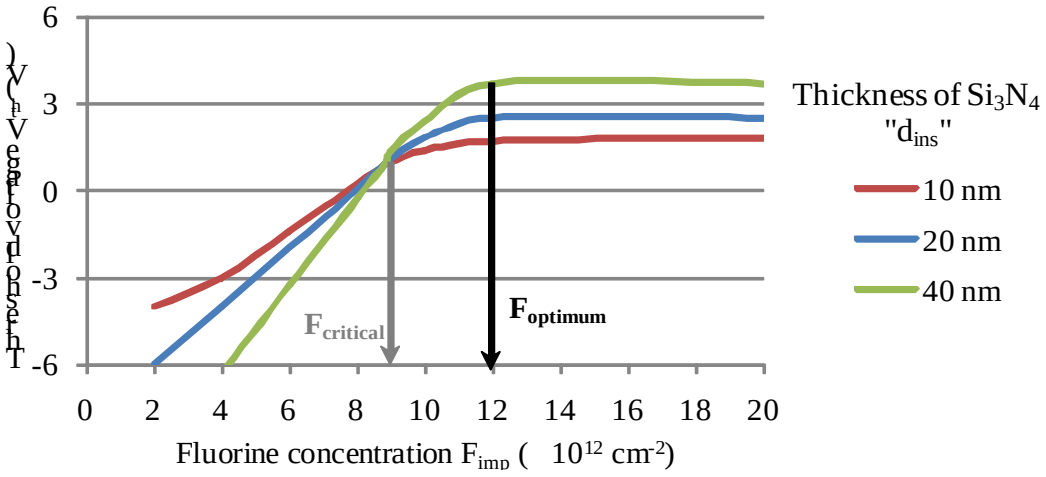

Figure 3.13 Variations of the threshold voltage with the Fluorine concentration at various thicknesses of the insulator

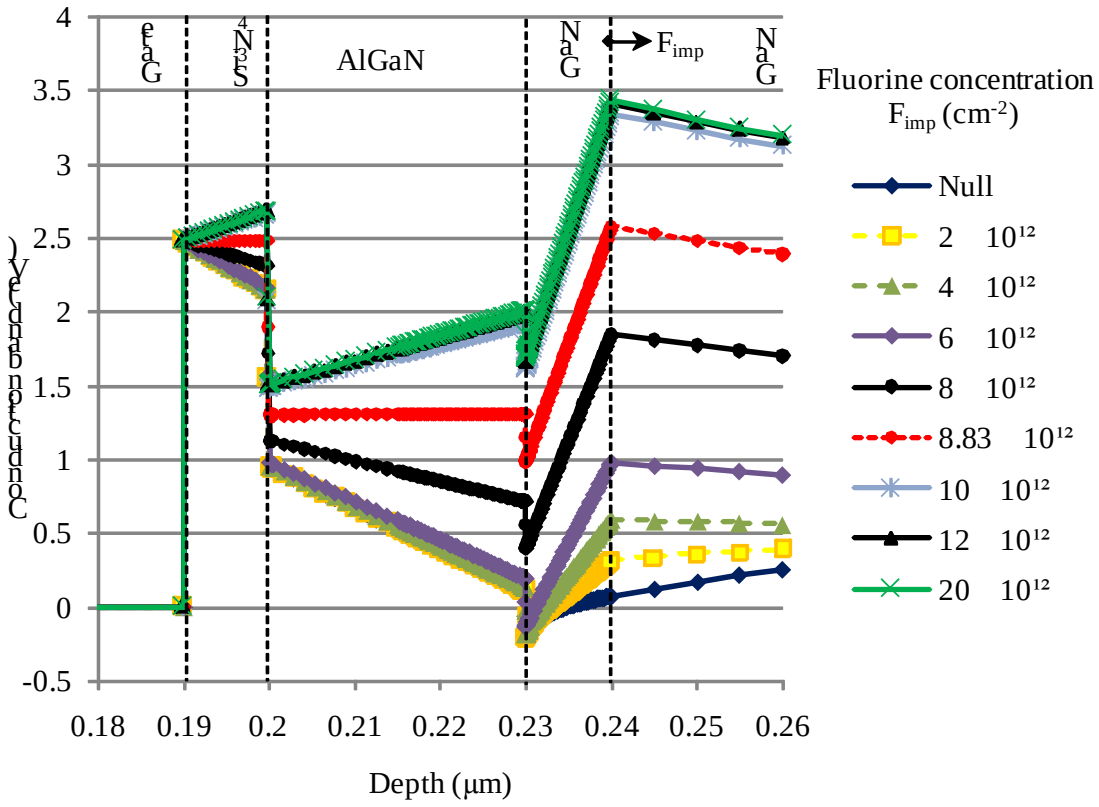

Figure 3.14 Band diagrams of MIS-HEMT at various Fluorine concentrations

Therefore, the threshold voltage will keep on increasing as long as the gap between the conduction band and the Fermi level is less than the bandgap. Once the gaps are equal,

Fluorine ions will be incapable of increasing the gap and hence lifting further the triangular well, which causes the increase in the threshold voltage.

It should be noted from figure 3.13, that all the curves corresponding to various d_{ins}, intersect at a common point. The Fluorine concentration associated with this point is named $F_{critical}$ and will be further discussed in the coming sections.

3.3.2. Variation of the threshold voltage with thickness of the insulator

To further explore the effect of the thickness of the insulator on the threshold voltage, d_{ins} is varied from 10 nm to 160 nm. The variations of the threshold voltage with the thickness of the insulator at various Fluorine concentrations are shown in figure 3.15.

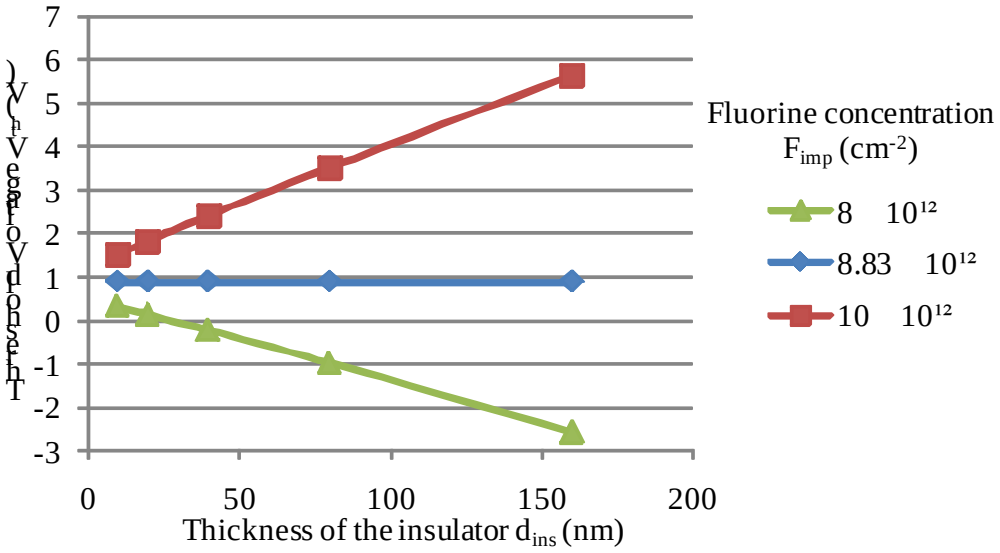

Figure 3.15 Variations of the threshold voltage with the thickness of the insulator at various Fluorine concentrations

It is clear that the variation of V_{th} with d_{ins} strongly depends on F_{imp}. The concentration of Fluorine $F_{critical}$, at which the threshold voltage is not affected by the thickness of the insulator, is equal to 8.83×10^{-12} cm^{-2}. This concentration corresponds to the intersection point in figure 3.13.

For $F_{imp} < F_{critical}$, the threshold voltage decreases with increasing d_{ins}. On the other hand, when $F_{imp} > F_{critical}$, the threshold voltage increases with increasing d_{ins}. The different variations in the threshold voltage with respect to the thickness of the insulator is directly related to the direction of the y-component of the electric field "E_y" in the AlGaN layer, above the region where Fluorine ions are implanted. When $E_y = 0$, the threshold voltage will

be unaffected by the thickness of the insulator. If E_y is pointing towards the gate electrode, the threshold voltage will decrease with increasing the thickness of the insulator, and vice versa: if E_y points towards the substrate, the threshold voltage increases with increasing the thickness of the insulator.

The direction of E_y can be extracted from the profile of the conduction band shown in figure 3.14 ($E_y \propto dE_c/dy$; y = depth). In our simulation, the positive y-direction points towards the substrate. When $F_{imp} = F_{critical} = 8.83 \times 10^{12}$ cm^{-2}, the conduction band is constant and hence $E_y = 0$. At $F_{imp} = 8 \times 10^{12}$ $cm^{-2} < F_{critical}$ the conduction band is decreasing and then $E_y > 0$. At $F_{imp} = 1 \times 10^{13}$ $cm^{-2} > F_{critical}$, the conduction band is increasing and then $E_y < 0$.

3.3.3. Variations with the permittivity of the insulator

In this section, the effect of the permittivity of the insulator on the transfer characteristics is examined. Three different insulators are studied: SiO_2, Si_3N_4 and HfO_2 with a relative permittivity of 3.9, 7.5 and 25 respectively. Figure 3.16 shows the variations of the threshold voltage with the permittivity of the insulator at various Fluorine concentrations.

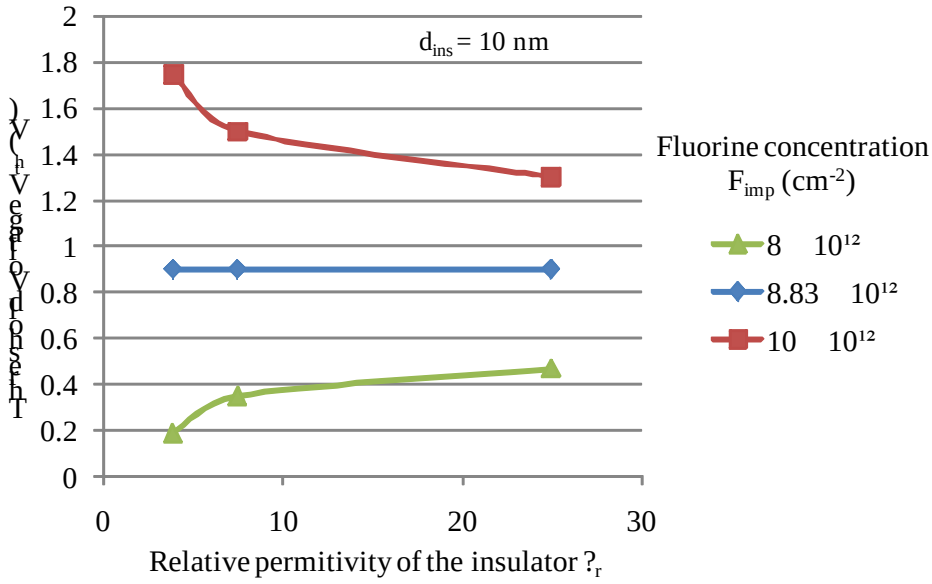

Figure 3.16 Variations of the threshold voltage with the permittivity of the insulator at various Fluorine concentrations

It can be noted that the variations with respect to the permittivity of the insulator mimics the variations with respect to the thickness of the insulator. When $F_{imp} = F_{critical}$, no variation in the threshold voltage is observed with increasing ε_r. For $F_{imp} < F_{critical}$, the threshold voltage

increases with increasing ε_r. On the other hand, when $F_{imp} > F_{critical}$, the threshold voltage decreases with increasing ε_r.

However, the rate of change in the threshold voltage with the thickness of the insulator depends on the permittivity of the material. Figure 3.17 shows the variations of the threshold voltage with the thickness of the insulator at $F_{imp} < F_{critical}$ for three different insulators. It can be seen that although the threshold voltage decreases with increasing the thickness of the insulator, the rate of decrease is more severe when the permittivity of the insulator is decreased.

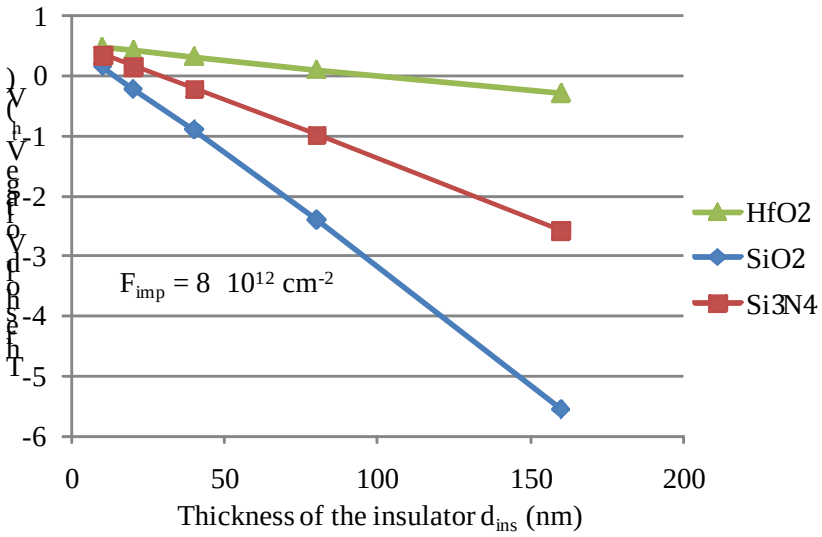

Figure 3.17 Variations of the threshold voltage with the thickness of the insulator at $F_{imp} < F_{critical}$ for three different insulators

The same applies for the rate of increase on the threshold voltage with the thickness of the insulator when $F_{imp} > F_{critical}$. As shown in figure 3.18, the threshold voltage increases with increasing the thickness of the insulator. However, the lower the permittivity of the insulator, the faster the increase in the threshold voltage.

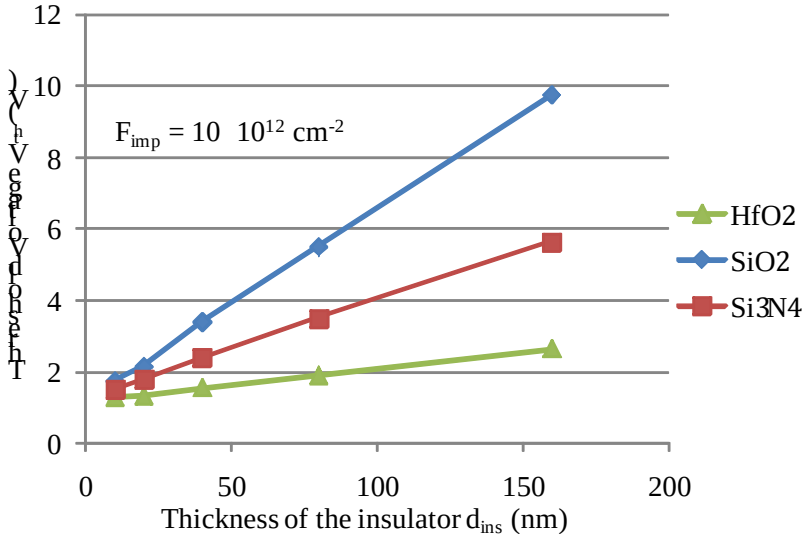

Figure 3.18 Variations of the threshold voltage with the thickness of the insulator at $F_{imp} > F_{critical}$ for three different insulators

3.4. Effect on the transconductance

For now, the threshold voltage can be increased by either increasing the Fluorine concentration or by increasing the thickness of the insulator with $F_{imp} > F_{critical}$. However, each approach has its own effect on the transconductance. Figure 3.19 shows the transconductance at various thicknesses of Si_3N_4 with $F_{imp} = 1\times10^{13}$ $cm^{-2} > F_{critical}$.

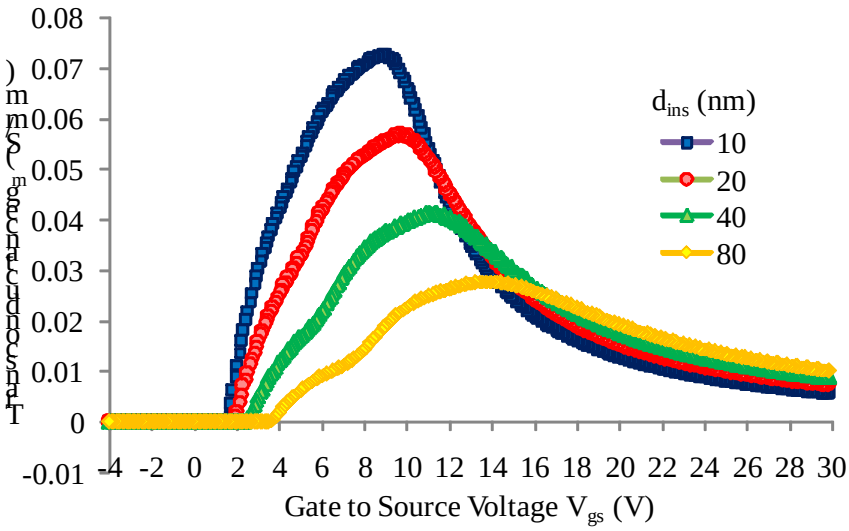

Figure 3.19 Variations of the transconductance with the thickness of the insulator at $F_{imp} > F_{critical}$

It can be seen that, although the threshold voltage increases with this technique, the transconductance peak decreases with increasing the thickness of the insulator. On the other hand, when the threshold voltage increases with increasing the Fluorine concentration, the transconductance remains the same up to a point (F_{imp} = 6×10^{12} cm^{-2}) where it undergoes a sudden drop (F_{imp} = 8×10^{12} cm^{-2}) as shown in figure 3.20.

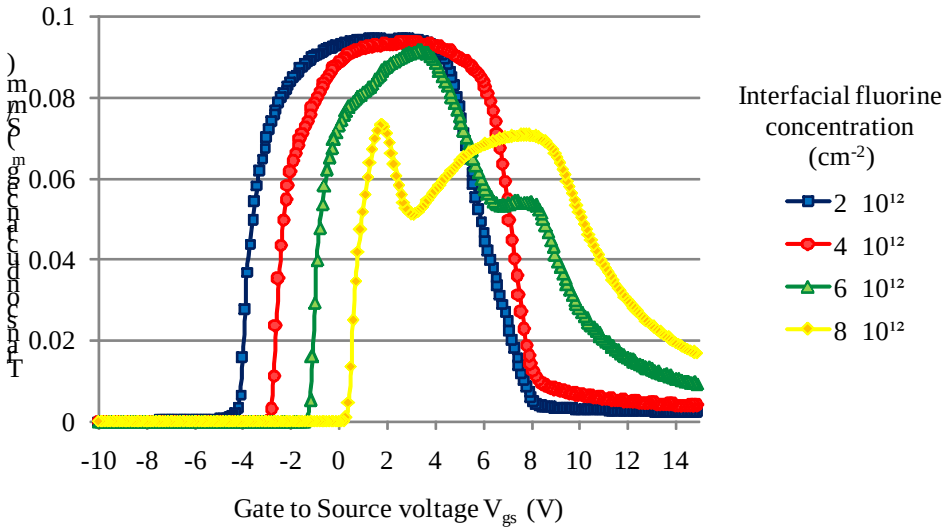

Figure 3.20 $g_m(V_{gs})$ of the MIS-HEMT at various Fluorine concentrations F_{imp} at d_{ins} = 10 nm

To explain this drop, the conduction current density is shown in figure 3.21 at V_{gs} = 6 V and V_{ds} = 10 V.

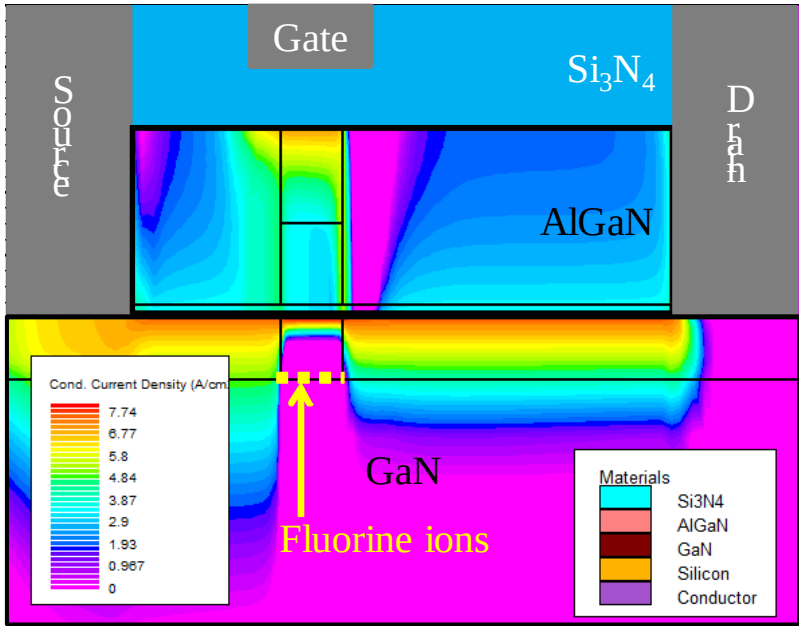

Figure 3.21 Conduction current density in the normally-off MIS-HEMT without an AlN interlayer

It can be seen that above the implanted Fluorine ions, the current no longer flows near the AlGaN/GaN interface but rather near the insulator/AlGaN interface. Since the mobility in the AlGaN layer is much lower than that at the AlGaN/GaN interface, a drop in the transconductance is obtained once the electrons migrate from the AlGaN/GaN interface to the insulator/Gate interface.

3.5. AlN interlayer for better transconductance

To resolve this problem, an AlN interlayer is added. Previous studies have used an AlN interlayer to increase the 2DEG density and prevent alloy scattering of channel electrons. However, in our case, the AlN layer is solely used to imprison the current at the AlGaN/GaN interface.

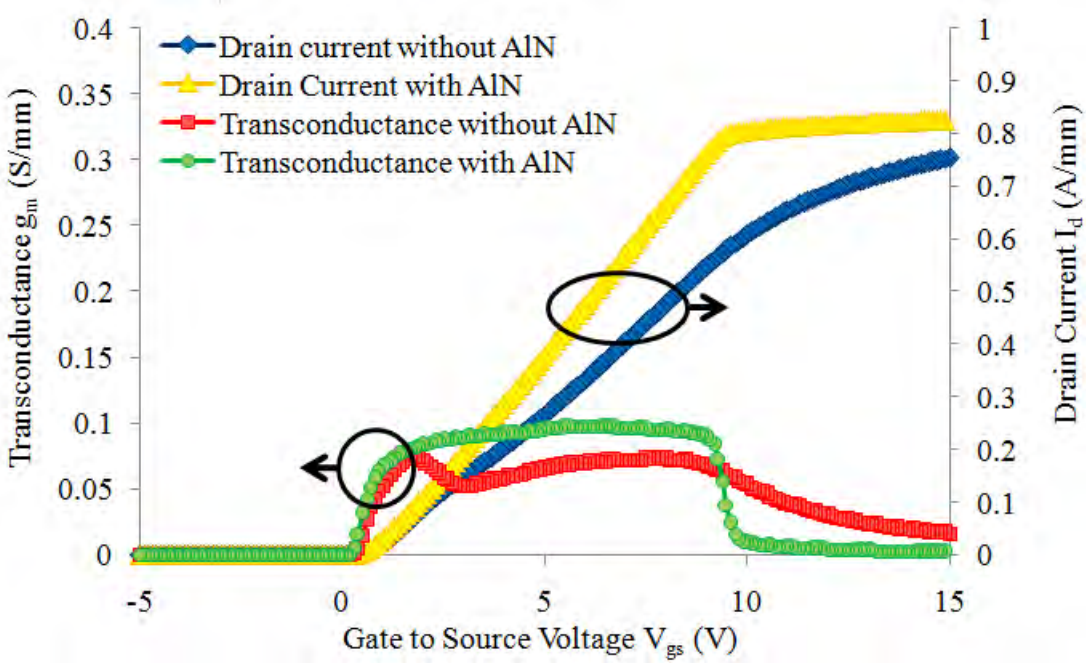

Figure 3.22 $I_d(V_{gs})$ and $g_m(V_{gs})$ of the MIS-HEMT with and without an AlN interlayer

Figure 3.22 shows the transfer characteristics of the normally-off HEMT with and without an AlN interlayer. The thickness of the AlN interlayer is 2 nm. Moreover, since the AlN interlayer increases the 2DEG density, higher Fluorine concentration is required to achieve a desired threshold voltage: $F_{imp} = 8\times10^{12}$ cm^{-2} in the MIS-HEMT without AlN and 9.4×10^{12} cm^{-2} in the MIS-HEMT with AlN. It can be seen that the added AlN interlayer improves the transconductance since it imprisons the current at the AlGaN/GaN interface, as shown in figure 3.23 which shows the conduction current density at V_{gs} = 6 V and V_{ds} = 10 V.

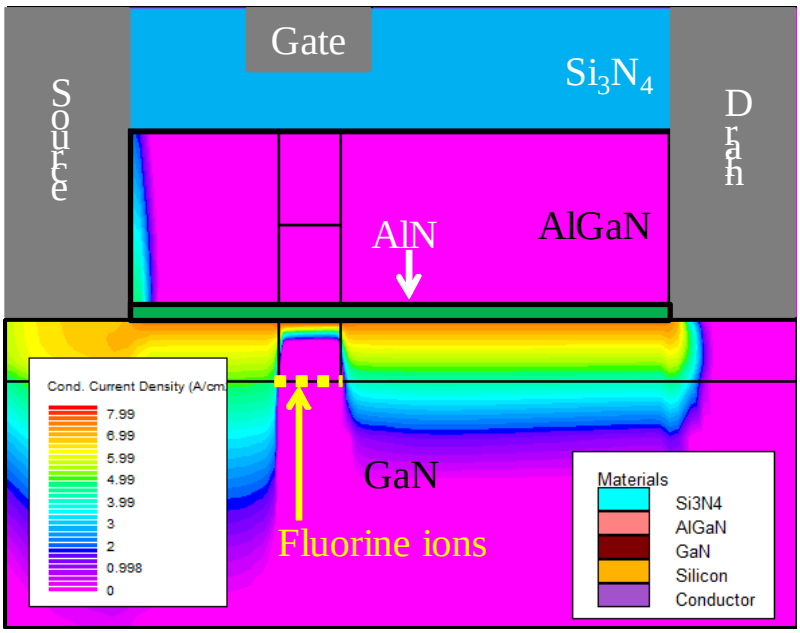

Figure 3.23 Conduction current density in the normally-off MIS-HEMT with an AlN interlayer

3.6. Conclusion

Fluorine implantation in the barrier layer is a well known technique used to achieve normally-off operation in HEMTs. However, when this technique is used, a small amount of Fluorine ions penetrate into the channel, presenting themselves as impurities leading to mobility degradation. In this chapter, the idea of implanting Fluorine below the channel, rather than above it, was explored. Simulation results have shown that the threshold voltage increases with increasing the Fluorine concentration. However, for this increase to happen, the distance between the Fluorine ions and the AlGaN/GaN interface "d" must be below a critical value $d_{critical}$. $d_{critical}$ decreases with increasing the Fluorine concentration. Moreover, when compared to implanting above this channel, implanting below the channel is more efficient when it comes to the Fluorine concentration required to achieve a certain threshold voltage, offers better confinement for the 2DEG below the gate and eliminates the scattering of channel electrons with Fluorine ions. Fortunately, the proposed technique neither affects the vertical breakdown voltage nor the off-state current. However, the forward gate voltage that decreases with increasing the Fluorine concentration, limits further increase in the threshold voltage. Therefore, to address the limitations of this technique, a sensitivity analysis was carried out for normally-off MIS-HEMTs with Fluorine implanted below the channel showing the effect of Fluorine concentration, permittivity and thickness of the insulator on the

performance of the device. Simulation results have confirmed the ability of Fluorine ions to increase the threshold voltage when implanted below the channel. However, a point is reached where further increase in the Fluorine concentration will not affect the threshold voltage. This is due to the fact that the gap between the Fermi level and the conduction band reaches the bandgap of the material in which Fluorine is implanted. Moreover, the effect of the thickness of the insulator on the threshold voltage strongly depends on the Fluorine concentration implanted. An increase in the thickness of the insulator will increase the threshold voltage if the concentration implanted is above $F_{critical}$ (in our simulation, $F_{critical} = 8.83 \times 10^{12}$ cm^{-2}), decrease it if the concentration implanted is below $F_{critical}$ and the threshold voltage is unaffected if the concentration implanted is equal to $F_{critical}$. The same behavior was obtained for the variation of threshold voltage with the permittivity of the insulator where three different behaviors were obtained depending on the implanted concentration. Although the idea of implanting Fluorine ions below the channel is capable of achieving normally-off operation, upon the application of high gate voltage in the case of MIS-HEMT, channel electrons above the Fluorine ions migrate from the AlGaN/GaN interface to the insulator/AlGaN interface causing a drop in the transconductance. To resolve this problem, an AlN interlayer can be added to imprison the electrons at the AlGaN/GaN interface.

Chapter 4
A normally-off HEMT with a buried p-GaN region

4.1. Introduction

For now, all the normally-off structures introduce agent inside or above the barrier layer. These agents lift the conduction band in the region where they are introduced causing an elevation in the triangular well at the AlGaN/GaN interface and hence increase the threshold voltage.

In this chapter, a new idea is explored: it is the introduction of a p-region under the gate and below the AlGaN/GaN interface. The conduction band will be uplifted in the p-region and will cause the triangular well at the AlGaN/GaN interface to elevate. Normally-off operation is achieved if the uplifting of the conduction band in the p-region is strong enough to elevate the triangular well above the Fermi level. Figure 4.1 shows the band diagram of a conventional normally-on HEMT and a normally-off HEMT using the proposed concept.

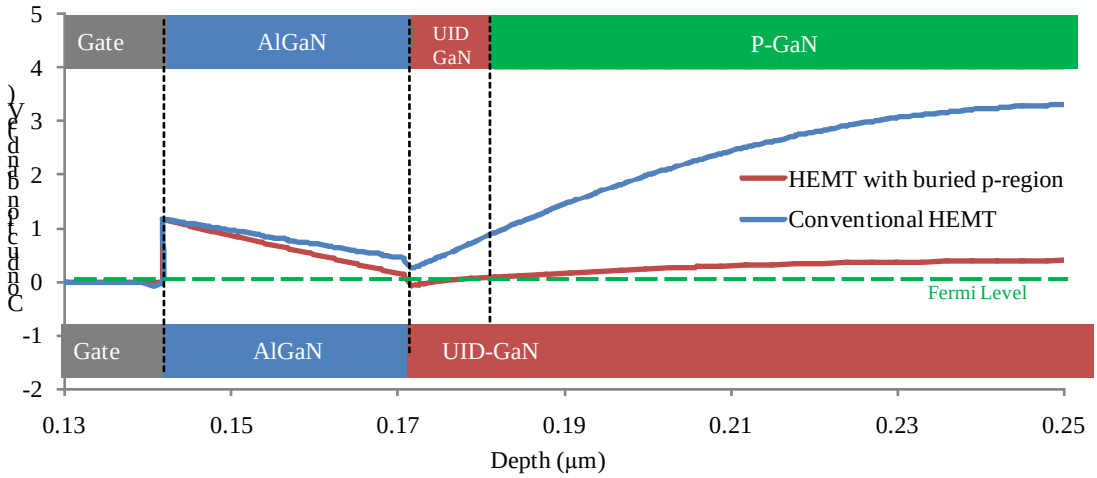

Figure 4.1 Band diagram of a conventional normally-on HEMT and the HEMT with a buried p-region showing normally-off operation in the later

The position of p-region below the channel in the UID-GaN layer gives rise to the name "buried p-region". A sensitivity analysis is performed, showing the effect of the doping concentration, position and dimensions of the p-region on the threshold voltage of the device. Moreover, the study includes the effect of a buried p-region in the case of the Gate Injection Transistor (GIT).

4.2. HEMT with buried p-region

The schematic cross-section of the simulated structure is shown in figure 4.2. The dimensions and physical parameters are taken the same as the normally-on HEMT used for calibration (figure 2.5). A p-GaN region is introduced below the AlGaN/GaN interface. The distance

between the top of the p-region and the AlGaN/GaN interface is "d". The thickness and width of the p-GaN region are named "P_{th}" and "P_w" respectively.

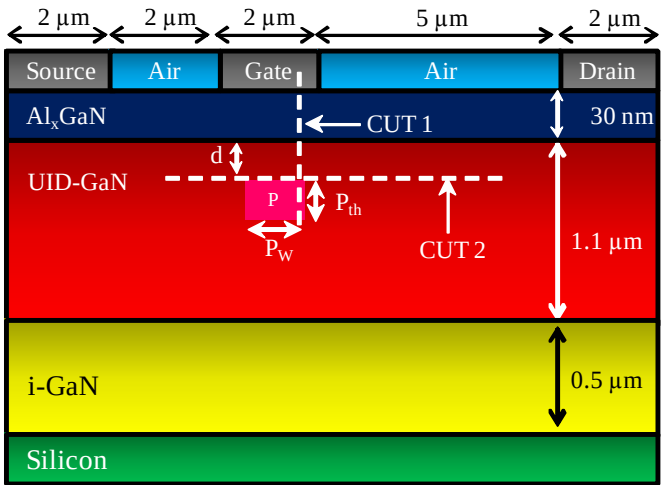

Figure 4.2 Schematic cross-section of the simulated HEMT with buried p-region

Before starting the sensitivity analysis, it is worth noting that all the variations in the threshold voltage will be explained from the shape of the band diagram through CUT 1 and CUT 2 in figure 4.2.

It is well known that in p-doped semiconductors the Fermi level shifts towards the valence band and, as the p-doping concentration increases, the shift increases. This shift can be seen as an increase in the gap between the conduction band and the Fermi level. In semiconductor devices, since at equilibrium the Fermi level is constant, the increase in the gap between the conduction band and the Fermi level will result in the uplifting of the conduction band in the region where p-dopants are introduced.

Consider a pure p-doped semiconductor without any surrounding influencing its band diagram. The Fermi level will be shifted towards the valence band and the energy gap between the conduction band and the Fermi level will be equal to E_{CF0}.

However, in semiconductor devices, the gap between the conduction band and the Fermi level and hence the uplifting of the former strongly depends on the environment surrounding the p-region. In this case, the gap between the conduction band and the Fermi level will vary inside the p-region and is denoted by E_{CF}. For E_{CF} to reach E_{CF0}, the p-region must achieve certain dimensions that will be discussed in the following chapter.

4.2.1. Effect of the width of the p-region P_w

Figure 4.3 shows an example of the variation of the threshold voltage with the width of the p-region "P_w".

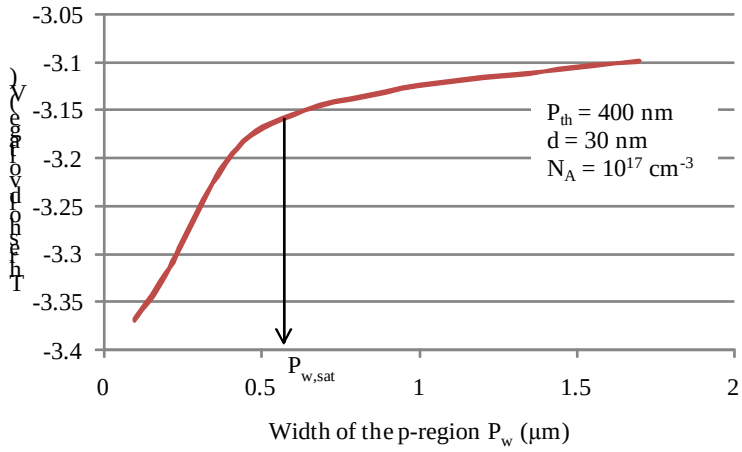

Figure 4.3 Variation of the threshold voltage with the width of the p-region

In this simulation, the doping concentration of the p-region N_A is considered constant throughout the p-region (uniform distribution) and equal to 10^{17} cm^{-3}. P_{th} and d are 400 nm and 30 nm respectively. The threshold voltage increases with increasing P_w until a point is reached where further increase in P_w barely affects the threshold voltage. Let $P_{w,sat}$ denotes the width above which no significant increase in the threshold voltage is observed. To explain these variations, the band diagrams along CUT 2 in figure 4.2, for different values of P_w, are shown in figure 4.4.

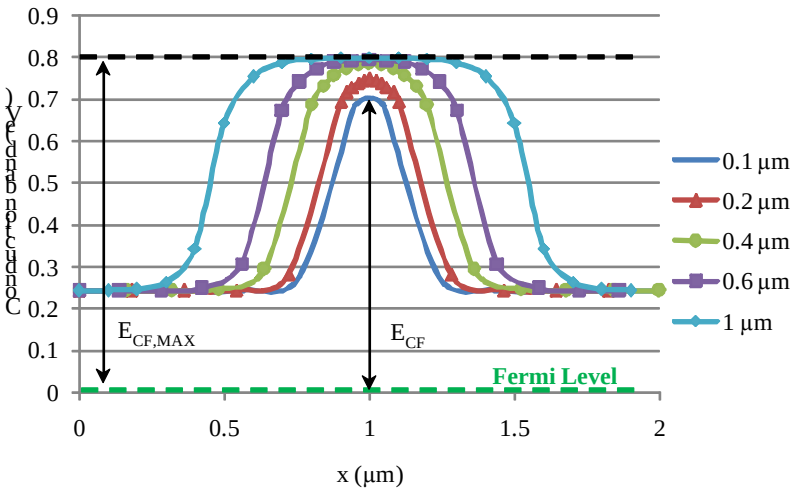

Figure 4.4 Band diagrams along CUT2 in figure 4.2 showing the uplifting of the conduction band in the p-region

For the p-region to properly establish itself inside a device, a certain width is required. The full potential of the p-region in shifting the threshold voltage is obtained once E_{CF} inside the p-region reaches its maximum value $E_{CF,MAX}$. It worth noting that the highest value $E_{CF,MAX}$ can reach is E_{CF0}. In figure 4.4, E_{cf} inside the p-region increases with increasing P_w. This corresponds to the increase in the threshold voltage with P_w. The width at which E_{CF} reaches $E_{CF,MAX}$ is $P_{w,sat}$. In figure 4.4, due to the positive bound charge at the AlGaN/GaN interface, $E_{CF,MAX}$ fails to reach E_{CF0} (E_{CF0} = 3.351 eV for a p-doping of 10^{18} cm^{-3}).

One of the most important aspects in the buried p-region is that its width "P_w" should not exceed the width of the gate. As mentioned before, the buried p-region will elevate the triangular well above the Fermi level. This will cause channel depletion above the p-region at zero gate voltage. However, the channel electrons below the gate can be restored by applying a positive gate voltage. Assume that the width of the p-region exceeds that of the gate, the channel electrons located above the p-region will be depleted, and, since the gate can only restore electrons located below it, some regions, even after the application of a positive gate voltage, will remain depleted as shown in figure 4.5. In that case, the HEMT will never turn on.

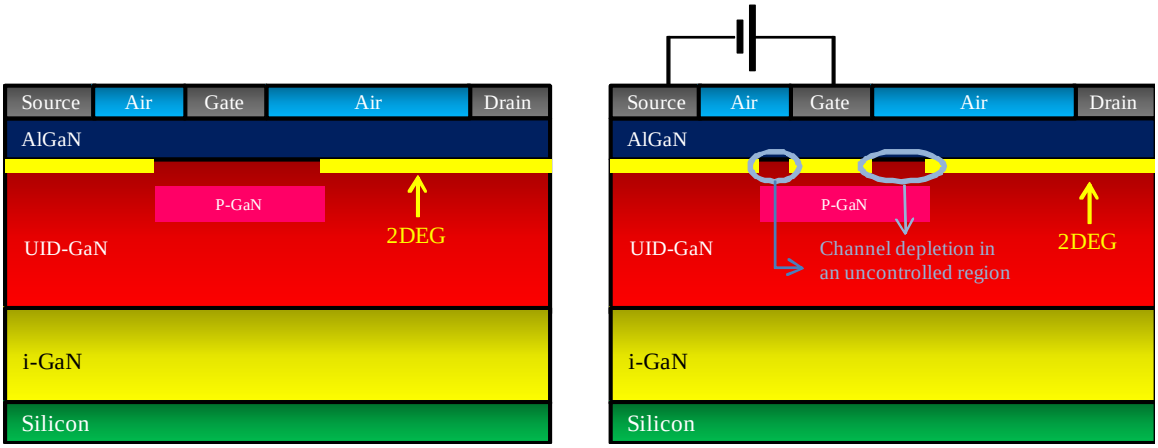

Figure 4.5 Schematic cross -section showing the distribution of the 2DEG before and applying a gate voltage for a HEMT with a buried p-region having a wider width than that of the gate. The device will never turn on regardless of the applied gate voltage

4.2.2. Effect of the thickness of the p-region P_{th}

Figure 4.6 shows an example of variations of the threshold voltage with the thickness of the p-region "P_{th}" at various doping concentrations.

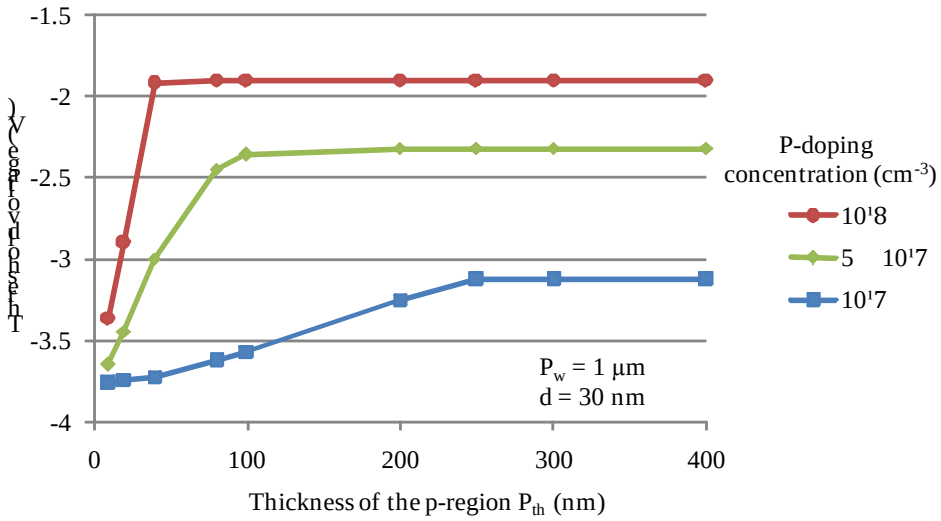

Figure 4.6 Variations of the threshold voltage with the thickness of p-region "P_{th}" at various doping concentrations

It is clear that the variations of the threshold voltage mimic the variation with P_w. The threshold voltage increases with increasing P_{th} until a point is reached (P_{th} = $P_{th,sat}$) where further increase in P_{th} does not affect the threshold voltage. Using a width of 1 µm ensures that p-region establishes itself in the horizontal direction. To see the variations of the band diagrams in the vertical direction, the conduction band along CUT1 in figure 4.2 is shown in figure 4.7 for various P_{th}.

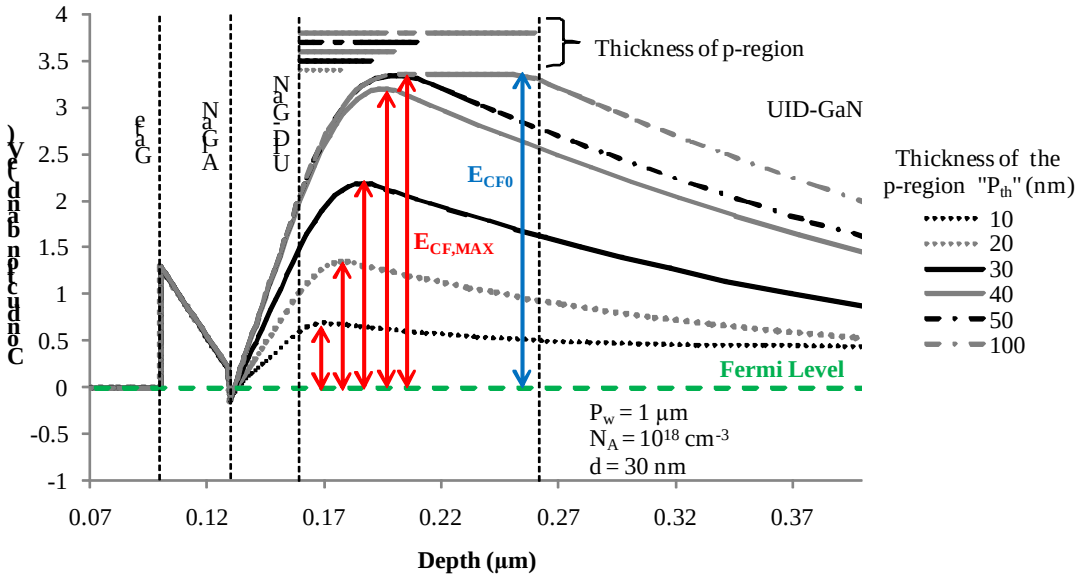

Figure 4.7 Band diagrams along CUT 2 in figure 4.2 showing the profile of the conduction band for different values of P_{th}

Although p-doping increases the gap between the Fermi level and the conduction band, when a p-doped region is inserted between 2 other layers, the gap is affected by its surrounding. For the gap of the sandwiched p-region (E_{CF}) to be equal to the gap of a p-region with no surrounding (E_{CF0}), a certain thickness, dependent on the doping concentration, must be obtained. In other words, inside a sandwiched p-doped region, E_{CF} will increase with increasing the thickness, and if the thickness is big enough, E_{CF} can reach a constant value ($E_{CF,MAX}$) equals to E_{CF0}. Once the thickness of the p-region allows $E_{CF,MAX}$ to reach E_{CF0}, no further increase in the threshold voltage will be obtained when further increasing P_{th}.

It can be seen from Figure 4.7, at the doping concentration of 10^{18} cm^{-3}, when the thickness is below 50 nm, the gap ($E_{CF,MAX}$) increases with increasing the thickness; however, it fails to reach 3.351 eV (E_{CF0} for a p-doping of 10^{18} cm^{-3}). On the other hand, when the thickness is 50 nm and above, the increase in the gap in the p-doped region reaches its limit which is 3.37 eV ($E_{CF,MAX} = E_{CF0}$).

To explain the decrease in $P_{th,sat}$ with increasing the doping concentration, the band diagrams along CUT 1 in figure 4.2 are shown in figure 4.8 for two doping concentrations.

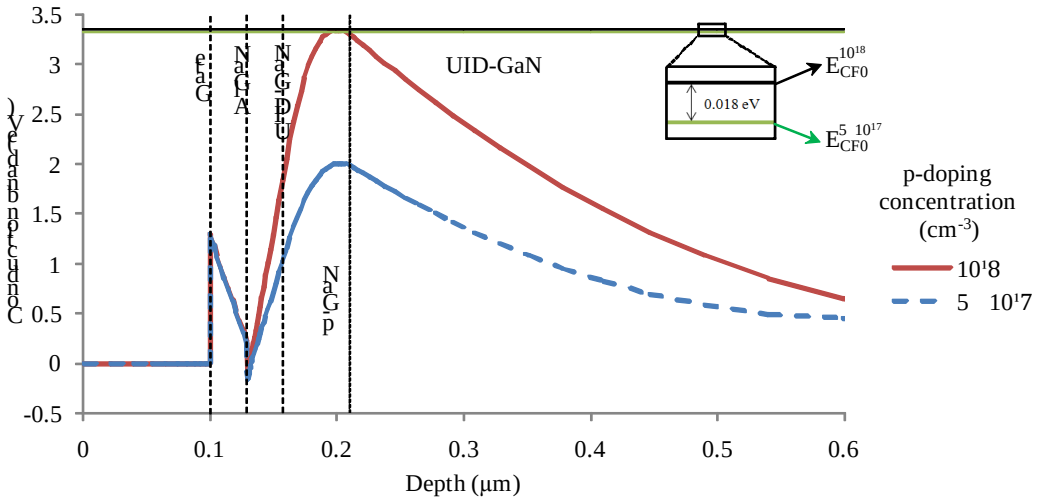

Figure 4.8 Band diagrams along CUT 2 in figure 4.2 showing the profile of the conduction band for two different doping concentrations at P_{th}=50 nm. With higher doping concentrations, shorter thicknesses are required for $E_{CF,MAX}$ to reach E_{CF0}

It can be seen that at, a thickness of 50 nm ($P_{th,sat}$ for a doping concentration of 10^{18} cm^{-3}; $P_{th,sat}^{10^{18}}$), $E_{CF,MAX}$ reaches E_{CF0} for a doping concentration of 10^{18} cm^{-3} but fails to do the same at the doping of 5×10^{17} cm^{-3}. With higher doping concentrations, shorter thicknesses are required for $E_{CF,MAX}$ to reach E_{CF0}.

Although the threshold voltage increases with increasing the thickness of the p-region, the threshold voltage remains negative and hence the HEMT remains normally-on. This is because, in the above studied structure, the p-region was not "strong" enough to lift the triangular well above the Fermi level. The positive bound charge at the AlGaN/GaN interface is pushing the triangular well downwards. So, in order to lift the triangular well above the Fermi level and hence achieve normally-off operation, either the downward push of the triangular well must be decreased or the effectiveness of the p-region must be increased.

4.2.3. Effect of x-mole fraction: decreasing the download push of the triangular well

As mentioned before, the positive bound charge at the AlGaN/GaN interface is pushing the triangular well downwards. This push increases with increasing the density of positive bound charge. The aim of inserting the p-region below the channel was to overcome the downward push of the triangular well by uplifting the conduction band in the vicinity of the AlGaN/GaN interface. But since the uplift of the conduction band in the p-region was insufficient to elevate the triangular well above the Fermi level, we suggest the decrease in the downward push of the triangular well. That can be done by decreasing the bound charge density at the interface by decreasing the x-mole fraction in the AlGaN layer. Indeed, a decrease in the x-mole fraction will reduce the strain in the AlGaN layer resulting in the reduction of the piezoelectric polarization field and hence lower bound charge. Note that, the bound charge can be reduced also by decreasing the thickness of the AlGaN layer as mentioned in section 1.7.3.

Figure 4.9 shows as example of variations of the threshold voltage with the thickness of the p-region at various x-mole fractions. It can be seen that, while a doping concentration of 5×10^{17} cm^{-3} fails to shift the threshold voltage to positive values at an x-mole fraction of 0.25, normally-off operation was achieved when the x-mole fraction was reduced to 0.15. In figure 4.10, the band diagrams show the uplifting of the conduction band above the Fermi level when the x-mole fraction is decreased.

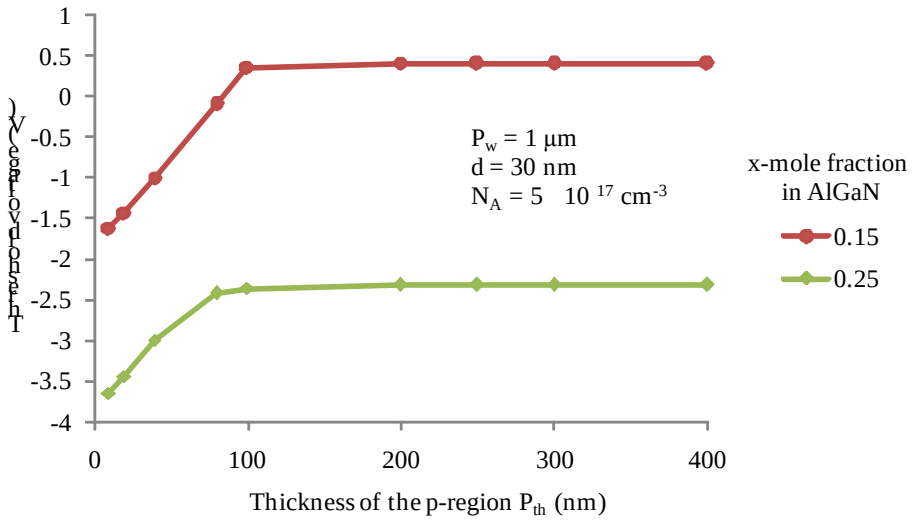

Figure 4.9 Variation of the threshold voltage with the thickness of p-region "P_{th}" at various x-mole fractions

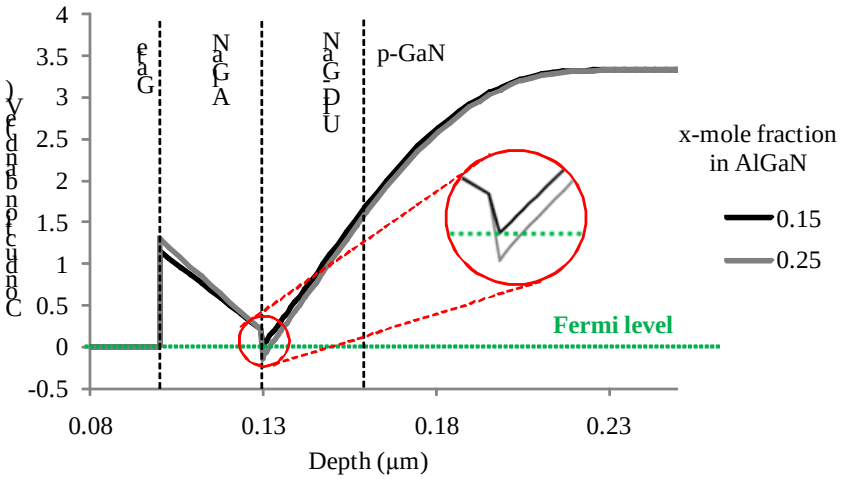

Figure 4.10 Band diagrams along CUT 2 in figure 4.2 showing the profile of the conduction band at two different doping x-mole fractions for P_{th}=200 nm. The elevation of the triangular well above the Fermi level is obtained at an x-mole fraction of 0.15 (see zoom)

The other way to achieve normally-off operation is to increase the effectiveness of the p-region. This can be done by either decreasing the distance between the p-region and the AlGaN/GaN interface or increasing the p-doping concentration N_A.

4.2.4. Effect of p-doping concentration

Figure 4.11 shows an example of variations of the threshold voltage with the doping concentration in the p-region at various distances "d" from the AlGaN/GaN interface. It can be seen that the threshold voltage increases with increasing the doping concentration.

However, there exists a doping concentration above which further increase in the doping concentration barely affects the threshold voltage. This can be seen at d = 30 nm, at doping concentrations beyond 10^{19} cm^{-3}. This phenomenon was not observed in the case of 10 and 20 nm since the doping concentration, at which the threshold voltage saturates shifts the threshold voltage to values beyond the forward gate voltage. The band diagram along CUT1 in figure 4.2, at d = 10 nm, is shown in figure 4.12 for various doping concentrations.

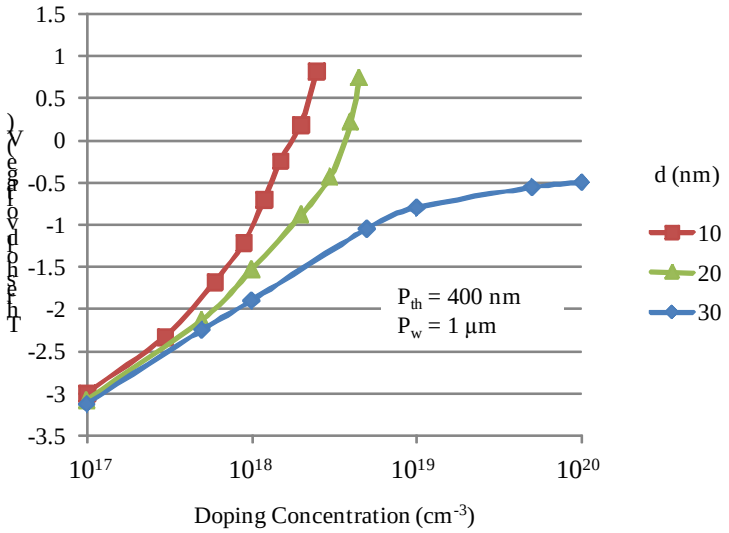

Figure 4.11 Variations of the threshold voltage with the doping concentration in the p-region at various distances

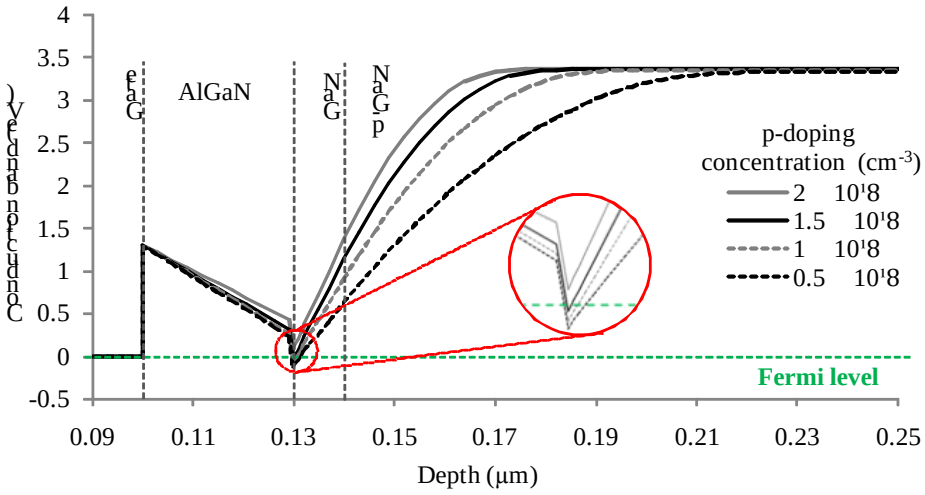

Figure 4.12 Band diagrams along CUT1 in figure 4.2 showing the profile of the conduction band at different p-doping concentrations; d = 10 nm

Normally-off operation is achieved at a doping concentration of 2×10^{18} cm^{-3}. This is shown in the zoomed part of figure 4.12 where the conduction band is uplifted above the Fermi level.

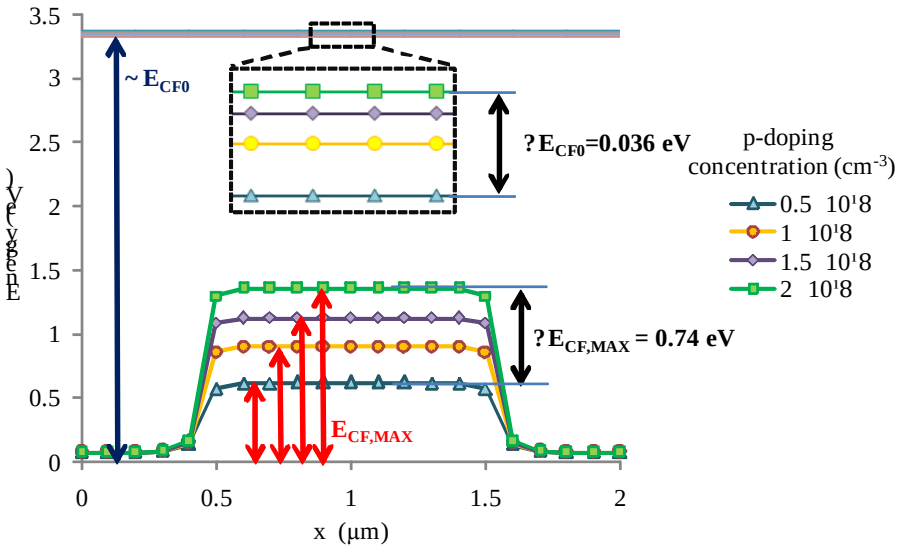

Figure 4.13 Band diagrams along CUT2 in figure 4.2 showing the profile of the conduction band at different doping concentrations; d = 10 nm

It is worth noting that the thickness and width of the p-region are always taken large enough to insure maximum efficiency in terms of shifting the threshold voltage. In our simulation: P_w = 1 µm and P_{th} = 400 nm. The band diagrams along CUT2 in figure 4.2, at d = 10 nm, are shown in figure 4.13 at various doping concentrations. It can be seen that the increase in the threshold voltage does not only come from the increase in E_{CF0} with doping concentration, but majorly from the rate of increase in E_{CF} inside the p-region (figure 4.12). In other words, when increasing the doping concentration, the increase in $E_{CF,MAX}$ is much higher than the increase in E_{CF0} ($\Delta_{ECF0} < \Delta_{ECF,MAX}$; figure 4.13).

4.2.5. Effect of the distance "d" between p-region and the AlGaN/GaN interface

The distance "d" between the top of the p-region and the AlGaN/GaN interface is one of the most sensitive parameters in this structure. An example of variations of the threshold voltage with the distance d is shown in figure 4.13 for different doping concentrations. Two important things can be noted out. First, the effectiveness of the p-region increases when the p-region approaches the AlGaN/GaN interface since the threshold voltage increases with decreasing d. However, the rate of increase strongly depends on the doping concentration. Secondly, the increase in the threshold voltage with the doping concentration depends on the

distance d. As the p-region starts approaching the AlGaN/GaN interface, the sensitivity of threshold voltage to the doping concentration starts to increase. For example, at d=10 nm the threshold voltage increases from -1.8 V to 0.18 V when the doping concentration is increased from 5×10^{17} cm^{-3} to 2×10^{18} cm^{-3}. On the other hand, when d = 60 nm, such increase in the doping concentration barely affects the threshold voltage.

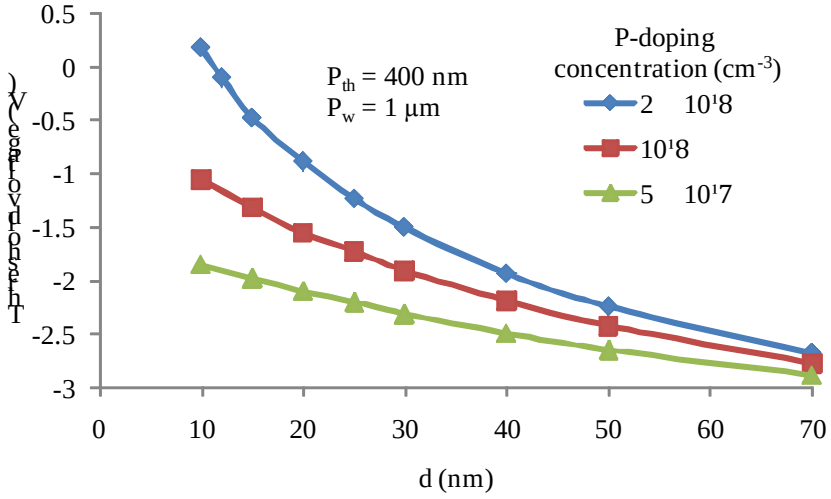

Figure 4.14 Variations of the threshold voltage with d at various doping concentrations

4.3. MIS-HEMT with a buried p-region

Although the buried p-region grants the HEMT normally-off operation, the gate leakage limits the increase in the threshold voltage. Therefore, an insulating layer is introduced below the gate to eliminate the gate leakage.

In this work, three different insulators are used: Silicon Oxide (SiO_2), Silicon Nitride (Si_3N_4) and Hafnium Oxide (HfO_2). An ideal case is studied in which no fixed charge is present inside the insulator or at the insulator/barrier interface. The aim of using different types of insulators is to see the effect of the permittivity of the insulator on the transfer characteristics of the device. The relative permittivity (ε_r) of SiO_2, Si_3N_4 and HfO_2 is 3.9, 7.5, and 25 respectively. The structure for all the coming MIS-HEMT simulations is shown in figure 4.15. P_{th}, P_w and d are equal to 400 nm, 1 µm and 10 nm respectively; The value of these parameters were chosen according to our previous studies.

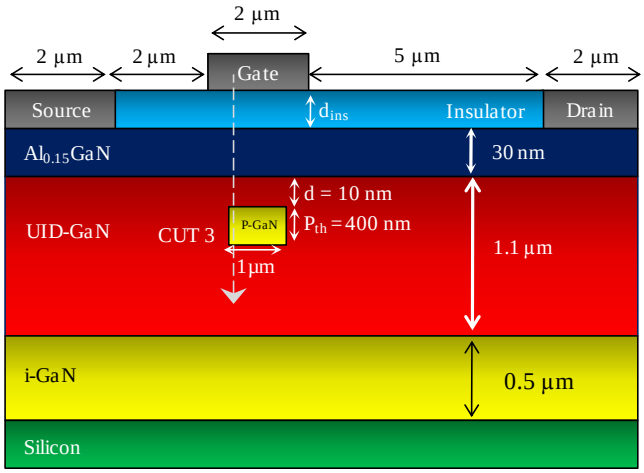

Figure 4.15 Schematic cross-section of the simulated MIS-HEMT with a buried p-region

4.3.1. Variation with doping concentration

In figure 4.16, the variations of the threshold voltage with N_A, at d_{ins} = 10, 20 and 40 nm, are illustrated. The insulator used is Si_3N_4. As in section 4.2.4, the threshold voltage increases with increasing N_A up to a point ($N_A = N_{A,Optimum}$) where further increase in the doping concentration barely affects the threshold voltage.

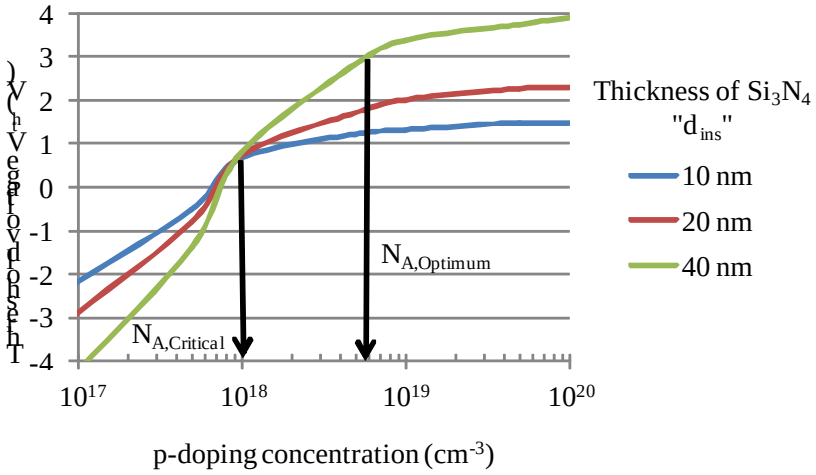

Figure 4.16 Variations of the threshold voltage with the p-doping concentration "N_A" at various thicknesses of the insulator

Moreover, all the curves corresponding to various d_{ins}, intersect at a common point. The doping concentration associated with this point is named $N_{A,critical}$ and will be further discussed in the coming sections.

4.3.2. Variations of the threshold voltage with thickness of the insulator

To further explore the effect of the thickness of the insulator on the threshold voltage, d_{ins} is varied from 10 nm to 160 nm. The variations of the threshold voltage with the thickness of the insulator at various p-doping concentrations are shown in figure 4.17.

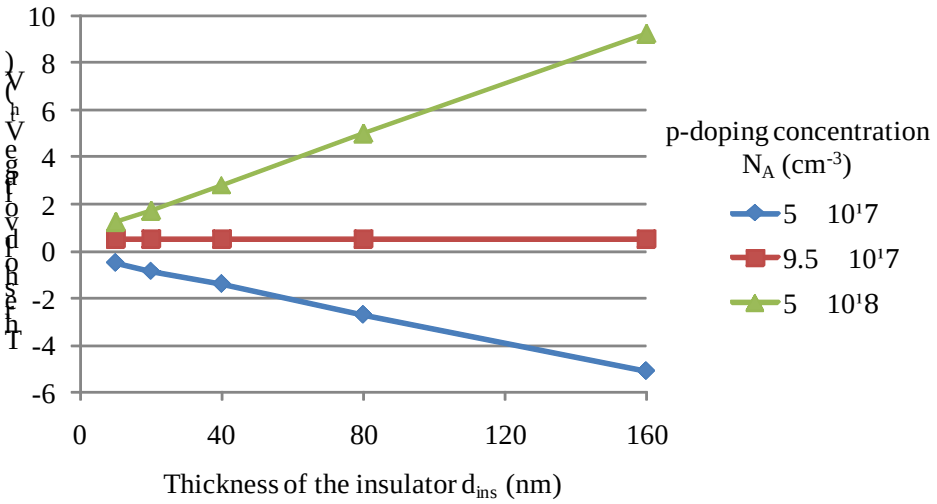

Figure 4.17 Variations of the threshold voltage with the thickness of the insulator at various p-doping concentrations

It is clear that the variation of V_{th} with d_{ins} strongly depends on N_A. The doping concentration $N_{A,critical}$ at which the threshold voltage is not affected by the thickness of the insulator, is equal to 9.5×10^{17} cm^{-3}. This concentration corresponds to the intersection point in figure 4.16.

For $N_A < N_{A,critical}$, the threshold voltage decreases with increasing d_{ins}. On the other hand, when $N_A > N_{A,critical}$, the threshold voltage increases with increasing d_{ins}.

4.3.3. Variations with the permittivity of the insulator

In this section, the effect of the permittivity of the insulator on the transfer characteristics is examined. Three different insulators are used: SiO_2, Si_3N_4 and HfO_2 with a relative permittivity of 3.9, 7.5 and 25 respectively. Figure 4.18 shows the variations of the threshold voltage with the permittivity of the insulator at various p-doping concentrations.

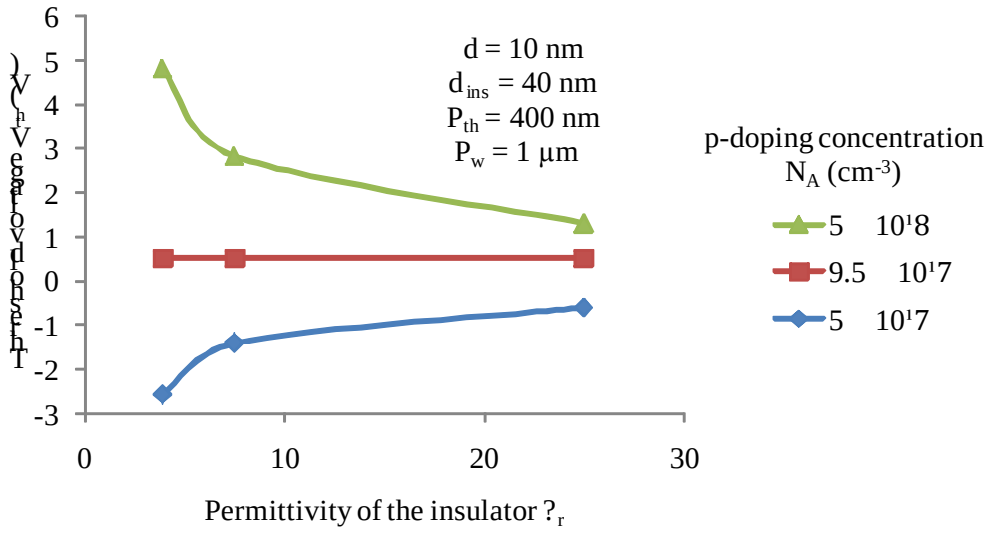

Figure 4.18 Variations of the threshold voltage with the permittivity of the insulator at various p-doping concentrations

It can be noted that the variations with respect to the permittivity of the insulator mimics the variations with respect to the thickness of the insulator. When $N_A = N_{A,critical}$, no variation in the threshold voltage is observed with increasing ε_r. For $N_A < N_{A,critical}$, the threshold voltage decreases with increasing ε_r. On the other hand, when $N_A > N_{A,critical}$, the threshold voltage increases with increasing ε_r.

However, the rate of change in the threshold voltage with the thickness of the insulator depends on the permittivity of the material. Figure 4.19 shows the variations of the threshold voltage with the thickness of the insulator at $N_A = 5 \times 10^{17} < N_{A,critical}$ for three different insulators. It can be seen that, although the threshold voltage decreases with increasing the thickness of the insulator, the rate of decrease is more severe when the permittivity of the insulator is decreased.

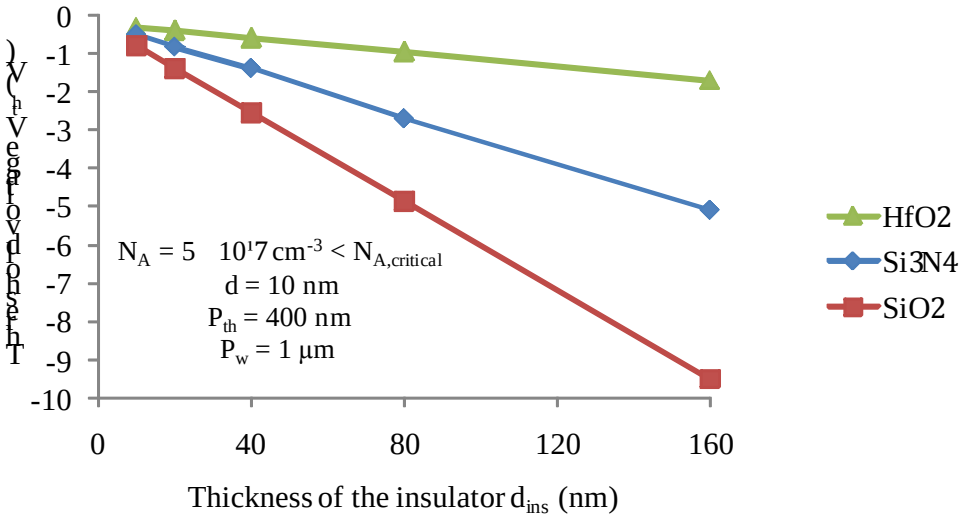

Figure 4.19 Variations of the threshold voltage with the thickness of the insulator at $N_A < N_{A,critical}$ for three different insulators

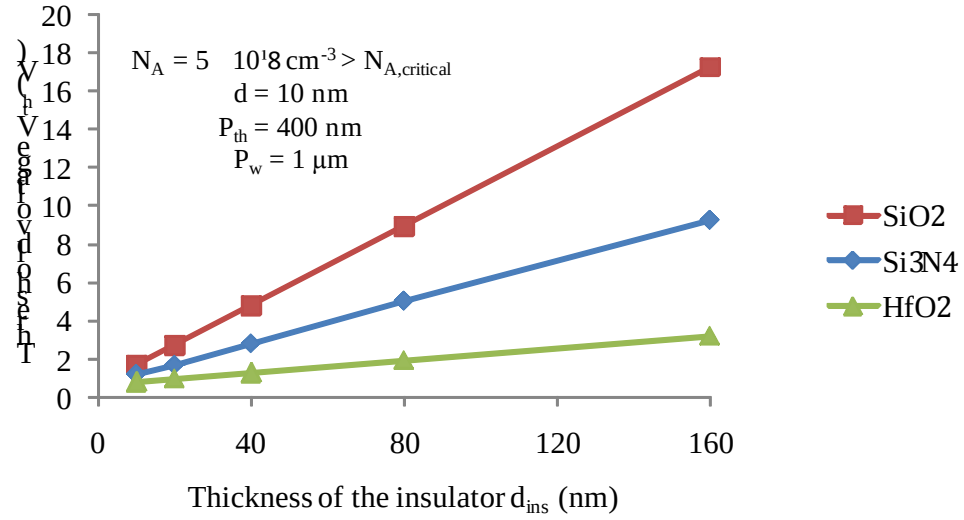

Figure 4.20 Variations of the threshold voltage with the thickness of the insulator at $N_A > N_{A,critical}$ for three different insulators

The same applies for the rate of increase on the threshold voltage with the thickness of the insulator when $N_A = 5 \times 10^{17} > N_{A,critical}$. As shown in figure 4.20, the threshold voltage increases with increasing the thickness of the insulator. However, as the permittivity of the insulator increases, the rate of increase of the threshold voltage increases.

4.4. Comparison between the HEMT with a buried p-region and the Gate Injection Transistor (GIT)

To address the advantages and drawbacks of the proposed structure, a comparison with a previously proposed normally-off Gate Injection Transistor (GIT) is performed.

4.4.1. Gate Injection Transistor

The Gate Injection Transistor is a normally-off HEMT that uses a p-region above the AlGaN layer (barrier layer) only below the gate [37]. Its schematic cross-section is shown in figure 4.21. The conduction band is lifted in the p-region causing the triangular well at the AlGaN/GaN interface to elevate. Normally-off operation is achieved when the uplift of the conduction band in the p-region is strong enough to elevate the triangular well above the Fermi level. The band diagram of the GIT along CUT3 in figure 4.21 is shown in figure 4.22, pointing out the mechanism used in this structure to achieve normally-off operation.

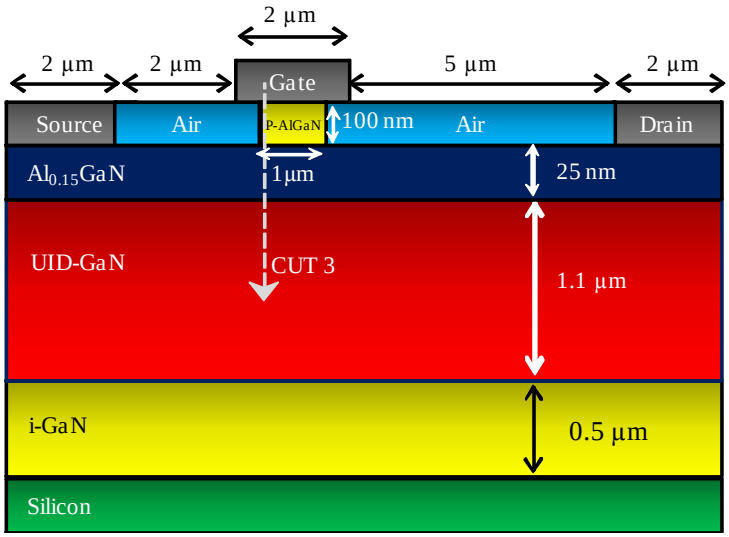

Figure 4.21 Schematic cross-section of the simulated Gate Injection Transistor (GIT). This structure is compared to our proposed structure (HEMT with buried p-region)

Similar to the HEMT with buried p-region, the threshold voltage of GIT is affected by the doping concentration and dimensions of the p-AlGaN region as well as the distance between the p-region and the AlGaN/GaN interface. In all the coming simulations of the GIT, the dimensions of the p-AlGaN region are optimized in way to obtain a maximum shift in the threshold voltage.

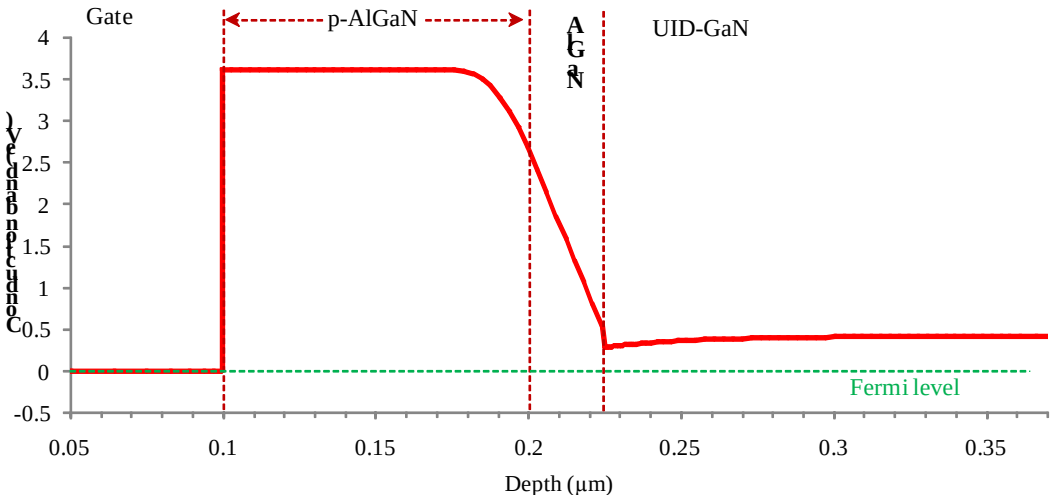

Figure 4.22 Band diagram of the Gate Injection Transistor showing the uplifting of the conduction band in the p-AlGaN region which elevates the triangular well above the Fermi level at the AlGaN/GaN interface

4.4.2. HEMT with a buried p-region versus GIT

In this section, a comparison with the GIT is performed aiming to point out the advantages and drawbacks of our proposed structure. In the proposed GIT, the optimized thickness and x-mole fraction of the AlGaN layer are 25 nm and 0.15 respectively. The x-mole fraction of the p-AlGaN cap layer is 0.15 [38].

For a fair comparison between the proposed structure and the GIT, the same physical parameters are used for both structures (thickness and doping of GaN and AlGaN). In both cases, the thickness and width of the p-GaN region are 100 nm and 1 µm respectively. Moreover, the distance between the p-region and the AlGaN/GaN interface is 25 nm in both cases (thickness of AlGaN layer = "d" = 25 nm). The p-doping concentration will be increased until normally-off operation in both structures is achieved. The chosen “normally-off” criterion is a threshold voltage of 0.5 V.

The schematic cross-section of the simulated normally-off GIT is shown in figure 4.21. As for our proposed structure, the schematic cross-section is the same as the one shown in figure 4.2, expect for the thickness and x-mole fraction that are reduced to 25 nm and 0.15 respectively.

An example of variations of the threshold voltage and the forward gate voltage are shown for the GIT in figure 4.23 and for the HEMT with buried p-region in figure 4.24. These values are extracted at V_{ds}=1 V.

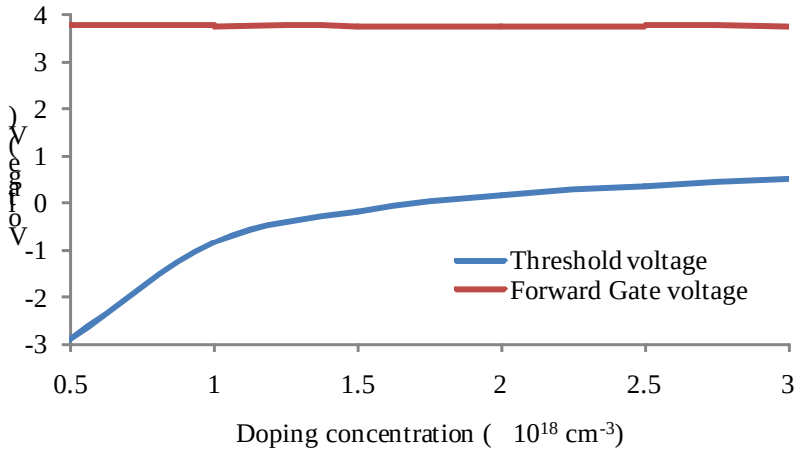

Figure 4.23 Variations of threshold voltage and forward gate voltage of the GIT with the doping concentration. A threshold voltage of 0.5 V was achieved at a doping concentration of 3×10^{18} cm^{-3}; at this doping concentration, the forward gate voltage was 3.7 V. Values are extracted at V_{ds} =1 V

To achieve a threshold voltage of 0.5 V, a doping concentration of 3×10^{18} cm^{-3} is required in the case of GIT while 5×10^{17} cm^{-3} is sufficient in our proposed structure. Therefore, the proposed structure is more efficient when it comes to the doping concentration required to achieve normally-off operation. On the other hand, the forward gate voltage is much higher in the case of the Gate Injection Transistor. This is attributed to the use of p-AlGaN gate in the GIT rather than a Schottky gate. The low forward gate voltage in our proposed structure limits the increase in the threshold voltage to higher values.

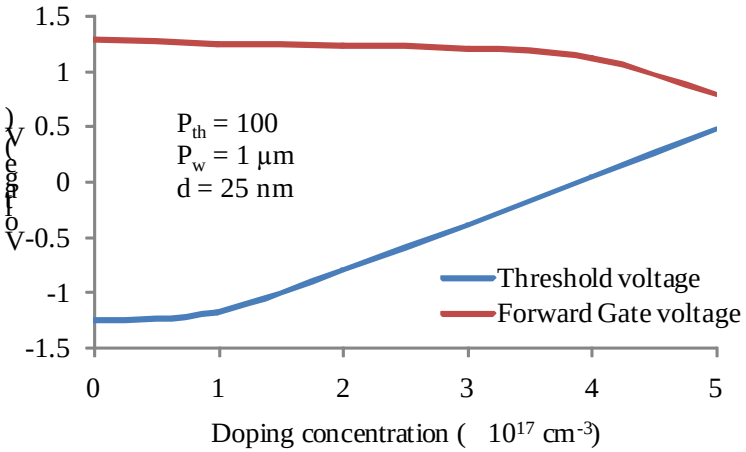

Figure 4.24 Variations of threshold voltage and forward gate voltage of our proposed with the doping concentration. A threshold voltage of 0.5 V was achieved at doping concentration of 5×10^{17} cm^{-3}; at this doping concentration, the forward gate voltage was 0.8 V. Values are extracted at V_{ds} =1 V

To address the quality of the triangular well in which the channel electrons are confined, the band diagrams for both structures, along CUT1 in figure 4.2 and CUT3 in figure 4.23, are shown in figure 4.25. It is clear that the confinement of the 2DEG is superior in our case. This better confinement will lead to higher mobility. However, in our simulation the mobility of the 2DEG, in all cases, was fixed to 1500 cm^2/v.sec. This hinders the comparison of the on-state resistance and transconductance for the two structures.

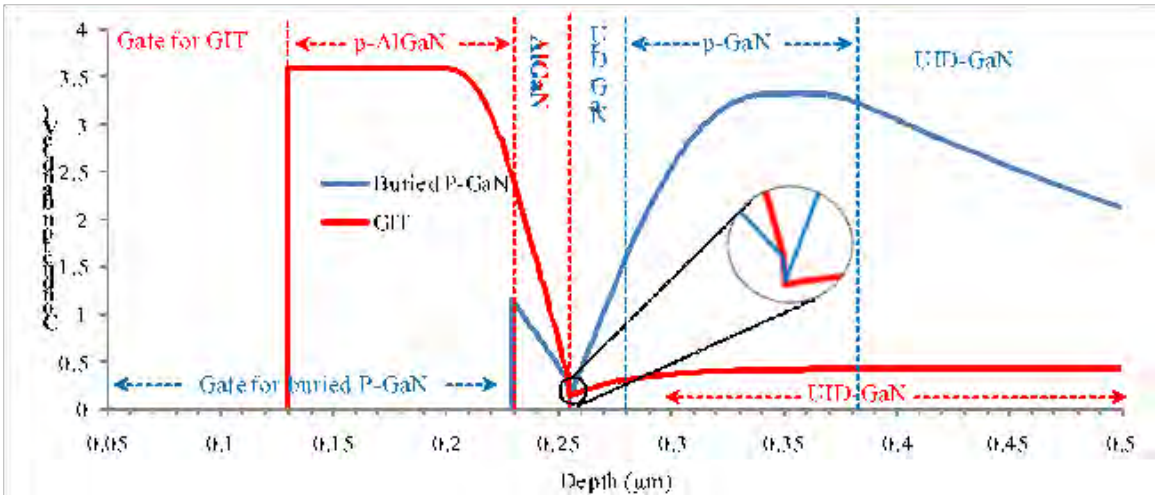

Figure 4.25 Band diagrams of the Gate Injection Transistor and the HEMT with a buried p-GaN region corresponding to a threshold voltage of 0.5 V with a p-doping concentration of 3 × 10^{18} cm^{-3} and of 5×10^{17} cm^{-3} respectively. The zoomed part shows a better triangular well in the case of HEMT with a buried p-GaN region

4.4.3. Hybrid normally-off GIT with a buried p-region

One of the main potentials of the buried p-region is that it is not only an alternative solution to achieve normally-off operation but also a complementary one. Indeed, the buried p-region can combined with all the proposed normally-off HEMTs. For example: recessed gate and buried p-region, Fluorine implantation in the barrier and a buried p-region or GIT with a buried p-region.

In the GIT, the p-AlGaN region increases the forward gate voltage allowing the structure to attain high current densities and push the limits that hinders further increase in the threshold voltage, while, in the proposed structure, as we attempt to increase the threshold voltage, the forward gate voltage decreases.

On the other hand, in the structure with buried p-region, there is the advantage of approaching the AlGaN/GaN interface without the necessity to decrease the thickness of the

AlGaN layer, which plays an important role in increasing the 2DEG density at the interface (figure 1.20). This is a very important point since, as mentioned before, the effectiveness in shifting the threshold voltage increases as the agent approaches the AlGaN/GaN interface.

To merge the advantages of the two structures, a GIT with a buried p-region is studied. The schematic cross-section of the hybrid structure is shown in figure 4.26.

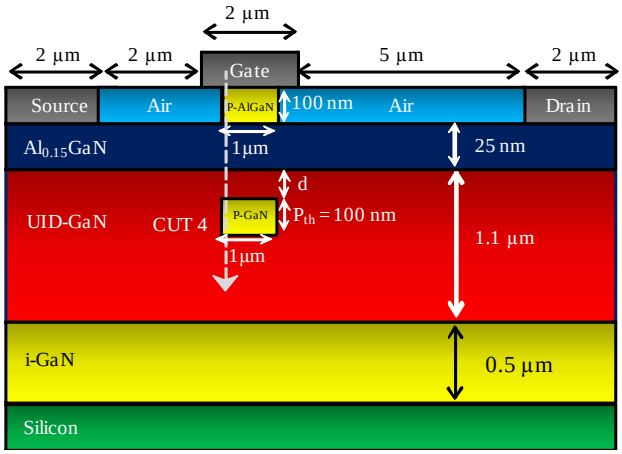

Figure 4.26 Schematic cross-section of the hybrid Gate Injection Transistor (GIT) with a buried p-GaN region

The width and thickness of both p-regions are 1 µm and 100 nm respectively. The distance between the buried p-region and the AlGaN/ GaN interface is 25 nm. The AlGaN thickness is 25 nm and the x-mole fraction of the AlGaN layers is 0.15.

An example of variations of the threshold voltage and the forward gate voltage with doping concentration in both regions are shown in figure 4.27.

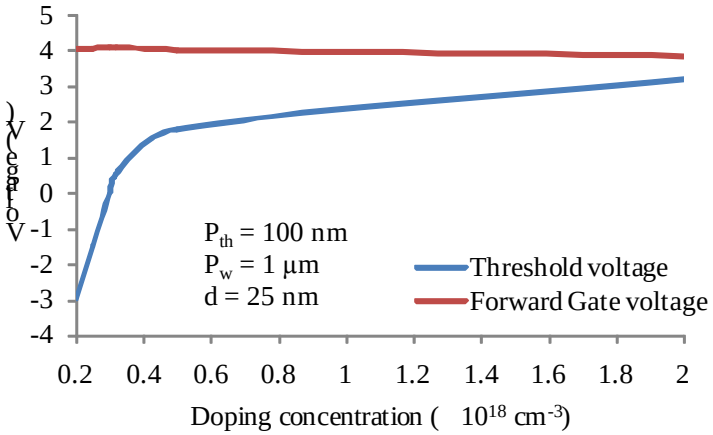

Figure 4.27 Variations of threshold voltage and forward gate voltage of the GIT with buried p-region with the doping concentration. A threshold voltage of 0.5 V was achieved at doping concentration of 3.2×10^{17} cm^{-3}; at this doping concentration, the forward gate voltage was 3.7 V. Values are extracted at V_{ds} =1 V

It can be seen that the threshold voltage increases with increasing the doping concentration. Moreover, the high forward gate voltage is inherited from the GIT.

It is important to point out that a relatively low doping concentration is required to achieve a threshold voltage of 0.5 V when compared to the GIT and to the HEMT with a buried p-region. This is because the triangular well at the AlGaN/GaN interface is uplifted from both sides as shown in figure 4.28.

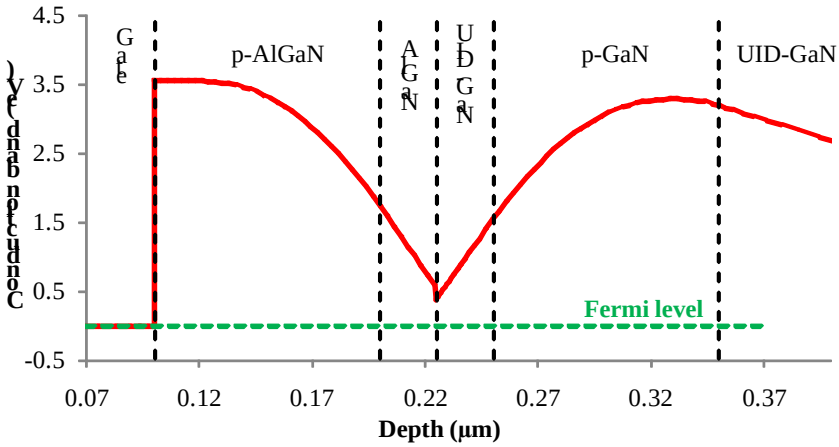

Figure 4.28 Band diagram of the Gate Injection Transistor with a buried p-GaN region corresponding to a threshold voltage of 0.5 V with a p-doping concentration of 3.2 × 10^{17} cm^{-3} in both p-regions

To obtain the maximum shift in the threshold voltage, the hybrid structure is studied with "d" decreased to 10 nm and the thickness of the buried p-region increased to 400 nm.

An example of variations of the threshold voltage and the forward gate voltage with doping concentration in both regions are shown in figure 4.29. It can be seen that high threshold voltages can be achieved at reasonable p-doping concentration.

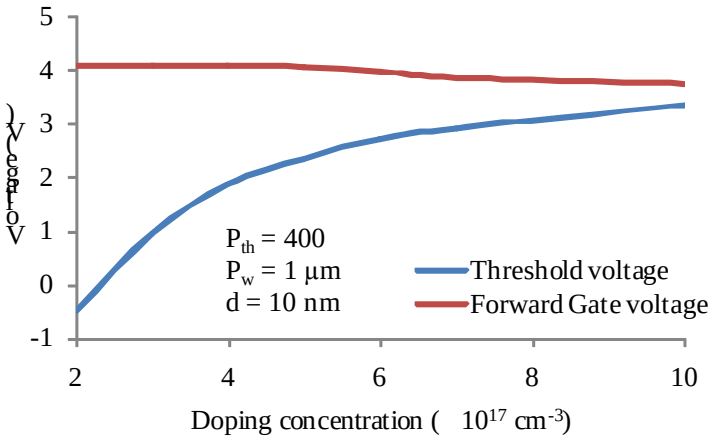

Figure 4.29 Threshold voltage and forward gate voltage of the GIT with buried p-region at various doping concentrations. With optimized parameters high threshold voltages can be reached at reasonable doping concentrations. Values are extracted at V_{ds} =1 V

4.5. New structures easing the fabrication of normally-off HEMTs with a buried p-region

Although the idea of burying a p-region to achieve normally-off operation seems to be promising, the challenges to fabricate such structure remain a big challenge.

The first option is the ion implantation. After growing a GaN layer Mg ions can be implanted in the region that is to be under the gate. Afterwards, a thin GaN layer will be introduced (10-30 nm) and then comes the barrier layer. Although this technique was used before by [77][78] to create Current Blocking Layer (CBL) in Current Aperture Vertical Electron Transistor (CAVET), the resulting doping concentration is relatively low. The second option is the localized epitaxial growth of the p-GaN and its neighboring UID-GaN regions. However, such growth is very challenging and relatively expensive.

These challenges provoke us to think of a way to facilitate the experimental production of a buried p-region. The outcome was the proposal of two new normally-off structures that uses the concept of burying a p-region while remedying the challenges of achieving it.

4.5.1. Structure #1

4.5.1.1. Device design and fabrication process

The schematic cross-section of the first proposed structure is shown in figure 4.30.

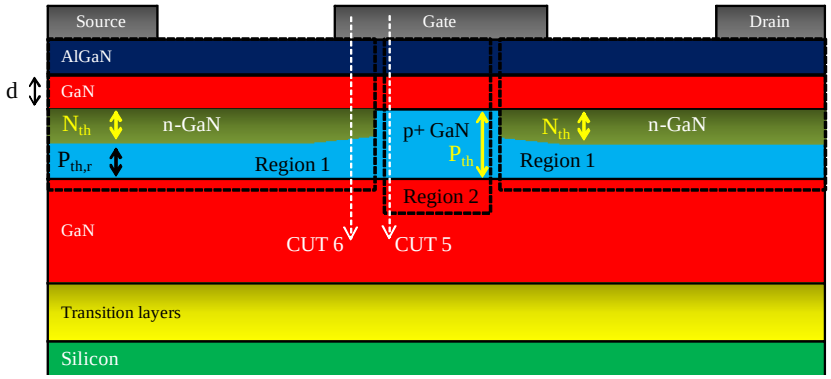

Figure 4.30 Schematic cross-section of structure #1

To achieve this structure experimentally, the following can be done: after the growth of the GaN layer on a substrate, an epitaxial p-layer is grown all over the GaN layer. Afterwards, using ion implantation, n-wells are created in Region 1. Then comes a thin GaN layer (10-50 nm) and finally the barrier layer (AlGaN layer), electrodes and passivation. Fabrication steps

are shown in figure 4.31. It is worth recalling the importance of such technique in serving as both independent and complementary solution for the normally-off HEMTs.

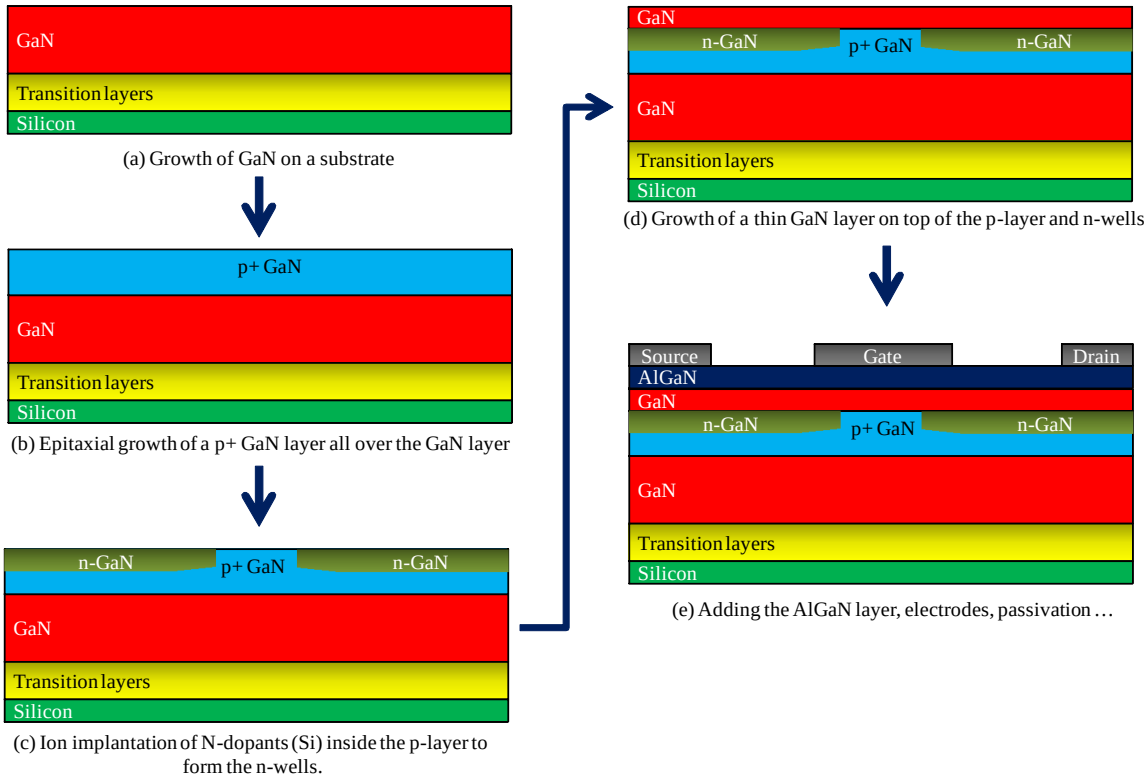

Figure 4.31 Major steps in the fabrication of structure #1

As shown in figure 4.30, the regions where the n-wells are introduced are named Region 1. The remaining region is called region 2. The thickness of the p-layer in region 2 is named P_{th} since it plays the role of the buried p-region (as in section 4.2). The thicknesses of the n-wells are named N_{th}. The remaining thickness of the p-layer in region 1 is named $P_{th,r}$ since it represents the remainings of the p-layer after introducing the n-wells: $P_{th,r} = P_{th} - N_{th}$. The distance between the p-region and the AlGaN/GaN interface "d" is the thickness of the thin GaN layer (figure 4.31 (d)).

4.5.1.2. Conditions for operation

We have previously shown that, in order to achieve normally-off operation, a buried p-region with optimized thickness and doping concentration must be brought close enough to the AlGaN/GaN interface to cause channel depletion. Moreover, in section 4.2.1, it was mentioned that the width of the buried p-region should not exceed the gate width; otherwise the device will remain off regardless of the applied gate voltage.

In the structure shown in figure 4.30, the p-region spans across the whole device. For this device to operate as a normally-off transistor, three conditions must be satisfied:

1 - Region 1 should expand laterally so that the width of region 2 is less than the gate width.

2 - The channel must be depleted in region 2 at V_{gs} = 0 V.

3 - The channel in region 1 should not be depleted at V_{gs}= 0 V.

The second condition was studied in details in chapter 4 where we address the effect of the position, dimensions and doping concentration of the p-region on the threshold voltage. Positive threshold voltage indicates channel depletion at V_{gs} = 0 while negative threshold voltage signals the survival of channel electrons; and the smaller the threshold voltage, the higher the population of channel electrons after the introduction of the p-region. The depleted channel electrons in region 2 can be restored upon the application of a positive gate voltage.

As for the third condition, assuming no N-dopants are introduced (N_{th} = 0), $P_{th,r}$ became equal to P_{th}. This will cause channel depletion in region 1 and the device will remain off regardless of the applied gate voltage. However, after the introduction of the N-dopants, channel electrons in region 1 are retrieved for three reasons:

1- The thickness of the p-layer ($P_{th,r}$) is decreased.

As the depth of the n-wells increases, $P_{th,r}$ decreases ($P_{th,r} = P_{th} - N_{th}$). In section 4.2.2 we have shown that for $P_{th} \leq P_{th,sat}$, the threshold voltage decreases with decreasing P_{th}. This means that, as the thickness of the p-region decreases, the 2DEG density in the channel above it increases.

2- The distance between the remaining p-layer and the AlGaN/GaN interface is increased.

In region 2, the distance between the p-region and the AlGaN/GaN interface equals: N_{th} + d. Therefore, as N_{th} increases, the p-region goes further from the AlGaN/GaN interface. This, according to section 4.2.5, will decrease the threshold voltage which means increasing the 2DEG density above the p-region.

3- The n-GaN well standing between the p-region and the AlGaN/GaN interface has an effect on the 2DEG concentration.

In n-type semiconductors, the Fermi level shifts towards the valance band while, in p-type semiconductors, it shifts towards the conduction band. At equilibrium, the shift in the Fermi level is manifested by an upward push in the conduction band in p-type semiconductors and

by a downward push in n-type semiconductors. In region 1, the n-wells are sandwiched between the p-layer and the AlGaN/GaN interface. If the downward push in the n-region is strong enough to compensate the upward push in the p-region, the channel will remain populated with electrons.

4.5.1.3. Band diagram

In this section, the band diagram is studied in regions 1 and 2 along CUT 5 and CUT 6 of figure 4.30. The doping concentration and thickness of the p-layer are 10^{18} cm^{-3} and 100 nm respectively. For simplicity, the doping concentration in the n-wells "N_{well}" is taken uniform. The thickness and doping concentration of the n-wells are 40 nm and 2×10^{18} cm^{-3} respectively. The thickness of the thin GaN layer between the AlGaN/GaN interface and the p-layer is d = 10 nm.

The band diagram along CUT5 is shown in figure 4.32. It can be seen that the uplift in the p-region elevates the triangular above the Fermi level causing channel depletion at zero gate voltage. This is the reason behind the normally-off operation, as discussed in section 4.2.

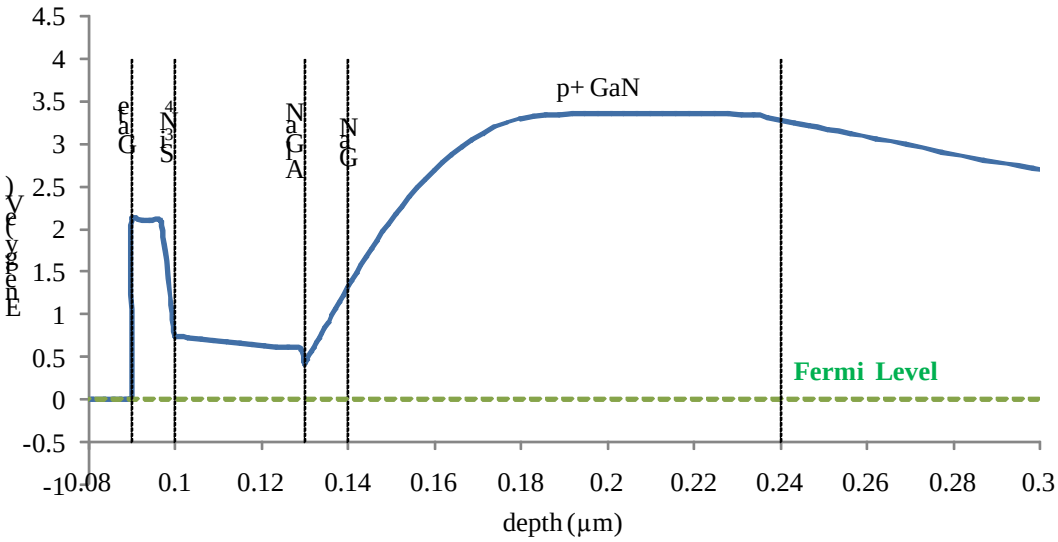

Figure 4.32 Band diagram along CUT 5 in figure 4.30 showing the elevation of the triangular well above the Fermi level, due to uplift of the conduction band in the p-region

The band diagram along CUT 6 is shown in figure 4.33. It can be seen that, although the conduction band is uplifted in the p-region, the n-wells prevent the elevation of the triangular well above the Fermi level and hence the channel electrons remain populating at the AlGaN/GaN interface in region 1.

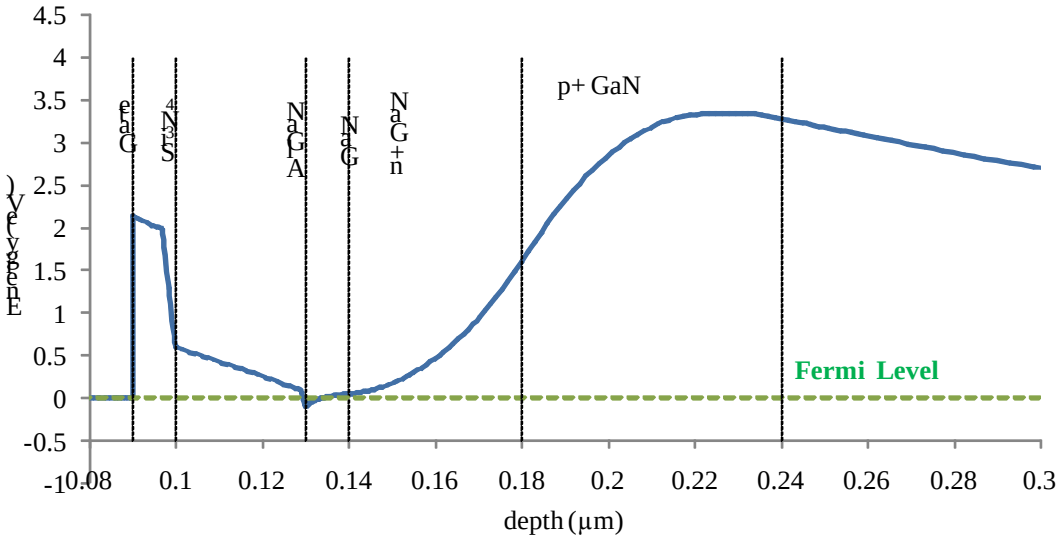

Figure 4.33 Band diagram along CUT 6 in figure 4.30 showing the shielding effect of the n-wells

Since the parameters in region 2 control the 2DEG density below the gate, the threshold voltage can be controlled by varying "P_{th}","N_A" and "d". On the other hand, the parameters in region 1, N_{th}, N_{well} and d, control the 2DEG density elsewhere and are responsible for controlling the current density of the device.

4.5.1.4. Sensitivity analysis

In this section, a sensitivity analysis is carried out showing the effect of the thickness (N_{th}) and the doping concentration (N_{well}) of the n-well on the transfer characteristics of the device. In all the presented simulations, the thickness and x-mole fraction of the AlGaN layer are 30 nm and 0.15 respectively. A 10 nm Si_3N_4 layer is used as a gate insulator. All the other parameters are taken the same as the normally-on HEMT used for calibration is section 2.3.3. The schematic cross-section of the device under simulation is shown in figure 4.34.

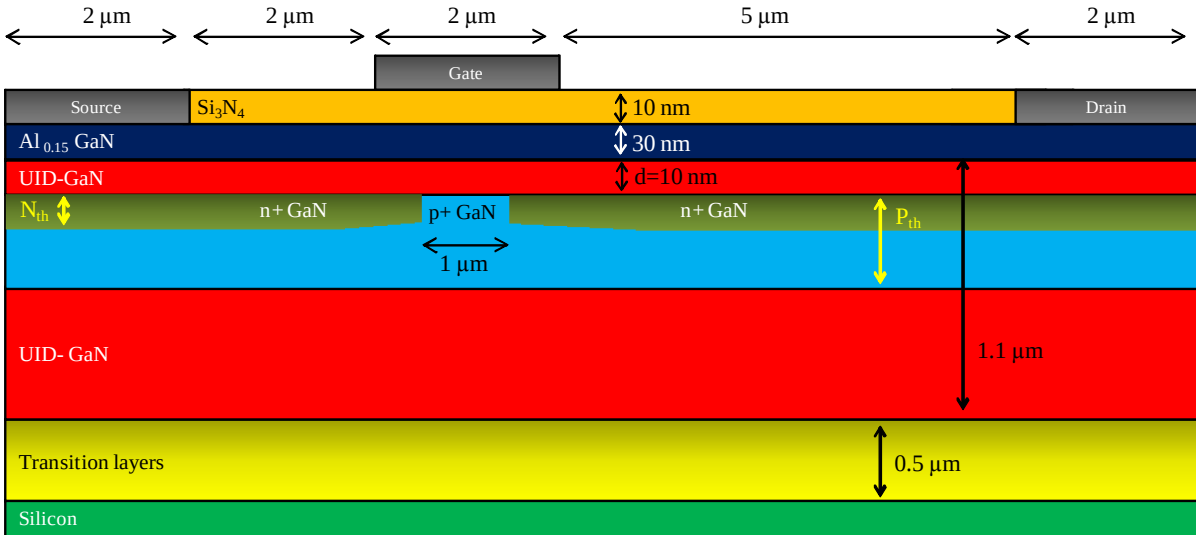

Figure 4.34 Schematic cross-section of the simulated structure

The variation of the drain current with N_{th} is shown is shown in figure 4.35. The doping concentration N_A and thickness P_{th} of the p-layer are 10^{18} cm^{-3} and 100 nm respectively. The doping concentration in the n-well is $N_{well} = 10^{18}$ cm^{-3}. As expected, the threshold voltage is not affected by N_{th}. However, as N_{th} increases, the 2DEG density increases, resulting in a higher current density.

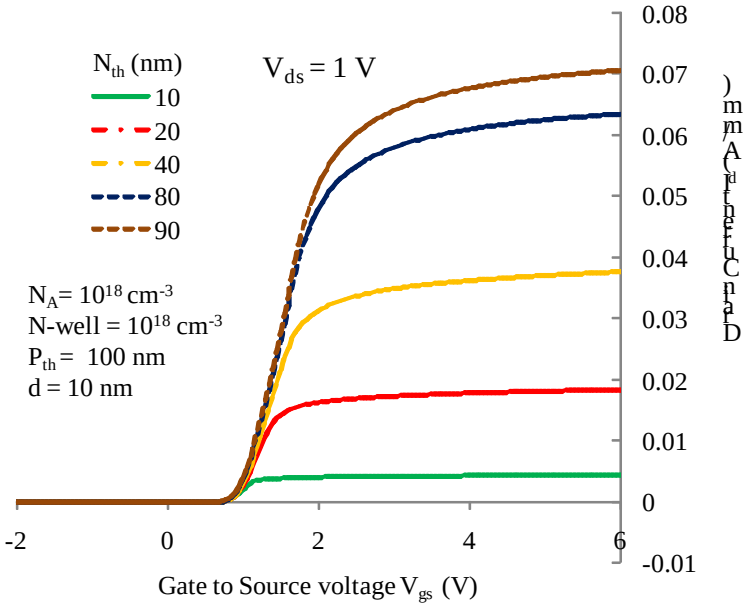

Figure 4.35 $I_{ds}(V_{gs})$ transfer characteristics of structure #1 for different N_{th}

If N_{th} increases to reach P_{th}, the simulated structure will look like the one simulated in section 4.2 (figure 4.15). Therefore the same results are expected as shown in figure 4.36. It is worth noting that the resulting doping concentration in the n-wells (*superposed* regions) is $N_s = N_{well} - N_A$. Figure 4.37 shows the variation of the Drain current with N_{th} for various N_s at

V_{gs} = 5 V. The current level of the conventional normally-off HEMT with buried p-region (figure 4.15) is shown in a dark black dotted line. The point of intersection between this dotted line and the simulated curves corresponds to the thickness of n-well (N_{th}) required to completely shield the channel electrons from the effect of the p-layer in region 1. When N_s increases, thinner thicknesses (N_{th}) are required to achieve the conventional level. Moreover, for high Ns, the current level surpasses the conventional level since the electrons in the n-wells start participating in the conduction current.

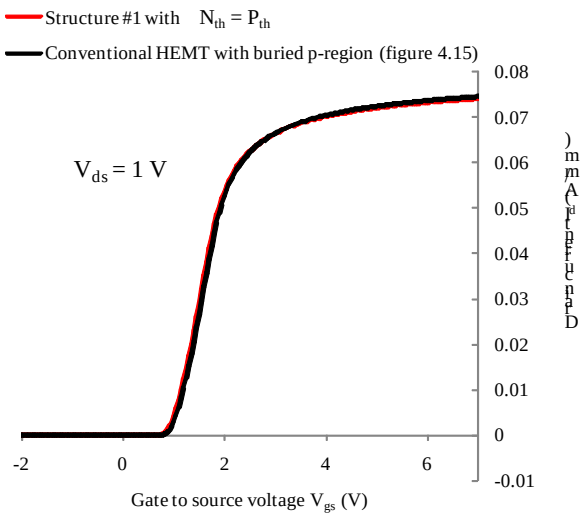

Figure 4.36 *$I_{ds}(V_{gs})$ transfer characteristics of structure #1 at $N_{th} = P_{th}$ and the structure shown in figure 4.15 (conventional HEMT with a buried p-region). A clear match is obtained since the two structures became identical when $N_{th} = P_{th}$*

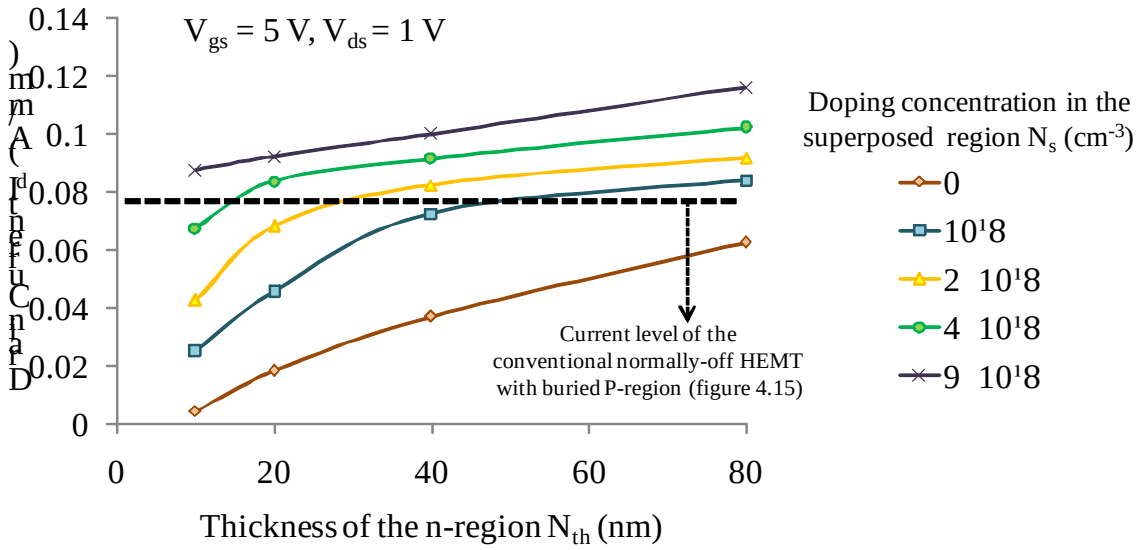

Figure 4.37 Variations of the Drain current with N_{th} for various N_s at V_{gs} = 5 V.

4.5.2. Structure #2

4.5.2.1. Device design and fabrication process

In section 4.5.1.2, we have stated the three reasons causing the survival of channel electrons in region 1 which are the decrease in $P_{th,r}$, the increase in the distance d and the downward push of the conduction band in the n-wells. However, the third reason alone is sufficient to restore the channel electrons in region 1. With that being said, a new structure is proposed using solely the downward push in the n-well to retrieve the channel. The schematic cross-section of structure #2 is shown in figure 4.38.

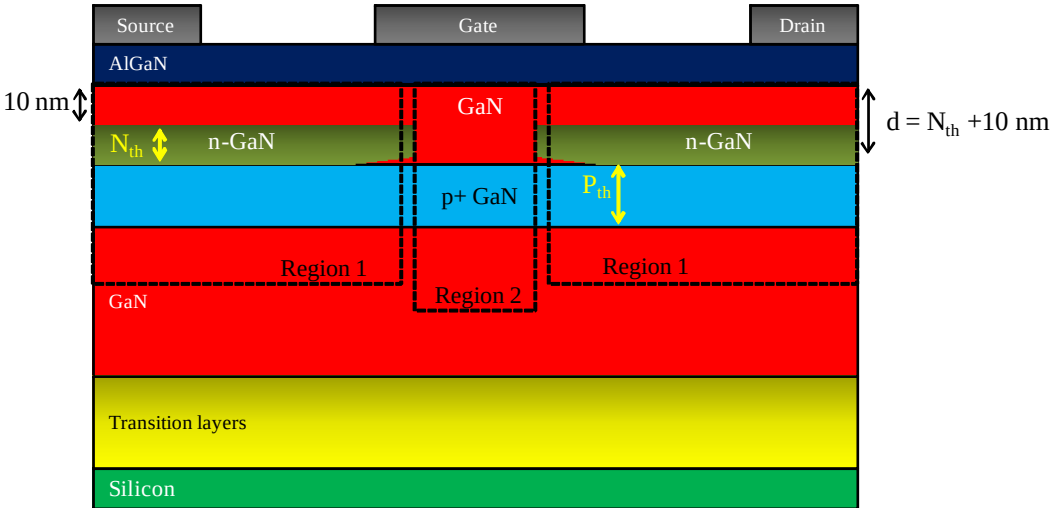

Figure 4.38 Schematic cross-section structure #2

To achieve this structure experimentally, the following can be done: after the growth of the GaN layer on a substrate, an epitaxial p-layer is grown all over the GaN layer. Then a GaN layer with a thickness equals to N_{th} is grown. Afterwards, using ion implantation, n-wells are created in Region 1 in the GaN layer. Then comes another thin GaN layer (10-50 nm) and finally the barrier layer (AlGaN layer), electrodes and passivation. The fabrication steps are shown in figure 4.39.

The growth of the other thin GaN layer (step 4.39 (e)) can be skipped. However, this will cause mobility degradation due to impurity scattering since the channel electrons in region 1 are inside the n-wells. Moreover, the existence of highly doped n-wells at the AlGaN/GaN interface reduces the confinement of channel electrons causing deterioration in their mobility.

When compared to the previous structure #1 (figure 4.30) the disadvantage of structure #2 is that the distance between the p-region and the AlGaN/GaN interface, in region 2, is increased from "d" to "d + N_{th}". On the other hand, smaller doping concentration is needed in the

n-wells to retrieve the channel electrons since in the first structure, the ion implantation is performed in a p-layer. In other words, the resulting doping in the n-wells in structure #1 is $N_s = N_{well} - N_A$ while, in this case, the resulting doping in the n-wells is $N_s = N_{well} + N_{GaN}$ (N_{GaN} is the doping concentration of the GaN layer placed after the growth of the p-layer (figure 4.39 (c))).

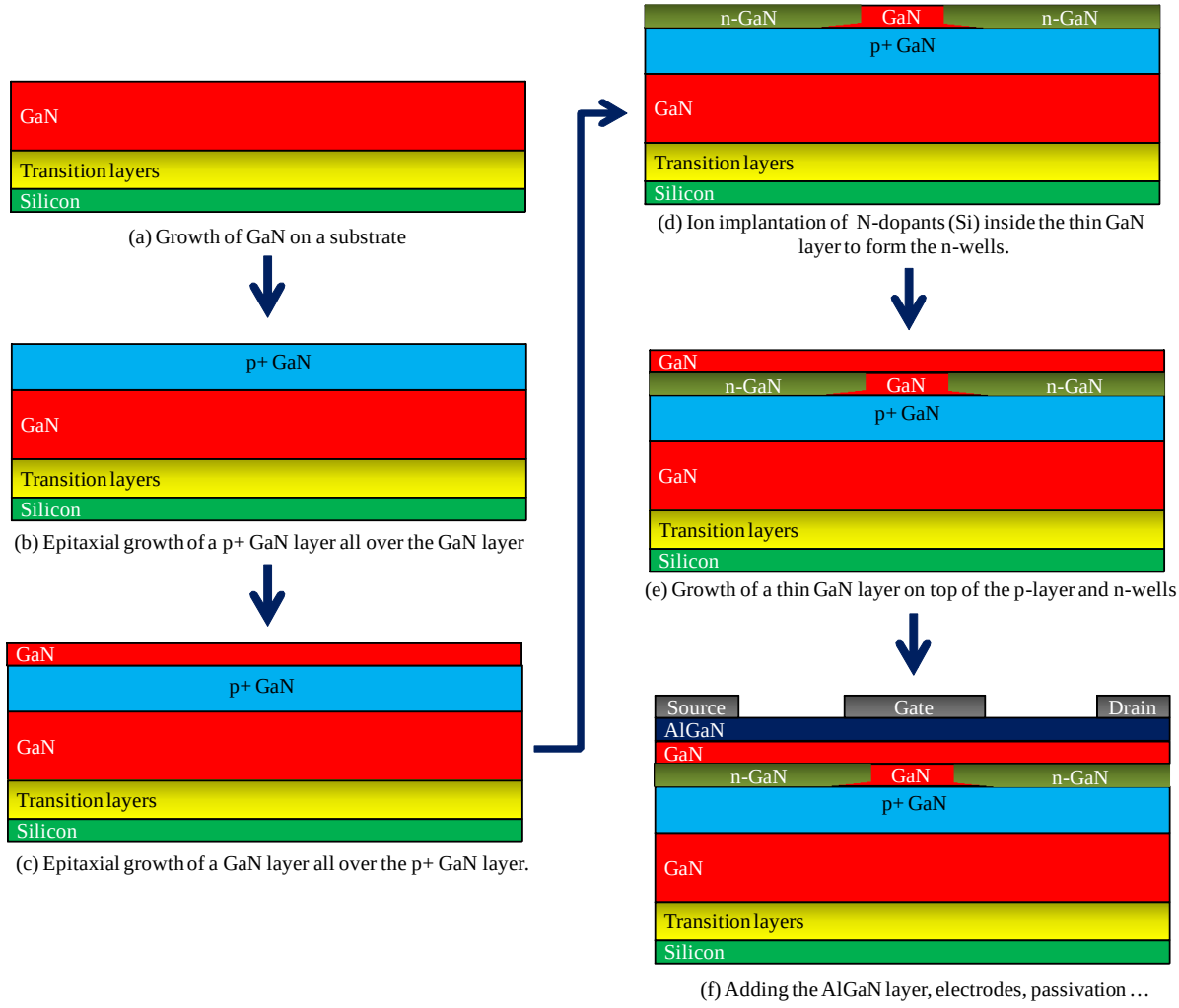

Figure 4.39 Major steps in the fabrication of structure #2

4.5.2.2. Sensitivity analysis

The variation of the drain current with N_s is shown in figure 4.40. The doping concentration N_A and thickness P_{th} of the p-layer are 10^{18} cm^{-3} and 100 nm respectively. The thickness of the n-well is N_{th} = 10 nm. N_{th} is taken small to keep the p-layer in region 2 close to the AlGaN/GaN interface. As shown in figure 4.40, the threshold voltage is not affected by N_s. However, as N_s increases, the 2DEG density increases, resulting in a higher current density.

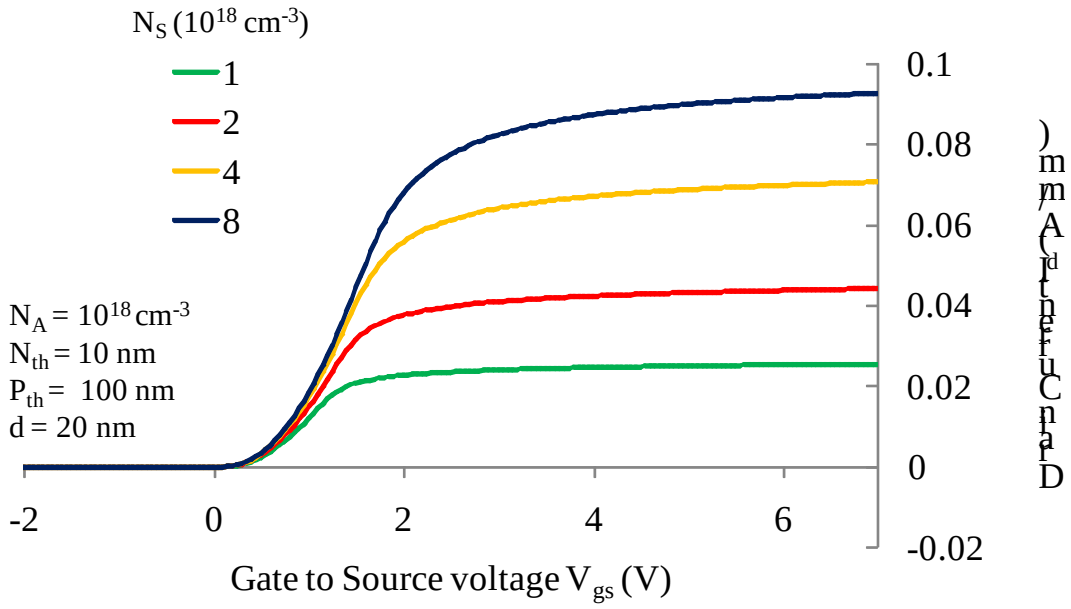

Figure 4.40 $I_d(V_{gs})$ transfer characteristics of structure #2 for different N_s

When compared to the transfer characteristics of structure #1 (figure 4.36), for the same P_{th} and N_A, a lower threshold voltage is obtained (0 V < 2 V). This is because the distance between the p-region and the AlGaN/GaN interface in structure #1 is smaller than that in structure #2 ($d < d + N_{th}$; 10 < 20 nm).

4.6. Conclusion

A new design with normally-off operation is achieved by burying a p-region below the channel of the HEMT. The conduction band in the p-region is uplifted, causing the triangular well at the AlGaN/GaN to elevate above the Fermi level. A sensitivity analysis was carried out to show the effect of the position, dimensions and doping concentration of the p-region on the threshold voltage. Simulation results have shown that the effectiveness of the p-region in shifting the threshold voltage increases as the p-region approaches the AlGaN/GaN interface. As for the dimensions of the p-region, the threshold voltage will increase with increasing the dimensions until a point is reached where further increase does not affect the threshold voltage. Moreover, the increase in the threshold voltage with the doping concentration strongly depends on the distance "d" between the p-region and the AlGaN/GaN interface. The sensitivity of the threshold voltage to the p-doping concentration decreases with increasing "d". If the p-region is able to increase the threshold voltage but fails to achieve normally-off operation, the x-mole fraction in the AlGaN layer can be decreased to further shift the threshold voltage to positive values.

However, the low forward gate voltage of the HEMT limits further increase in the threshold voltage. Therefore, the MIS-HEMT with a buried p-region is studied, showing the effect of doping concentration, permittivity and thickness of the insulator on the performance of the device. Simulation results have shown that the effect of the thickness of the insulator on the threshold voltage strongly depends on the p-doping concentration N_A. An increase in the thickness of the insulator will increase the threshold voltage if $N_A > N_{A,critical}$ (in our simulation, $N_{A,critical} = 9.5 \times 10^{17}$ cm^{-3}), decrease it if $N_A < N_{A,critical}$ and the threshold voltage is unaffected if $N_A = N_{A,critical}$. The same behavior was obtained for the variations of threshold voltage with the permittivity of the insulator where three different behaviors were obtained depending on N_A.

The proposed design is compared to the well-known Gate Injection Transistor (GIT). Although the GIT attains a higher forward gate voltage, our proposed structure is more efficient when it comes to the doping concentration required to achieve normally-off operation and offers better confinement for the 2DEG below the gate.

To merge the advantages of the two structures, the GIT with a buried p-region was studied. The resulting structure is able to achieve normally-off operation at relatively low doping concentrations and inherited the high forward gate voltage from the GIT.

Although the use of a buried p-region to achieve normally-off operation seems to be very promising, the fabrication of a localized highly doped buried p-region remains a big challenge. To overcome the fabrication challenges, two new normally-off structures were proposed. Although these structures still use the idea of burying a p-region to achieve normally-off operation, the way the p-region is created tackles the experimental challenges. The main idea in the two structures is to grow, below the channel, a p-layer that spans over the whole device. Afterwards, n-wells are created, everywhere except under the gate, inside the p-layer or between the p-layer and the AlGaN/GaN interface. The aim of these wells is to compensate the upward push in the conduction band created by the p-layer. Although the n-wells do not affect the threshold voltage, the drain current intensity increases as the doping concentration and the thickness of the n-wells increase.

Chapter 5
General conclusion and future work

5.1. General conclusion

AlGaN/GaN HEMTs are very promising candidates for high frequency applications with high power and low noise, such as microwave and millimeter wave communications, imaging and radars. With the high field strength offered by GaN and the high mobility of the two dimensional-electron-gas (2DEG) present in the HEMT, this device can attain high breakdown voltage with low on state resistance surpassing the limitation of conventional silicon devices. While power switching applications strongly demand normally-off operation, conventional HEMTs attain a channel populated with electrons at zero gate voltage making them normally-on. Several normally-off structures have been proposed such as recessed gate structures, Fluorine ion treatment, p-GaN gate structures, thin AlGaN barrier, and Gate Injection Transistor. However the threshold voltage of these structures is less than 3 V which is the threshold voltage required to prevent the misoperation caused by noise. With the gate leakage preventing further increase in the threshold voltage, an insulating layer is introduced under the gate giving rise to the MIS-HEMT.

In this work, two normally-off concepts were proposed. To examine their electric characteristics, a commercial TCAD simulation tool from Silvaco is used. The simulator was calibrated using experimental data from a normally-on HEMT device. The energy and density of the acceptor traps as well as the density of the two dimensional electron gas were tuned so that the simulated transconductance, threshold voltage and off state current matches the ones experimentally measured. Moreover, the transition layers were substituted by an intrinsic GaN layer. The thickness of this layer is increased to fit the vertical breakdown voltage of the device.

In the previously proposed normally-off HEMTs, there is an introduction of an external agent, such as negative Fluorine ions or p-doped layer, inside the barrier layer or at the top of it. In this work, we suggest the introduction of the same agents used before but this time under the channel rather than above it. This led to the proposition of two normally-off HEMT designs. The first is a HEMT with Fluorine implanted below its channel and the second is a HEMT with a buried p-GaN region.

In both structures, the agents should be buried only below the gate electrode. Otherwise the device will remain off regardless of the applied gate voltage. Simulation results have shown that the threshold voltage increases with increasing the concentration of the agent. Moreover, the effectiveness of the agent increases as it approaches the AlGaN/GaN interface.

When compared to structures with agents introduced above the channel, our approach is more effective when it comes to the concentration required to achieve normally-off operation and offers better confinement for the 2DEG density below the gate. On the other hand, burying a p-region or Fluorine ions below the channel reduces the forward gate voltage, which limits further increase in the threshold voltage.

To further increase the threshold voltage, an insulating layer is introduced below the gate, giving rise to the MIS-HEMT. Simulation results have confirmed the ability of buried agents to increase the threshold voltage. However, a point is reached where further increase in the concentration will not affect the threshold voltage. This is due to the fact that the gap between the Fermi level and the conduction band reaches the bandgap of the material in which the agents are introduced. Moreover, the effect of the thickness of the insulator on the threshold voltage strongly depends on the concentration of the agent. There exists a critical concentration ($F_{critical}$ or $N_{A,critical}$) at which no increase in threshold voltage is obtained when increasing the thickness of the insulator. The threshold voltage increases with the thickness of the insulator if the concentration is higher than the critical level and decreases if it is below it. The same behavior is obtained for the variation of threshold voltage with the permittivity of the insulator where three different behaviors were obtained depending on the concentration of the agent. The threshold voltage of the proposed structures can reach values higher than 3 V without affecting the 2DEG mobility.

The importance of the proposed structures is their ability to serve as an independent and complementary solution to achieve normally-off operation. For example, the HEMT with a buried p-GaN region can be combined with the Gate Injection Transistor. The resulting HEMT can achieve normally-off operation at relatively low p-doping concentration and inherits the high forward gate voltage from the GIT.

Although, the use of a buried p-region to achieve or help develop a normally-off HEMT seems to be very promising, the fabrication of a localized highly doped buried p-region remains a big challenge. In the final chapter, two new normally-off structures are presented. Although these structures still use the idea of burying a p-region to achieve normally-off operation, the way the p-region is created tackles the experimental challenges. The proposed structures are the only normally-off HEMT concepts that do not require etching. The main idea in the two structures is to grow, below the channel, a p-layer that spans over the whole device. Afterwards, n-wells are created, everywhere except under the gate, inside the p-layer or between the p-layer and the AlGaN/GaN interface. The aim of these wells is to

compensate the upward push in the conduction band created by the p-layer. Although the n-wells do not affect the threshold voltage, the drain current intensity increases as the doping concentration and the thickness of the n-wells increase.

5.2. Future work

It is axiomatic that the next step would be confirming the simulation results by fabricating the proposed structures. Since the fluorine equivalent interface charge density and position are not yet linked to experimental parameters, we plan on fabricating the normally-off HEMT with a buried p-region. Furthermore, several amends can be made in the simulation for more informative and accurate results.

5.2.1. Structure for fabrication

The schematic cross-section of the normally-off structure we plan to fabricate is shown in figure 5.1. The structure is the same as the one simulated in section 4.34, except for the added AlN interlayer between the thin UID-GaN layer and the AlGaN barrier layer.

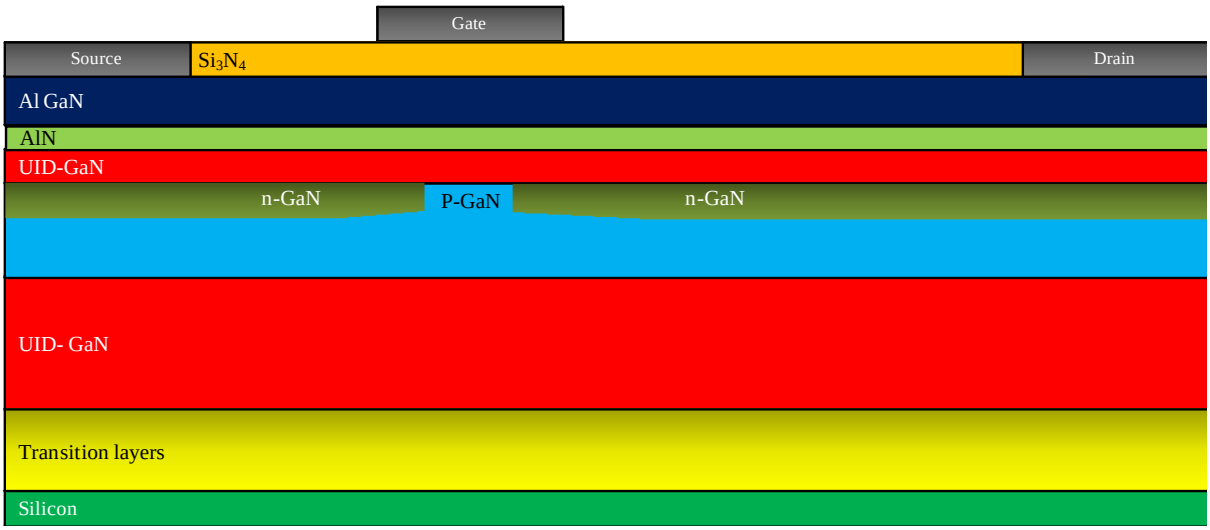

Figure 5.1 Schematic cross-section of the structure we plan to fabricate

5.2.2. Develop and implement a new mobility model

In sections 3.2.2 and 4.4.2 we have shown that, in the proposed structures, the confinement of the 2DEG below the gate increases. This will increase the mobility of the 2DEG. However, in our simulations, the mobility of the 2DEG was fixed to 1500 cm^2/v.sec. In section 2.3.4.1, to fit the experimental results from a normally-off HEMT with Fluorine implanted in the barrier layer, the mobility of the 2DEG was used as a fitting parameter and reduced from 1500 cm^2/v.sec to 500 cm^2/v.sec to account for the scattering between the channel electrons and Fluorine ions.

Therefore, it would be better to develop a new mobility that takes into account the confinement of the 2DEG and the scattering between the channel electrons and the Fluorine ions and implement it in the simulation software.

5.2.3. Linking the equivalent interfacial charge to the Gaussian profile

Since ATLAS lacks the ability of introducing fixed charge in a Gaussian profile, when simulating the effect of the implanted Fluorine ions, an equivalent interfacial charge with a profile similar to the delta function was used. For more informative results, the link between the experimental profile and the equivalent interfacial charge should be done. Another solution would be the use of different simulation softwares, such as Synopsys, where the introduction of fixed negative charge in a Gaussian profile is possible.

5.2.4. AC and transient analysis

Although several structures were proposed, only the DC performance was examined. This work can be extended by performing AC and transient analysis to the proposed structures.

References

[1] M. Toyota, Z. L. Liang, Y. Akita, H. Miyata, S. Kato, and T. Kurosu, “Application of Power Electronics Technology to Energy Efficiency and CO_2 Reduction,” *Hitachi Rev.*, vol. 59, no. 4, p. 141, 2010.

[2] I. Batarseh, “The Power MOSFET,” in *Power Electronics Handbook*, 2001, pp. 78–79.

[3] T. Egawa, “Development of Next generation Devices Amidst Global Competition Due to Their Huge Market Potential,” *Ultimate in Vacuum ULVAC*, no. 63, pp. 18–21, 2012.

[4] B. J. Baliga, *Fundamentals of power semiconductor devices*. Springer, 2010.

[5] E. Bahat-Treidel, “GaN Based HEMTs for High Voltage Operation,” Technischen Universität Berlin, Germany, 2012.

[6] D. A. Grant and J. Gowar, *Power MOSFETs: Theory and Applications*. Wiley-Interscience, 1989.

[7] *Gallium Nitride Processing for Electronics, Sensors and Spintronics*. .

[8] M. T. Veety, *Four Terminal Gallium Nitride MOSFETs*. 2011.

[9] S. Wetzel, T. Ager, S. Fisher, B. K. Meyer, I. Grzegory, and S. Porowski, “Strongly localized donor level in oxygen doped gallium nitride,” presented at the International conference on physics of semiconductors, Berlin, Germany, 1996.

[10] A. Hiroshi, K. Masahiro, H. Kazumasa, and A. Isamu, “P-Type Conduction in Mg-Doped GaN Treated with Low-Energy Electron Beam Irradiation (LEEBI), and,” vol. 28, p. L2112, 1989.

[11] D. Balaz, “Current collapse and device degradation in AlGaN/GaN heterostructure field effect transistors,” University of Glasgow, 2011.

[12] E. S. Hellman, “The Polarity of GaN: a Critical Review,” *MRS Internet J. Nitride Semicond. Res.*, vol. 3, p. e11, 1998.

[13] E. Cho, *Gallium Nitride Based Heterostructure Growth and Application to Electronic Devices and Gas Sensors*. ProQuest, 2009.

[14] C.-H. Chang, H.-T. Hsu, L.-C. Huang, C.-Y. Chiang, and E. Y. Chang, “Dept. of Mater. Sci. & Eng., Nat. Chiao-Tung Univ., Hsinchu, Taiwan,” in *Microwave Conference Proceedings (APMC), 2012 Asia-Pacific*, 2012, pp. 941–943.

[15] S. L. Selvaraj, A. Watanabe, A. Wakejima, and T. Egawa, “1.4-kV Breakdown Voltage for AlGaN/GaN High-Electron-Mobility Transistors on Silicon Substrate,” *IEEE Electron Device Lett.*, vol. 33, no. 10, pp. 1375–1377, Oct. 2012.

[16] T. E. Kazior, R. Chelakara, W. Hoke, J. Bettencourt, T. Palacios, and H. S. Lee, “High performance mixed signal and RF circuits enabled by the direct monolithic heterogeneous integration of GaN HEMTs and Si CMOS on a silicon substrate,” in *Compound Semiconductor Integrated Circuit Symposium (CSICS) IEEE*, 2011, pp. 1–4.

[17] J. D. Brown, R. Borges, E. Piner, A. Vescan, S. Singhal, and R. Therrien, “AlGaN/GaN HFETs fabricated on 100-mm GaN on silicon (111) substrates,” *Solid-State Electron.*, vol. 46, no. 10, pp. 1535–1539, 2002.

[18] W. Saito, T. Nitta, Y. Kakiuchi, Y. Saito, K. Tsuda, I. Omura, and M. Yamaguchi, “On-Resistance Modulation of High Voltage GaN HEMT on Sapphire Substrate Under High Applied Voltage,” *IEEE Electron Device Lett.*, vol. 28, no. 8, pp. 676–678, Aug. 2007.

[19] X. L. Wang, C. M. Wang, G. X. Hu, J. X. Wang, T. S. Chen, G. Jiao, J. P. Li, Y. P. Zeng, and J. M. Li, “Improved DC and RF performance of AlGaN/GaN HEMTs grown by MOCVD on sapphire substrates,” *Solid-State Electron.*, vol. 49, no. 8, pp. 1387–1390, Aug. 2005.

[20] T. Egawa, G.-Y. Zhao, H. Ishikawa, M. Umeno, and T. Jimbo, “Characterizations of recessed gate AlGaN/GaN HEMTs on sapphire,” *Electron Devices IEEE Trans. On*, vol. 48, no. 3, pp. 603–608, 2001.

[21] V. Tilak, B. Green, V. Kaper, H. Kim, T. Prunty, J. Smart, J. Shealy, and L. Eastman, “Influence of barrier thickness on the high-power performance of AlGaN/GaN HEMTs,” *Electron Device Lett. IEEE*, vol. 22, no. 11, pp. 504–506, 2001.

[22] S. T. Sheppard, K. Doverspike, W. L. Pribble, S. T. Allen, J. W. Palmour, L. T. Kehias, and T. J. Jenkins, “High-power microwave GaN/AlGaN HEMTs on semi-insulating silicon carbide substrates,” *Electron Device Lett. IEEE*, vol. 20, no. 4, pp. 161–163, 1999.

[23] M.-A. di Forte Poisson, M. Magis, M. Tordjman, R. Aubry, N. Sarazin, M. Peschang, E. Morvan, S. L. Delage, J. di Persio, R. Quéré, B. Grimbert, V. Hoel, E. Delos, D. Ducatteau, and C. Gaquiere, “LP-MOCVD growth of GaAlN/GaN heterostructures on silicon carbide: application to HEMT devices,” *J. Cryst. Growth*, vol. 272, no. 1–4, pp. 305–311, Dec. 2004.

[24] K. K. Chu, P. C. Chao, M. T. Pizzella, R. Actis, D. E. Meharry, K. B. Nichols, R. P. Vaudo, X. Xu, J. S. Flynn, J. Dion, and G. R. Brandes, “9.4 W/mm Power Density AlGaN-GaN HEMTs on Free-Standing GaN Substrates,” *IEEE Electron Device Lett.*, vol. 25, no. 9, pp. 596–598, Sep. 2004.

[25] M. I. Nathan, “Persistent photoconductivity in AlGaAs/GaAs modulation doped layers and field effect transistors: a review,” *Solid-State Electron.*, vol. 29, no. 2, pp. 167–172, 1986.

[26] L. Shen, S. Heikman, B. Moran, R. Coffie, N.-Q. Zhang, D. Buttari, I. P. Smorchkova, S. Keller, S. P. DenBaars, and U. K. Mishra, “AlGaN/AlN/GaN high-power microwave HEMT,” *Electron Device Lett. IEEE*, vol. 22, no. 10, pp. 457–459, 2001.

[27] Y. Ando, Y. Okamoto, H. Miyamoto, T. Nakayama, T. Inoue, and M. Kuzuhara, “10-W/mm AlGaN-GaN HFET with a field modulating plate,” *IEEE Electron Device Lett.*, vol. 24, no. 5, pp. 289–291, May 2003.

[28] A. Asgari, “Effects of partially occupied sub-bands on two-dimensional electron mobility in AlGaN/GaN heterostructures,” *J. Appl. Phys.*, vol. 95, no. 3, p. 1185, 2004.

[29] M. Asif Khan, Q. Chen, C. J. Sun, M. Shur, and B. Gelmont, “Two-dimensional electron gas in GaN–AlGaN heterostructures deposited using trimethylamine-alane as the aluminum source in low pressure metal organic chemical vapor deposition,” *Appl. Phys. Lett.*, vol. 67, no. 10, p. 1429, 1995.

[30] O. Ambacher, B. Foutz, J. Smart, J. R. Shealy, N. G. Weimann, K. Chu, M. Murphy, A. J. Sierakowski, W. J. Schaff, L. F. Eastman, R. Dimitrov, A. Mitchell, and M. Stutzmann, “Two dimensional electron gases induced by spontaneous and piezoelectric polarization in undoped and doped AlGaN/GaN heterostructures,” *J. Appl. Phys.*, vol. 87, no. 1, p. 334, 2000.

[31] S. D. Burnham, K. Boutros, P. Hashimoto, C. Butler, D. W. S. Wong, M. Hu, and M. Micovic, “Gate-recessed normally-off GaN-on- Si HEMT using a new O_2-BCl_3 digital etching technique,” *Phys. Status Solidi C*, vol. 7, no. 7–8, pp. 2010–2012, Jun. 2010.

[32] W. Saito, Y. Takada, M. Kuraguchi, K. Tsuda, and I. Omura, “Recessed-gate structure approach toward normally off high-Voltage AlGaN/GaN HEMT for power electronics applications,” *IEEE Trans. Electron Devices*, vol. 53, no. 2, pp. 356–362, Feb. 2006.

[33] W. B. Lanford, T. Tanaka, Y. Otoki, and I. Adesida, “Recessed-gate enhancement-mode GaN HEMT with high threshold voltage,” *Electron. Lett.*, vol. 41, no. 7, pp. 449–450, 2005.

[34] C. Y. Chang, S. J. Pearton, C. F. Lo, F. Ren, I. I. Kravchenko, A. M. Dabiran, A. M. Wowchak, B. Cui, and P. P. Chow, "Development of enhancement mode AlN/GaN high electron mobility transistors," *Appl. Phys. Lett.*, vol. 94, no. 26, p. 263505, 2009.

[35] M. A. Khan, Q. Chen, C. J. Sun, J. W. Yang, M. Blasingame, M. S. Shur, and H. Park, "Enhancement and depletion mode GaN/AlGaN heterostructure field effect transistors," *Appl. Phys. Lett.*, vol. 68, no. 4, p. 514, 1996.

[36] V. Kumar, A. Kuliev, T. Tanaka, Y. Otoki, and I. Adesida, "High transconductance enhancement-mode AlGaN⁄GaN HEMTs on SiC substrate," *Electron. Lett.*, vol. 39, no. 24, p. 1758, 2003.

[37] H. Chonan, T. Ide, X.-Q. Shen, and M. Shimizu, "Effect of hole injection in AlGaN/GaN HEMT with GIT structure by numerical simulation," *Phys. Status Solidi C*, vol. 9, no. 3–4, pp. 847–850, Mar. 2012.

[38] Y. Uemoto, M. Hikita, H. Ueno, H. Matsuo, H. Ishida, M. Yanagihara, T. Ueda, T. Tanaka, and D. Ueda, "Gate Injection Transistor (GIT)- A Normally-Off AlGaN/GaN Power Transistor Using Conductivity Modulation," *IEEE Trans. Electron Devices*, vol. 54, no. 12, pp. 3393–3399, 2007.

[39] L.-Y. Su, F. Lee, and J. J. Huang, "Enhancement-Mode GaN-Based High-Electron Mobility Transistors on the Si Substrate With a P-Type GaN Cap Layer," *IEEE Trans. Electron Devices*, vol. 61, no. 2, pp. 460–465, Feb. 2014.

[40] J. Kim, S.-K. Hwang, I. Hwang, H. Choi, S. Chong, H.-S. Choi, W. Jeon, H. S. Choi, J. Y. Kim, Y. H. Park, and others, "High threshold voltage p-GaN gate power devices on 200 mm Si," in *Power Semiconductor Devices and ICs (ISPSD), 2013 25th International Symposium on*, 2013, pp. 315–318.

[41] O. Hilt, A. Knauer, F. Brunner, E. Bahat-Treidel, and J. Wurfl, "Normally-off AlGaN/GaN HFET with p-type Ga Gate and AlGaN buffer," in *Power Semiconductor Devices & IC's (ISPSD), 2010 22nd International Symposium on*, 2010, pp. 347–350.

[42] I. Hwang, J. Kim, H. S. Choi, H. Choi, J. Lee, K. Y. Kim, J.-B. Park, J. C. Lee, J. Ha, J. Oh, J. Shin, and U.-I. Chung, "p-GaN Gate HEMTs With Tungsten Gate Metal for High Threshold Voltage and Low Gate Current," *IEEE Electron Device Lett.*, vol. 34, no. 2, pp. 202–204, Feb. 2013.

[43] C.-S. Suh, A. Chini, Y. Fu, C. Poblenz, J. S. Speck, and U. K. Mishra, "p-GaN/AlGaN/GaN Enhancement-Mode HEMTs," in *Device Research Conference, 64th*, 2006, pp. 163–164.

[44] I. Hwang, J. Oh, H. S. Choi, J. Kim, H. Choi, J. Kim, S. Chong, J. Shin, and U.-I. Chung, "Source-Connected p-GaN Gate HEMTs for Increased Threshold Voltage," *IEEE Electron Device Lett.*, vol. 34, no. 5, pp. 605–607, May 2013.

[45] Y. Cai, Y. Zhou, K. M. Lau, and K. J. Chen, "Control of Threshold Voltage of AlGaN/GaN HEMTs by Fluoride-Based Plasma Treatment: From Depletion Mode to Enhancement Mode," *IEEE Trans. Electron Devices*, vol. 53, no. 9, pp. 2207–2215, Sep. 2006.

[46] T. Palacios, C.-S. Suh, A. Chakraborty, S. Keller, S. P. DenBaars, and U. K. Mishra, "High-performance E-mode AlGaN/GaN HEMTs," *IEEE Electron Device Lett.*, vol. 27, no. 6, pp. 428–430, Jun. 2006.

[47] Yong Cai, Yugang Zhou, K. J. Chen, and K. M. Lau, "High-performance enhancement-mode AlGaN/GaN HEMTs using fluoride-based plasma treatment," *IEEE Electron Device Lett.*, vol. 26, no. 7, pp. 435–437, Jul. 2005.

[48] K. J. Chen, L. Yuan, M. J. Wang, H. Chen, S. Huang, Q. Zhou, C. Zhou, B. K. Li, and J. N. Wang, "Physics of fluorine plasma ion implantation for GaN normally-off HEMT

technology," in *Electron Devices Meeting (IEDM), 2011 IEEE International*, 2011, pp. 19–4.

[49] H. Chen, M. Wang, and K. J. Chen, "Self-aligned enhancement-mode AlGaN/GaN HEMTs using 25 keV fluorine ion implantation," in *Device Research Conference (DRC), 2010*, pp. 137–138.

[50] H. Kambayashi, Y. Satoh, T. Kokawa, N. Ikeda, T. Nomura, and S. Kato, "High field-effect mobility normally-off AlGaN/GaN hybrid MOS-HFET on Si substrate by selective area growth technique," *Solid-State Electron.*, vol. 56, no. 1, pp. 163–167, Feb. 2011.

[51] W. Huang, Z. Li, T. P. Chow, Y. Niiyama, T. Nomura, and S. Yoshida, "Enhancement-mode GaN hybrid MOS-HEMTS with $R_{on,sp}$ of 20 mohm-cm^2," in *Power Semiconductor Devices and IC's, 2008. ISPSD'08. 20th International Symposium on*, 2008, pp. 295–298.

[52] Z. Dong, S. Tan, Y. Cai, H. Chen, S. Liu, J. Xu, L. Xue, G. Yu, Y. Wang, D. Zhao, and others, "5.3 A/400V normally-off AlGaN/GaN-on-Si MOS-HEMT with high threshold voltage and large gate swing," *Electron. Lett.*, vol. 49, no. 3, pp. 221–222, 2013.

[53] S. Yagi, M. Shimizu, M. Inada, Y. Yamamoto, G. Piao, H. Okumura, Y. Yano, N. Akutsu, and H. Ohashi, "High breakdown voltage AlGaN/GaN MIS–HEMT with SiN and TiO_2 gate insulator," *Solid-State Electron.*, vol. 50, no. 6, pp. 1057–1061, Jun. 2006.

[54] C. Liu, E. F. Chor, and L. S. Tan, "Enhanced device performance of AlGaN/GaN HEMTs using HfO_2 high- *k* dielectric for surface passivation and gate oxide," *Semicond. Sci. Technol.*, vol. 22, no. 5, pp. 522–527, May 2007.

[55] M. Kanamura, T. Ohki, T. Kikkawa, K. Imanishi, T. Imada, A. Yamada, and N. Hara, "Enhancement-Mode GaN MIS-HEMTs With n-GaN/i-AlN/n-GaN Triple Cap Layer and High-k Gate Dielectrics," *IEEE Electron Device Lett.*, vol. 31, no. 3, pp. 189–191, Mar. 2010.

[56] C.-T. Chang, T.-H. Hsu, E. Y. Chang, Y.-C. Chen, H.-D. Trinh, and K. J. Chen, "Normally-off operation AlGaN/GaN MOS-HEMT with high threshold voltage," *Electron. Lett.*, vol. 46, no. 18, pp. 1280–1281, 2010.

[57] Z. Tang, Q. Jiang, Y. Lu, S. Huang, S. Yang, X. Tang, and K. J. Chen, "600-V Normally Off SiN_x/AlGaN/GaN MIS-HEMT With Large Gate Swing and Low Current Collapse," *IEEE Electron Device Lett.*, vol. 34, no. 11, pp. 1373–1375, Nov. 2013.

[58] W. Choi, O. Seok, H. Ryu, H.-Y. Cha, and K.-S. Seo, "High-Voltage and Low Leakage Current Gate Recessed Normally-Off GaN MIS-HEMTs With Dual Gate Insulator Employing PEALD SiN_x/RF-Sputtered HfO_2," *IEEE Electron Device Lett.*, vol. 35, no. 2, pp. 175–177, Feb. 2014.

[59] Ting-En Hsieh, Edward Yi Chang, Yi-Zuo Song, Yueh-Chin Lin,, Huan-Chung Wang, Shin-Chien Liu,, Sayeef Salahuddin, and Chenming Calvin Hu,, "Gate Recessed Quasi-Normally OFF Al_2O_3/AlGaN/GaN MIS-HEMT With Low Threshold Voltage Hysteresis Using PEALD AlN Interfacial Passivation Layer," *IEEE Electron Device Lett.*, vol. 35, no. 7, pp. 732–734, Jul. 2014.

[60] S. Quan, X.-H. Ma, X.-F. Zheng, and Y. Hao, "An Ultrathin AlGaN Barrier Layer MIS-HEMT Structure for Enhancement-Mode Operation," *Chin. Phys. Lett.*, vol. 30, no. 2, p. 028503, Feb. 2013.

[61] M. Ťapajna and J. Kuzmík, "Control of Threshold Voltage in GaN Based Metal Oxide Semiconductor High Electron Mobility Transistors towards the Normally-Off Operation," *Jpn. J. Appl. Phys.*, vol. 52, no. 8S, p. 08JN08, Aug. 2013.

[62] M. Ťapajna and J. Kuzmík, “A comprehensive analytical model for threshold voltage calculation in GaN based metal-oxide-semiconductor high-electron-mobility transistors,” *Appl. Phys. Lett.*, vol. 100, no. 11, p. 113509, 2012.

[63] *ATLAS User’s Manual DEVICE SIMULATION SOFTWARE*. Santa Clara, CA, 2011: SILVACO,.

[64] J. D. Albrecht, R. P. Wang, P. P. Ruden, M. Farahmand, and K. F. Brennan, “Electron transport characteristics of GaN for high temperature device modeling,” *J. Appl. Phys.*, vol. 83, no. 9, pp. 4777–4781, May 1998.

[65] D. M. Caughey and R. E. Thomas, “Carrier mobilities in silicon empirically related to doping and field,” *Proc. IEEE*, pp. 2192–2193, 1967.

[66] S. Selberherr, *Analysis and simulation of semiconductor devices*. Wien, Austria; New York: Springer-Verlag, 1984.

[67] A. G. Chynoweth, “Ionization Rates for Electrons and Holes in Silicon,” *Phys. Rev.*, vol. 109, no. 5, pp. 1537–1540, Mar. 1958.

[68] R. Van Overstraeten and H. De Man, “Measurement of the ionization rates in diffused silicon p-n junctions,” *Solid-State Electron.*, vol. 13, no. 5, pp. 583–608, May 1970.

[69] E. T. Yu, X. Z. Dang, P. M. Asbeck, S. S. Lau, and G. J. Sullivan, “Spontaneous and piezoelectric polarization effects in III–V nitride heterostructures,” *J. Vac. Sci. Technol. B*, vol. 17, no. 4, pp. 1742–1749, 1999.

[70] O. Madelung, *Semiconductors: Basic Data*. Springer-Verlag GmbH, 1996.

[71] H. Kim, S.-J. Park, and H. Hwang, “Thermally oxidized GaN film for use as gate insulators,” *J. Vac. Sci. Technol. B Microelectron. Nanometer Struct.*, vol. 19, no. 2, p. 579, 2001.

[72] I. H. Oğuzman, E. Bellotti, K. F. Brennan, J. Kolník, R. Wang, and P. P. Ruden, “Theory of hole initiated impact ionization in bulk zincblende and wurtzite GaN,” *J. Appl. Phys.*, vol. 81, no. 12, pp. 7827–7834, Jun. 1997.

[73] B. P. Luther, S. E. Mohney, T. N. Jackson, M. A. Khan, Q. Chen, and J. W. Yang, “Investigation of the mechanism for Ohmic contact formation in Al and Ti/Al contacts to n-type GaN,” *Appl. Phys. Lett.*, vol. 70, no. 1, pp. 57–59, Jan. 1997.

[74] T. Mattila, A. P. Seitsonen, and R. M. Nieminen, “Large atomic displacements associated with the nitrogen antisite in GaN,” *Phys. Rev. B*, vol. 54, no. 3, p. 1474, 1996.

[75] J. Piprek, *Semiconductor Optoelectronic Devices: Introduction to Physics and Simulation*. Academic Press, 2003.

[76] Y. Zhang, M. Sun, S. J. Joglekar, T. Fujishima, and T. Palacios, “Threshold voltage control by gate oxide thickness in fluorinated GaN metal-oxide-semiconductor high-electron-mobility transistors,” *Appl. Phys. Lett.*, vol. 103, no. 3, p. 033524, Jul. 2013.

[77] S. Chowdhury, B. L. Swenson, M. H. Wong, and U. K. Mishra, “Current status and scope of gallium nitride-based vertical transistors for high-power electronics application,” *Semicond. Sci. Technol.*, vol. 28, no. 7, p. 074014, Jul. 2013.

[78] S. Chowdhury, B. L. Swenson, and U. K. Mishra, “Enhancement and Depletion Mode AlGaN/GaN CAVET With Mg-Ion-Implanted GaN as Current Blocking Layer,” *IEEE Electron Device Lett.*, vol. 29, no. 6, pp. 543–545, Jun. 2008.